Granular chains, an alternative to study confined polymer dynamics.

Paul Rambach

To cite this version:

Paul Rambach. Granular chains, an alternative to study confined polymer dynamics.. Statistical Mechanics [cond-mat.stat-mech]. Université PSL; Université de Mons, 2020. English. NNT : . tel-02970536

HAL Id: tel-02970536
https://theses.hal.science/tel-02970536

Submitted on 18 Oct 2020

HAL is a multi-disciplinary open access archive for the deposit and dissemination of scientific research documents, whether they are published or not. The documents may come from teaching and research institutions in France or abroad, or from public or private research centers.

L'archive ouverte pluridisciplinaire **HAL**, est destinée au dépôt et à la diffusion de documents scientifiques de niveau recherche, publiés ou non, émanant des établissements d'enseignement et de recherche français ou étrangers, des laboratoires publics ou privés.

THÈSE DE DOCTORAT
DE L'UNIVERSITÉ PSL

Préparée à l'Université de Mons
Dans le cadre d'une cotutelle avec l'ESPCI

Les chaines granulaires, une voie pour étudier la dynamique des polymères confinés

Granular chains, an alternative to study confined polymer dynamics

Soutenue par
Paul RAMBACH
Le 22 septembre 2020

Ecole doctorale n° 564
ED *Physique en Île-de-France*

Spécialité
Physique

Composition du jury :

Roberto, LAZZARONI	Pr., UMONS	*Président, Rapporteur*
Günter, REITER	Pr.,, Freiburg Univ.	*Rapporteur*
Jorg, BASCHNAGEL	Pr., Strasbourg Univ.	*Examinateur*
Françoise, BROCHARD-WYATT	Pr. émérite, Institut Curie (UPMC)	*Examinateur*
Menon, NARAYANAN	Pr., Amherst Massachusetts Univ.	*Examinateur*
Elie, RAPHAEL	Pr., ESPCI	*Examinateur*
Pascal, DAMMAN	Pr., Mons Univ.	*Directeur de thèse*
Thomas, SALEZ	Dr., Bordeaux Univ.	*Directeur de thèse*

General introduction

A macromolecule, *i.e.* a polymer chain, is a large molecule composed of identical or different repeating structural subunits, called monomers. Typically, the number of monomer units N vary from 10^2 to 10^4 but may reach the order of 10^6–10^9. The simplest and the most basic polymer structure is a linear chain but more complex topologies exist and comprise linear-chain segments jointed in various regularly or randomly branched structures. This rather crude definition tends to relegate polymers to an abstract notion. On the contrary, polymers are very much present in our daily life: nylon, latex, polystyrene, cellulose, collagen, keratine, protein, DNA... What makes them so ubiquitous and primordial is their ability to change their conformational state in a response to varying environmental conditions or to specific triggers – chemical (ionic strength and pH) or physical (temperature and illumination) stimuli but also specific interactions (molecular recognition forces) – and this ability is conferred by their long-chain nature. Mastering the fine tuning of conformational changes in individual macromolecules is the key to most technological applications. Indeed, in the medicine realm, one would control the biological response of artificial materials or biomedical devices operating in contact with biofluids (blood and serum). Also, one would then be able to design drug-delivery systems that would target specific cells or tissues while, at the same time, be invisible to the immune system. Besides, polymeric antiviral and antibacterial drugs possess advantages over traditional small molecules therapeutics such as higher efficiency, wide spectrum of action, and ability of redesign for new emerging targets. For instance, the formation of polymer–virus complexes may interact and block specific receptors on the viral surface responsible for virus–cell interactions. Even though the bulk mechanical, electrical, and thermal properties of polymers are astonishing, thin polymer films and therefore, the influence of confinement on the extended, flexible conformations of the macromolecules have attracted much interest lately.

In this work, we will mainly be interested in the chain dynamics, specially when repulsive interactions come at play. A better understanding of this dynamics would improve our knowledge about crucial phenomena at the cellular level. For instance, the transport of RNA across the nuclear pore or the injection of viral DNA plasmid by bacteriophages into a bacteria. Alas, studying repulsive polymers in confined geometries

is as experimentally difficult as it is biologically relevant. In spite of recent advances in « nanorheology », from the Brownian motion of local probes, or in computer simulation, designing experiments matching the biological parameters is extremely challenging. All this leads to unchallenged theoretical tools. Even the straightforward problem of polymer translocation remains lively debated. As a way out of this impasse, we propose to use granular chains as a macroscopic equivalent of polymers. First we were interested in the internal structure of a stack of granular chains at rest and we rationalized it with a polymer analogy. Then we added energy in our experimental system via mechanical excitations which appears to be analogous to the equilibration with a thermal bath. Finally, we studied the dynamics of chains in specific confined geometries and compared it to both molecular dynamics simulations and theoretical tools.

Remerciements

An obligatory step on the path to a complete thesis manuscript is the acknowledgement and recognition to the people without which this work would not have been possible.
Even though being mandatory, it is a real pleasure to thank them.

First, all of my jury members who had the kindness to read my work : Jorg Bashnagel, Françoise Brochard-Wyart, Roberto Lazzaroni, Narayanan Menon, Günther Reiter and Elie Raphaël – who was just like a co-director.
Second, my two co-directors : Pascal Damman and Thomas Salez. It goes without saying that I owe you two my deepest gratitude.

Et troisièmement, je tiens à remercier tous les membres du laboratoire Influx, team bio et team granules. On a passé de très bons moments, et d'autres. Ce fut très humain et même si jamais je ne renierai mon parisianisme, je garde pour toujours une petite part de belge dans mon coeur. Il faut maintenant que je rentre "am baraque".

Enfin, je veux ici aussi remercier tous les membres de ma famille qui ne m'ont vu qu'en pointillé ces dernières années. Parmi tous les membres de ma famille, il y a ma doudou qui occupe une part toute particulière dans mon coeur. Elle m'offre le plus beau souvenir de Belgique : notre petit poisson !

Je dédie cette thèse à ma grand-mère Colette, à mon grand-père Philippe ainsi qu'à mon oncle Jean-Christophe.

ἕν οἶδα ὅτι οὐδὲν οἶδα

Contents

General introduction **i**

Remerciements **iii**

Part I What is the internal structure of a granular-chain assembly ? **1**

Part introduction **3**

1 How to understand the internal structure of matter ? **5**

1.1 The sphere, one shape for three states of matter 5

1.1.1 Crystal 5

1.1.2 Gaz 6

1.1.3 Liquid 8

1.2 The packing of granular matter 9

1.2.1 An old problem 10

1.2.2 A range of packing densities 13

1.2.3 Jamming instead of packing 14

1.2.4 The conjecture of Edwards 17

1.3 The packing of non spherical particles 17

1.3.1 Direct observation of deviation 18

1.3.2 The sphere, the exception rather than the rule 18

1.4 The packing of granular-chains 20

1.4.1 Table-top observation 20

1.4.2 Direct method of investigation 22

2 Indirect method of investigation **25**

2.1 Experimental setup 25

2.1.1 Parameters of the experiments 25

2.2 Preliminary observations 29

2.2.1 Experiments with glass beads 29

2.2.2 Experiments with granular chains 29

3 **Avalanche dynamics** **33**

3.1 Definition of an event 33

3.2 Cumulative distribution of event sizes 34

4 **Mean behaviour** **37**

4.1 Role of indentation depth 37

4.2 Role of chain size 38

4.3 Self-amplification of friction 39

4.3.1 The capstan 40

4.3.2 Interleaved phonebooks 41

4.3.3 Typical equation governing self-amplification 42

4.4 Interlocking points 42

4.4.1 A semi-dilute regime for self-amplified friction 45

4.4.2 Master curve 47

Part II Can a vibrated system be described by statistical physics ? **49**

Part introduction **51**

5 **How to thermostatize an experiment with vibrations ?** **53**

5.1 The experimental setup 53

5.1.1 The apparatus 53

5.1.2 Granular temperature 55

5.2 A thermostating bath 56

5.2.1 The generalized Langevin equation 57

5.2.2 Different possible baths 59

6 **A macroscopic Brownian particle in a double well trap** **65**

6.1 The double-well arena 65

6.2 Particle's positions 66

6.3 Mean escape time 69

Part III How is a long chain translocating ? **71**

Part introduction **73**

7 **A first approach to translocation** **75**

7.1 Biological context 75
7.2 Experimental investigations of macromolecule translocation 79
7.3 Two modes of translocation 80
  7.3.1 Description of the simulation 81
  7.3.2 Free translocation 83
  7.3.3 Confined translocation 91

8 Free translocation mechanisms 95

8.1 Sung and Park's theoretical approach 96
  8.1.1 Derivation of the potential – End-to-end distance distributions . . 96
  8.1.2 Free energy 103
  8.1.3 Fokker-Planck equation 105
  8.1.4 Langevin equation 106
8.2 Panja's theoretical approach 107
  8.2.1 Anomalous diffusion of a monomer - Rouse dynamics 108
  8.2.2 Anomalous diffusion of a monomer - self-avoiding chain 111
  8.2.3 Memory kernel and anomalous diffusion 114
  8.2.4 Impact of anomalous diffusion on chain free translocation through a pore 114
  8.2.5 Concluding remarks 117

9 Chain initially confined 119

9.1 Pressure driven translocation 120
  9.1.1 Mean escape time from the cavity 122
  9.1.2 Mean first passage time 125
9.2 Example of another biased translocation 126
  9.2.1 Ratchet translocation 126
9.3 Concluding remarks 127

General conclusion and outlooks 129

Bibliography 131

List of Figures

1.1 (a) Particles composing a cubic cristal, by Haüy [63] (b) Globular particles constituting a snowflake crystal, by Dalton [27] (c) X-ray diffraction pattern by ZnS, Knipping, Friedrich and Laue 1912 [50]. 6
1.2 (a) Painting by Joseph Wright, 1768, entitled Experiment on a bird in the air pump and representing a scientific experiment performed in a salon to entertain the audience. (b) Drawing taken from [85] explaining collisions between two spheres. 8
1.3 Bernal in his office trying to recreate a sphere packing. Photos taken from [46]. 9
1.4 General agreement between experimentally and calculated radial distributions, taken from [47]. 9
1.5 Stack of cannonballs. Photo taken from Wikipedia, credit Nedra. 10
1.6 Mathematician Johannes Kepler and drawings in his pamphlet on snowflakes [67], now located at the Thomas L. Fisher Library at the University of Toronto. 11
1.7 Drawing of four disks on a lattice and the definition of R, h, r and θ_i. . . . 12
1.8 (a) Face centered cubic (fcc). (b) Hexagonal close packed (hcp). Photos taken from Wikipedia, credit to Christophe Dang Ngoc Chan. 13
1.9 (a) Evolution of the packing density with the container size [113]. (b) Time evolution of the density of a shaken packing, from [70]. 14
1.10 (a) Force chains, taken from Bob Behringer's home page [7]. (b) Distribution of contact number, taken from [33]. 15
1.11 Unified jamming diagramm, with T the temperature on an axis, τ the shear stress on a another axis and the inverse of Φ, the packing fraction, on the last axis. Therefore, increasing one parameter while keeping the other two fixed leads to an unjamming transition. Taken from [77]. 16
1.12 (a) Archetypal Volume/Temperature diagram showing the transition point between solid (glass & crystal) and liquid. (b) Pressure/Packing fraction diagram also exhibiting the transition between solid and liquid but for an assembly of spheres. In both cases, the solid state is made from two different branches. Taken from [121]. 16
1.13 An article in Science 1973 [115]. 17

1.14 On the left column, heaps of rather spherical particles – photos taken from the internet. On the right, column-like stacks of staples, rods and stars, photos taken from [121, 122, 49]. 18
1.15 (a)Volume fraction and (b) coordination number against aspect ratio, both exhibiting a particuliar behaviour for the sphere shape. Adapted from [34]. 19
1.16 Packing fraction against aspect ratio for rod-like particles. On the left, the data are plotted with a linear scale while on the right the same data are represented in a log-log graph. The solid curve corresponds to the theoretical expression given by Eq.1.7, in good agreement for great aspect ratios. Taken from [103]. 20
1.17 Pile of granular-chains, with lengths of 3, 5, 10 and 30 monomers as indicated in the upper left corner of each photo. Taken from our work [37]. . . 21
1.18 Densest achievable state for stacks of chains with different lengths N and stacks of rods with different aspect ratios length over diameter L/D. The solid red curves correspond to the function $f : x \to 1/x$. Data reproduced from [130] and [104]. 22
1.19 (a) Uniaxial compression test. (b) Stress strain curves. (c) Definition of a loop. Taken from [17]. 23
1.20 Image reconstructed from the X-ray tomography of a chain packing. Taken from [75]. 23

2.1 Vertical indentation setup we used to measure the mechanical response of a stack of chains. 26
2.2 Modelisation of the granular chain. 26
2.3 Measured resisitive force against depth of indentation for different types of container. 27
2.4 Measured resisitive force against depth of indentation for different indentation speeds. 28
2.5 (a) Force chains are visible thanks to the photoelasticity of the grain material [3]. (b) Measured resisitive force against depth of indentation for unconnected beads. 29
2.6 Zoom on the indenter when in (a) beads and (b) chains. 30
2.7 Experimental curves of resisitive force against depth of indentation for simple beads and chains of 10 monomers. 30
2.8 Measured resisitive force against depth of indentation for granular chains for (a) different lengths and (b) chains of 10 monomers. 31

3.1 Typical indentation curve and definition of an avalanche size. Blue dots in the inset are figurative for data points. 34
3.2 Mean cumulative size of avalanches. The dashed and the finely dashed lines are guide to the eye for power laws $x^{-3/2}$ and $x^{-1/2}$ respectively. . . 35

4.1 (a) Mean resistive force F and (b) logarithm of the ratio F/F_0 against indentation depth z for different chain lenghts $\mathcal{N}$. The red curves are linear guides for the eye. 38
4.2 Rate of the exponential increase of the resitive force $d\log(F)/dz$ againts the chain's length $\mathcal{N}$. The red dashed curve corresponds to the best power law fit $\sim \mathcal{N}^{0.46}$. 39
4.3 (a) Making fire with friction. (b) Avoiding friction with magnetic levitation. (c) The Chinese finger trap, images taken from Wikipedia. 40
4.4 Schematic of a capstan. 41
4.5 Schematic of two interleaved sets of sheets, taken from [1]. 41
4.6 Schematic view of the internal structure of polymer solution and melt, taken from [53]. 43
4.7 Evolution of the excluded volume with temperature: v is negative for $T \leq \theta$ and positive for $T \geq \theta$. Taken from [16]. 44
4.8 Blob picture: the chain, in red, can be seen as a chain of blobs, black circles, of size ξ. 46
4.9 (a) Effect of dilution on the resistive force. (b) Evolution of the slope of (a), $d\log(F/F_0)/dz$, with the volume fraction of chain. 47
4.10 Comparison between the measured resistive force and the theoretical expectation from Eq.4.18 for the two investigated cases: melt ($\Phi = 1$) and semi-dilute. 48

5.1 Setup we used to perform vibrated experiments. 54
5.2 (a) Evolution of the temperature T, measured as a kinetic energy, with y the depth, measured for a binary mixture of particles of radii 5 and 4 mm, taken from [127]. (b) Evolution of the temperature E, measured as a kinetic energy, with y the depth, on two different axis, adapted from [126]. For both graphs, the measure of depth is opposite to gravity. 55
5.3 (a) Observed deviation from Maxwell-Boltzmann distribution in vibrated particle experiments in [109]. (b) The use of a dimer bath negates these deviations, taken from [6]. 60
5.4 (a) Black metallic bead (diameter 4.5 mm) immerged in a layer of small plastic beads (1 mm diameter) and (b) part of the trajectory of the black bead during an experiment with a shaker excitation frequency of 30 Hz and acceleration of 24 m.s^{-2}. The grey nuances are an indicator of the course of time. 61
5.5 (a) Black metallic bead (diameter 4.5 mm) immerged in a layer of metallic dimers (2 mm diameter) and (b) part of the trajectory of the black bead during an experiment with a shaker excitation frequency of 30 Hz and acceleration of 24 m.s^{-2}. The grey nuances are an indicator of the course of time. 61

5.6 Black metallic bead (diameter 4.5 mm) on top of (a) a glued layer of plastic beads (2 mm diameter) and (b) the 3D-printed arena. In (c) part of the trajectory of the black bead during an experiment with a shaker excitation frequency of 30 Hz and acceleration of 24 m.s^{-2}. The grey nuances are an indicator of the course of time. 62
5.7 Probability density function (PDF) of the one step increment Δx for different solvant bath (a) small plastic beads (b) dimers (c) glued beads. The solid blue lines represent a Gaussian fit with σ as the standard deviation of the distribution. 63
5.8 VACF of the metallic bead moving on top of the glued beads layer. Just the first lagtimes are represented here. 64

6.1 (a) and (b) Perspective views of the two different potentials we used. . . . 65
6.2 Schematic side view of the potentials with barrier heigths $z_1 = 1$ mm (Potential 1) and $z_2 = 3$ mm (Potential 2). 66
6.3 Example of a trajectory in a double well trap. The red finely dashed lines correspond to the shapes of the well. The X-axis is defined as the line joining the centers of the well. 66
6.4 Example of the position probability on (a) the X-axis and (b) the Y-axis for four accelerations "acc": $\gamma = 9, 11, 13$ and 15 m.s^{-2}. 67
6.5 Position probability distributions modelled by Gaussian functions for the different potentials and accelerations on the (a) X-axis and (b) the Y-axis. . 67
6.6 Evolution of the fitting parameter (a) α and (b) τ with the shaker's acceleration γ. 68
6.7 Evolution of the produt $\alpha^2\tau$ with the shaker's acceleration γ. 69
6.8 (a) Probability for the bead to be located in the right or the left well. The black dashed line correponds to the probability 1/2. (b) Mean escape time from a well. The solid lines are best fits to $a.\exp(b/\gamma)$. 69

7.1 Schematics of the architecture of the cell membrane. Taken from Wikipedia, credit to Mariana Ruiz. 75
7.2 Three pathways across the cell membrane, by (a) diffusion or (b) through a membrane pore (b) and (c) via endocytosis. 76
7.3 (a) The internal structure of a prototypal animal cell: (1) Nucleolus (2) Nucleus (3) Ribosomes (4) Vesicle (5)Rough endoplasmic reticulum (6) Golgi apparatus (7) Cytoskeleton (8) Smooth endoplasmic reticulum (9) Mitochondrion (10) Vacuole (11) Cytosol (12) Lysosome (13) Centriole (14) Cell membrane. Taken from Wikipedia, credit to Kelvinsong. (b) A schematic of the cystoskeleton; in blue are the microtubules, in green intermediate filaments and in red actin filaments. Taken from [92]. 77
7.4 Artistic rendering of the T4 architecture. Adapted from Wikipedia, credit to Oona Räisänen. 78

7.5 T4 injection into a cell. Taken from Wikipedia, credit to Dr. Graham Beards. 79
7.6 T4 replication sequence. Taken from [83]. 79
7.7 (a) Examples of a "current blockade" caused by a polymer entering the pore and partly blocking the ions flows. Unsuccessful attempts of polymer translocation result in current blockades of very short durations see *e.g.* (3) as opposed to (1) and (2). Taken from [88]. (b) Schematic representation of the device allowing measurement of macromolecule translocation. Taken from [14]. 80
7.8 Free translocation: (a) initial configuration and (b) at later times ; Translocation outside a cavity: (c) cavity initially closed until equilibrium is reached then (d) an opening is created. 81
7.9 (a) Time evolution of the number of translocating monomers for a self-avoiding chain long of 54 monomers. Translocation ends when $s = 0$ or $s = 54$, figurated by the black dashed lines. (b) Probability distribution of the position of the center of mass of the chain at three different times for a self-avoiding chain long of 74 monomers. At first the probability is centered around the origin, then gradually a hole in the distribution appears at the origin, due to the translocation. 84
7.10 Waiting time for ideal and self avoiding chains of different lengths. Whatever the chain length, the longest waiting time corresponds to the translocation of the mid monomer. For each chain length, the waiting time for an ideal chain is shorter than the one for a self-avoiding chain. 85
7.11 Time evolution of the scaled monomer index $x(t) = s^*(t) - N/2$ in the pore for ideal and self-avoiding chains of different lengths. 85
7.12 (a) Mean translocation time and (b) Mean equilibration time for ideal and self-avoiding chains of different lengths. The solid line curves are obtained via a power law best fit with the exponent already chosen while the dashed line curves corresponds to a power law best fit with the exponent as a fitting parameter. 86
7.13 Normalized time evolution of the rescaled monomer index in the pore for ideal and self-avoiding (SA) chains of different lengths. 87
7.14 Distribution of translocation times for ideal and self-avoiding chains of different lengths. 89
7.15 Results from numerical solutions of Langevin equations for a 1D random walk with (a) 1 or (b) 2 absorbing boundaries. 90
7.16 (a) Time evolution of the number of monomers translocating for two self-avoiding chains of different lengths and for different cavity radii. (b) Mean escape time of a self-avoiding chain, with different lengths, out of a cavity, with different radii. 92
7.17 (a) Mean translocation time with respect to the rescaled radius of cavity $R/N^{3/4}$. (b) Empirical attempt to rescale the mean escape time by N^4. . . 92

8.1 Snapshots of the the translocation process of an ideal chain and a self-avoiding one as per our simulations. The blue beads stand for the wall particles, the green particles are related to the ideal chain and the yellow ones to the self-avoiding chain. 95

8.2 Illustration of the different conformations adopted by an ideal (in green) and a self-avoiding (in yellow) chain with 54 monomers whether (a) free or (b) tethered to a wall. The wall is made of the blue particles and the red particles are the end monomers of the chains. 96

8.3 Probability distributions of end-to-end distance for free (left column) and fixed (right column) ideal (top row) and self-avoiding (bottom row) chains. 97

8.4 Probability distribution of the end-to-end distance for an ideal chain, freely evolving in 2D. In the upper pannel the black solid curves are a best fit with the function $a(x/b)\exp(-(x/b)^2)$, where a and b are the fitting parameters. The bottom left pannel represents the evolution of the product ab and the bottom right pannel the evolution of b with the chain length N. 98

8.5 Probability distribution of the end-to-end distance for a self-avoiding chain, freely evolving in 2D. In the upper pannel the black solid curves are a best fit with the function $a(x/b)\exp(-(x/b)^2)$, where a and b are the fitting parameters. The bottom left pannel represents the evolution of the product ab and the bottom right pannel the evolution of b with the chain length N. 100

8.6 Probability distribution of the end-to-end distance for an ideal chain in 2D, tethered to a wall. In the upper pannel the black solid curves are a best fit with the function $a(x/b)\exp(-(x/b)^2)$, where a and b are the fitting parameters. The bottom left pannel represents the evolution of the product ab and the bottom right pannel the evolution of b with the chain length N. 101

8.7 Probability distribution of the end-to-end distance for a self-avoiding chain in 2D, tethered to a wall. The red dashed lines correspond to a best fit with the function $a(x/b)^{31/9}\exp(-(x/b)^4)$. 102

8.8 Probability distribution of the end-to-end distance for a self-avoiding chain in 2D, tethered to a wall. In the upper pannel the black solid curves are a best fit with the function $a(x/b)\exp(-(x/b)^2)$, where a and b are the fitting parameters. The bottom left pannel represents the evolution of the product ab and the bottom right pannel the evolution of b with the chain length N. 103

8.9 Effect of the wall as a free energy barrier for an ideal chain ($\nu = 1/2$, blue curve) and a self-avoiding chain ($\nu = 3/4$, red curve) of 1000 monomers. This barrier, given by $f(x) = \nu \ln(x(N-x))$, is relatively flat and reached its maximum for the mid monomer. 105

8.10 (a) Comparison between MD simulations (LAMMPS) and numerical results from Eq.8.32 for the translocation trajectory s of an ideal chain of 100 monomers. (b) Evolution of the mean translocation time τ_{trans} with the chain size N. Dots are data points and solid lines are best fits with the function aN^b with a and b as fitting parameters. 107
8.11 Comparison between the MSD of a monomer located in the middle (solid line) and the one of the chain's center of mass (dashed line) of an ideal chain of length 54. 111
8.12 Comparison between the MSD of a monomer located in the middle (solid line) and the one of the chain's center of mass (dashed line) of a self-avoiding chain of length 54. 112
8.13 Snapshots of a vibrated 50 monomers long granular chain taken at different times. The black beads are the ones tracked during the experiment. . . 113
8.14 Time evolution of the MSD of a tagged bead located at the center of a granular chain from our vibrated experiment. 113
8.15 MSD of the monomer number in the pore for an ideal (in blue) and a SA (in red) chain of length $N = 153$. 116

9.1 Snapshots of a self-avoiding chain with $N = 298$ monomers escaping a cavity, from LAMMPS simulations at times (a) $t = 0$ (b) t_1 (c) $t_2 = 3 \cdot t_1$ and (d) $t_4 = 12 \cdot t_1$. 120
9.2 (a) Raw and (b) Normalized by N^3 pressures P for a self-avoiding chain in a closed circular 2D cavity. 121
9.3 (a) Determination of the cavity's radius at which deviation from theoretical law starts (dashed lines). The solid black line correponds to the function R^{-6}. (b) Evolution of R_{crit} with the chain's length. 122
9.4 Figure already displayed in the first chapter of this part Fig.7.17 but redisplayed here for sake of simplicity. 122
9.5 Evolution of the rescaled, by $N^{5/2}$, mean escape time with the degree of initial confinement R/R_{F}. 123
9.6 Number of monomers oustide the cavity with respect to a normalized time $T = tN_0/R^4$. 125
9.7 Mean first passage time for the first monomer of the chain to escape the cavity. 126
9.8 Initial configurations when the chain has: (a) One head ratchet , (b) One head ratchet & ratchet in the middle and (c) A ratchet every 10 monomers. 127
9.9 Cumulative waiting time for a self-avoiding chain of length 54 with different number of ratchets amongst its monomers. 127

Part I

What is the internal structure of a granular-chain assembly ?

What is the meaning of human life, or of organic life altogether? To answer this question at all implies a religion. Is there any sense then, you ask, in putting it? I answer, the man who regards his own life and that of his fellow-creatures as meaningless is not merely unfortunate but almost disqualified for life. [...] The fairest thing we can experience is the mysterious. It is the fundamental emotion which stands at the cradle of true art and true science. He who knows it not and can no longer wonder, no longer feel amazement, is as good as dead, a snuffed-out candle. It was the experience of mystery – even if mixed with fear – that engendered religion. A knowledge of the existence of something we cannot penetrate, of the manifestations of the profoundest reason and the most radiant beauty, which are only accessible to our reason in their most elementary forms – it is this knowledge and this emotion that constitute the truly religious attitude; in this sense, and in this alone, I am a deeply religious man. I cannot conceive of a God who rewards and punishes his creatures, or has a will of the type of which we are conscious in ourselves. An individual who should survive his physical death is also beyond my comprehension, nor do I wish it otherwise; such notions are for the fears or absurd egoism of feeble souls. Enough for me the mystery of the eternity of life, and the inkling of the marvellous structure of reality, together with the single-hearted endeavour to comprehend a portion, be it never so tiny, of the reason that manifests itself in nature.

Albert Einstein, *the world as I see it*, 1949 [43]

Part introduction

The question raised by Albert Einstein about the meaning of life may well be the first and the last one in the human history. In the following pages we will not claim to answer it, we will rather stand by his last assessment, leaving the mystery of it and studying its manifestation in nature, and we will actually stand by the ″tiny″ portion part.

What is the world made of ? This existential question was raised early in history by philosophers all around the globe. However, since our western culture has been shaped by the ancient greek philosophers we will restrict ourselves to their conception of the world.

In broad brush strokes, around the Mediterranean circa V$^{\text{th}}$ century BC, matter at the macroscopical level was thought to be an assembly of elementary parts and two main philosophical schools have opposing points of view on the quality of these elementary parts. On one hand, the atomists consider that matter is made of invisible particles, all from the same substance, and the diversity observed at the macroscopical scale deriving from the different internal organization of the atoms. On the other hand, the peripateticians envisage four elementary substances earth, water, air and fire that blend in different proportions. The main debate centered not around the existence or the quality of these elementary parts but rather on what is between them. For the atomists, between the ″being″ there was ″non being″ that may be seen as the void, while for the peripateticians there was a fifth substance, the ″quinte essence″, called aether. The real stumbling block between these two doctrines was the possibility or not of the ″non being″.

While the doctrine of the peripatetician enabled a representation of the spiritual world as well as the physical world, the atomistic doctrine could not encompass the faculty we all possess: thinking. We may thus believe that because the model proposed by the peripateticians was more fulfilling than the atomism, it prevailed. This conception of the world is usualy referred to as the Aristotelian paradigm, as he is its main founding father.

Even though this paradigm prevailed it was quasi non-existant in Europe until the Renaissance and the Italian princes who had had these ancient texts translated, copied and largely circulated in whole Europe. It is admitted that the peripatetician school became widespread again while the atomists suffered from the same prejudice, its failure to integrate the divine.

However, contemporary scientists, penetrated with the same questions than their ancient Greek peers, discovered inconsistencies with this paradigm. For instance, Copernic pointed out that the Earth could not be at the center of the universe and Newton theory of gravitation cast away the notion that motion could only arise from action through contact. Gradually, the Aristotelian paradigm was proven wrong, yet none of these scientists completely refuted it. The impossibility of the void, closely related to the existence of a higher intelligence, was too deeply rooted in the western culture. Instead, science and metaphysic became increasingly independent, until Laplace famously replied to Napoleon about the role of God in his *System of the World* "Sire, je n'ai pas eu besoin de cette hypothèse" (which can be translated in "Sire, I did not need this hypothesis").

For all that, atomism was still not accepted by all scientists until the works of Boltzmann, Gouy, Einstein, Smochulokwski and Perrin, who definitely proved the existence of atoms in the early XX$^{\text{th}}$ century.

The debate over the existence of the void is still open, notably because of a corollary question about the concept of action at a distance. While earth, water, air and fire have lost their importance in science by then, the fifth element "aether" is still in the race. Einstein who first opposed to it finally gave a lecture in 1920 at the Leyden University entitled Ether and the theory of relativity, which he concluded by :

Recapitulating, we may say that according to the general theory of relativity space is endowed with physical qualities; in this sense, therefore, there exists an ether. According to the general theory of relativity space without ether is unthinkable; for in such space there not only would be no propagation of light, but also no possibility of existence for standards of space and time (measuring-rods and clocks), nor therefore any space-time intervals in the physical sense. But this ether may not be thought of as endowed with the quality characteristic of ponderable media, as consisting of parts which may be tracked through time. The idea of motion may not be applied to it. [41]

In this chapter, we will characterize the assembly of granular chains by understanding its internal structure. We will, then, exhibit the drastic effect of the geometry of a chain compared to simple spheres. Finally, through the prism of a polymer melt, we will rationalize the mechanical response of such an assembly to a vertical indentation.

Chapter 1

How to understand the internal structure of matter ?

In physics, a model is the rationalization of the key features of an observed phenomenon. Usually, to do so, one has to make assumptions and approximations. When dealing with an abstract concept, such as a particle, one often needs a visual support. Perhaps due to its associated metaphysical qualities, the spherical shape is the most commonly used visual support.

1.1 The sphere, one shape for three states of matter

1.1.1 Crystal

During the XVIIth and XVIIIth centuries, scientific experiments and discoveries were often displayed in the salons as entertainment. In this regard, curiosity cabinets would frequently include collections of crystals from all around the globe for their amazing beauties and symmetries. It is actually in one of these curiosity cabinets that Haüy accidentally broke an Iceland spath crystal and revealing in the process that the two new parts of the crystal presented the same symmetries as the unbroken one [26]. While the crystals were usually classified according to sensorial qualities (color, hardness, taste...), Haüy endeavored to classifying them according to their internal structure[1]. From his first experience of breaking a crystal, Haüy discovered that every crystal would consist in a core that retained a primitive shape. He described the regularity in the facets of a crystal as stemming from an arrangement of periodically repeated well defined geometrical units: rhomboids, see Fig.1.1a.
This first physical classification of crystals was improved a few years later, notably by Dalton and Berzelius [27, 13], with the newly discovered proportions in chemical com-

---

[1] *Je me suis borné à un genre de recherches plus à ma portée, en me proposant de déterminer la forme des molécules constituantes des crystaux, et la manière dont elles sont arrangées entre elles dans chaque crystal. C'est cette combinaison que j'appelle Structure* [63].

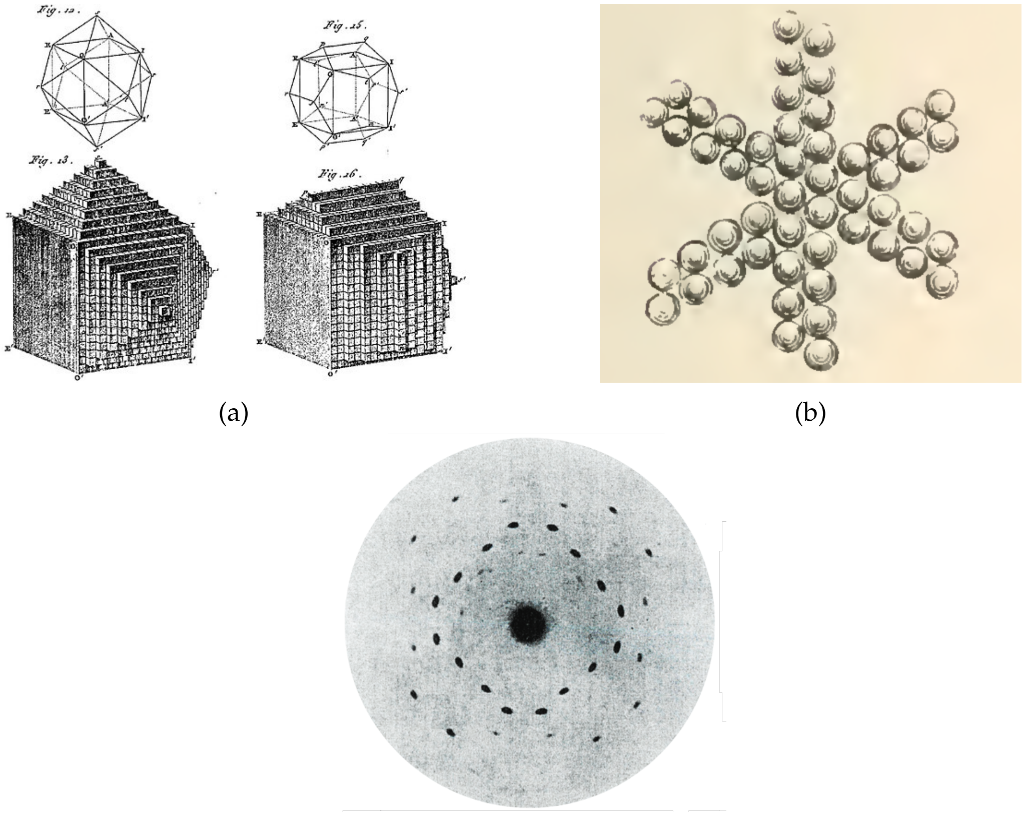

(a) (b)

(c)

Figure 1.1 – (a) Particles composing a cubic cristal, by Haüy [63] (b) Globular particles constituting a snowflake crystal, by Dalton [27] (c) X-ray diffraction pattern by ZnS, Knipping, Friedrich and Laue 1912 [50].

pounds. The internal structure of a crystal was indeed envisioned as a repetition of a geometrical unit but this unit was now seen as a chemical arrangement of different molecules, with the spherical shape, see Fig.1.1b. In the words of Berzelius:
Crystallization exhibits to us the effects of the natural arrangement of the ultimate particles of various compound bodies ; but we are scarcely yet sufficiently acquainted with chemical synthesis and analysis to understand the rationale of this process. The rhomboidal form may arise from the proper position of 4, 6, 8 or 9 globular particles, the cubic form from 8 particles, the triangular form from 3, 6 or 10 particles, the hexadral prism from 7 particles, etc [13].
It was not until 1912 that the observation of X-ray diffraction by a crystal (suflide zinc, ZnS) paved the way to finally seing the spacing of the atoms and thus the internal structure of a crystal, see Fig.1.1c and [50].

1.1.2 Gaz

In parallel to the advances made in the understanding of the crystal structure, scientists also explored the properties of the gas state, sometimes referred as elastic fluid. This crowded field of research is almost a byproduct of a fluid experiment.

Originally, as Gallileo reported in his "Dialogue concerning two new sciences"[51], the fountaineers of Treviso were unable to pump water above a height of thirty-two feet. According to Galileo, water rises because nature abhors vacuum and thus it needs to be filled. However, this limited rise of water is due to a limited repulsion of nature to vacuum. A contrario, Torricelli thought this limitation in the rise of water was due to the balance with the weight of the air column above the water basin. To test his hypothesis, he devised an experiment with a liquid approximately thirteen times denser than water, mercury. The maximal height of the resulting column of mercury was indeed approximately thirteen times smaller than the water column. Besides creating the first barometer, Torricelli exhibited in the process another striking trait : the initially completely filled tube of mercury had its upper sealed end emptied when the tube was placed in a mercury reservoir. Where had the mercury gone and what had replaced it? This experiment reopened the debate amongst scientists as well as philosophers about the question of the existence of the vacuum. From this vacuum experiment, sometimes called rarefied air, derived many scientific results, some amused in the salons see Fig.1.2a, others with greater impact, *e.g.* the known Boyl-Mariotte law, stating that the product of the volume occupied by a gas by the pressure it exerts is a function of the temperature.

As to the internal structure of a gas, even though since the beginning of the XIXth century its visualization is an assembly of particles, it is mid century that huge progresses have been made thanks to Clausius, Maxwell and Boltzmann.

Clausius described a gas as particles in constant motion and their motion is linear until they elastically collide with another particle [23].

Maxwell improved this model by considering that the velocities of the particles cannot be the same, but are part of a distribution of velocities. This use of statistics in physics is one of the greatest improvement of this century, see Fig.1.2b and [85, 84].

Boltzmann, at the end of the XIXth century, refined this velocity distribution by bridging kinetic energy and thermodynamic quantities.

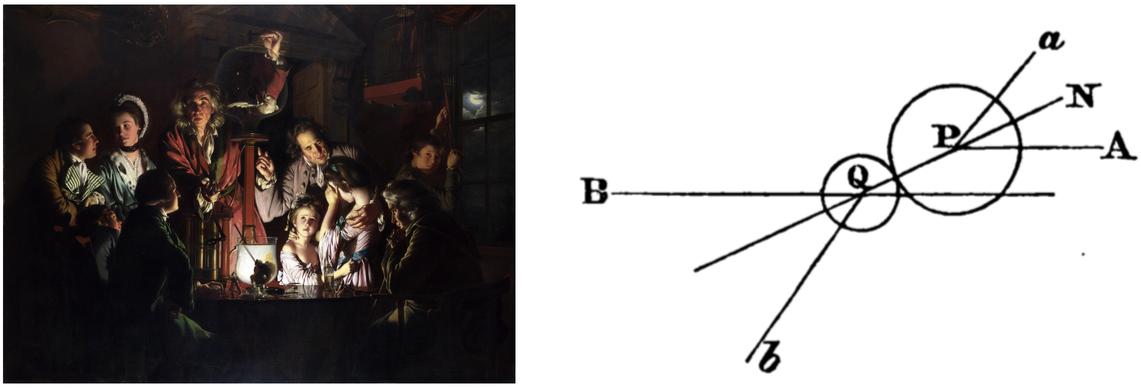

(a) (b)

Figure 1.2 – (a) Painting by Joseph Wright, 1768, entitled Experiment on a bird in the air pump and representing a scientific experiment performed in a salon to entertain the audience. (b) Drawing taken from [85] explaining collisions between two spheres.

1.1.3 Liquid

At the dawn of the XXth century, the internal structure of crystals and gas was rather well modeled by an assembly of spherical particles. This assembly is dense and ordered in a crystal while it is dispersed, random and in constant motion in a gas. Yet, borrowing the words of J.D. Bernal : *Compared with the progress of the molecular theories of gases and the lattice theory of crystalline solids, there has been little success in accounting for the phenomena of the liquid state in terms of the position and the known laws of the interaction of their constituent molecules* [11].

With this in mind, Bernal, a cristallographer by training, tackled the question of the structure of liquids via the prism of spheres' packing. Before him, there were mainly two paths for modeling the structure of liquids. Both were a derivation from the already known features of either a gas [15] or a crystal [68]. It is indeed appealing to do so since the common experience in phase transitions for water is ice to liquid to vapour when increasing gradually the temperature. Hence the internal structure of liquids thought to be a derivative of either crystal or gas.

However, experimental evidences of the molecular structure of liquids were obtained thanks to the discovery of X-rays [107, 116, 117] and neutrons diffraction. From these experimental data, it appeared that the structure of a liquid only possesses a short-range order, no further than two molecules.

Instead of using as a starting point the structure of a gas or a crystal, Bernal started with a broad description of the features he expected the liquid structure to exhibit : *homogeneous, coherent and essentially irregular assemblages of molecules containing no crystalline regions or holes large enough to admit another molecule* [11].

Bernal was then set to create a packing consistent with this description. He named it random close packing because the spheres had to be randomly distributed in space but with the constraint that no sphere could be inserted between two neighbouring ones.

His attempts in creating such arrangement were as numerous as different, from ball and spoke model, "crazy fishing" to thousands of shaken and compressed ball-bearings [46].

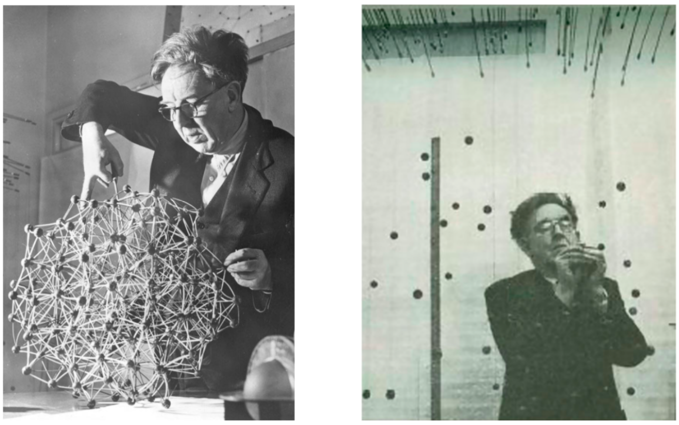

Figure 1.3 – Bernal in his office trying to recreate a sphere packing. Photos taken from [46].

Besides these hand-crafted packings, Bernal pioneered the use of the computational capacities to simulate random packings. With all these experimental devices, he was able to quantitatively compare the radial distribution calculated from the random close packing to the one measured from real liquid and the agreement was rather good, see Fig.1.4. In Bernal's own words, *We cannot consider this an absolute proof, but at any rate it cannot be disproved on the basis of the scattering results alone* [12].

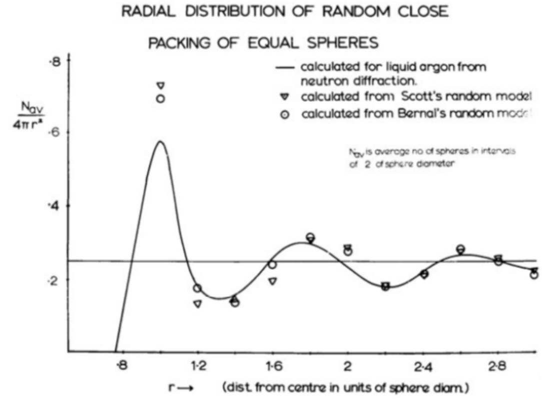

Figure 1.4 – General agreement between experimentally and calculated radial distributions, taken from [47].

1.2 The packing of granular matter

In his quest to decipher the structure of liquids, Bernal discovered that *in all the millennia that have passed in between, the real study of the nature of heaps had had to wait. It seemed too simple, in one respect, and too complicated in another* [12] and paved the way for a new

discipline: the study of granular matter. Surprisingly, the packing of spheres, that had been used to model three different states of matter, falls in neither of them. It is not a fluid since it can sustain a stress, yet it flows given the right amount of energy. It is not a gas since the constituent particles are in rather close contact. It is not a solid since there is no cohesive attraction between the particles.
In an article of La Recherche (1979), P.-G. de Gennes too appreciated that *One of the open questions in statistical mechanics is, in my opinion, the sand heap : its equilibrium slope, its avalanche dynamics, etc. In the coming years we will have to convince researchers that a dune is a topic of interest as beautiful as a galaxy or an atomic nucleus.*

1.2.1 An old problem

in the XVI$^{\text{th}}$ century, Sir Walter Raleigh, tasked his mathematical assistant, Thomas Harriot, to derive a formula to effortlessly count the number of cannonballs stacked on the deck of a war ship. They were stacked in the same manner as in Fig.1.5 and the appropriate formula to count them was easily derived by Thomas Harriot.

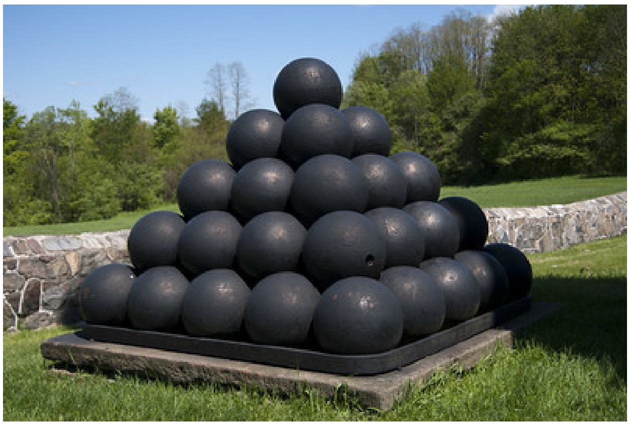

Figure 1.5 – Stack of cannonballs. Photo taken from Wikipedia, credit Nedra.

One way to count the total number of cannonballs is to sum the number of cannonballs on each layer of the stack. For a square based stack, the number of cannonballs on each layer is simply the square number of cannonballs on one side. Also, since each layer has the same side minus one cannonball than the layer just below, the total number of layers in a complete pyramid is the number of cannonballs on the side of the bottom layer. Hence, the total number of cannonballs in a square-based pyramid is :

$$N_{\text{tot}} = \sum_{i=1}^{N} i^2 = \frac{N(N+1)(2N+1)}{6} \tag{1.1}$$

with N being the number of cannonballs on one bottom side. Thus the pyramid in Fig. 1.5 is made of 55 cannonballs.

All in all, this is a relatively trivial problem. Yet, surely thanks to the epistolary correspondance between Thomas Harriot and Johannes Kepler, it prompted one of the most complicated questions. What is the optimal packing of a stack of spheres ?
In the legend, Kepler, one winter of 1611, while he had not received any salary from his emperor Rudolph II for some time, wrote a book as a Christmas present to one friend. In this book, entitled *De nive sexangula*, Kepler relates that, after contemplating the six edges of a snowflake, the hexagon shaped honeycomb and the arrangement of the pomegranates' seeds, he conjectured the arrangement of the cannonballs to be *the tightest possible, so that in no other arrangement could more pellets be stuffed into the same container*.

The so-called Kepler conjecture remained a conjecture for almost four centuries until a proof, given by Hales [61], transformed it into a theorem. [2]

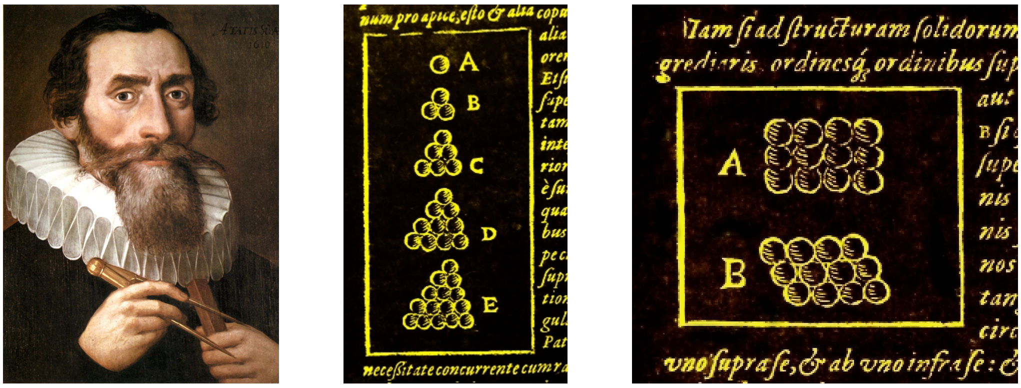
num pro apice, eſto & alia copu
A
B
C
D
E
neceſſitate concurrente cum ra
Iam ſi ad ſtructuram ſolidorum
grediaris ordinesq; ordinibus ſup
A
B
vno ſupra ſe, & ab vno infra ſe: &

Figure 1.6 – Mathematician Johannes Kepler and drawings in his pamphlet on snowflakes [67], now located at the Thomas L. Fisher Library at the University of Toronto.

Even though the Kepler conjecture remained elusive until very recently, Gauss demonstrated that if the arrangement was regular, namely on a lattice, the densest achievable density is :

$$\phi_{\max} = \begin{cases} \dfrac{\pi}{2\sqrt{3}} \simeq 0.91 & \text{if 2D,} \\ \dfrac{\pi}{3\sqrt{2}} \simeq 0.74 & \text{if 3D,} \end{cases} \tag{1.2}$$

This result, although easy to obtain because it comes from simple geometrical arguments, has in some ways changed the picture crystallographers had of crystals from a rhomboids assembly to a sphere packing.
Consider equal sized disks arranged on a regular lattice as in Fig.1.7. The density is defined as the ratio of the occupied area by the particles over the available area. In Fig.1.7, the available area is the blue shaded area of the parallelogram formed by the centers of the four disks. The occupied area is the portion of the disks that are in the previously described parallelogram. It is clear that the first step towards maximum density is to have the disks in contacts. Hence, the available area is given by the formula of a parallelogram

---

[2] As a sidetracking comment, the optimal packing of spheres in dimensions other than 1, 2, 3, 8 or 24 is still an unsolved problem.

of side two disk's radii, and the occupied area is given by the sum of the disks' areas inside the available area.

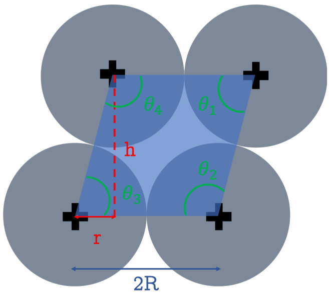

Figure 1.7 – Drawing of four disks on a lattice and the definition of R, h, r and θ_i.

This mathematically reads:

$$\begin{cases} A_{\text{available}} = 2Rh \\ A_{\text{occupied}} = \frac{1}{2}\sum_{i=1}^{4}\theta_i R^2 = \frac{1}{2}\left(\sum_{i=1}^{4}\theta_i\right)R^2 \end{cases} \tag{1.3}$$

It is a classical result that the sum of the angles of a quadrilateral is always 2π. Hence the occupied area is a constant equal to the area of one disk. Thus the maximum density problem corresponds to finding the smallest available area. This requirement is equivalent to find the smallest distance between centers, or with the notations of Fig.1.7, the smallest h possible or the largest r because of Pythagore's relation $h^2 = (2R)^2 - r^2$. It is clear that r is maximum when $r = R$, ie $h = \sqrt{(3)}R$. Finally, the maximum density is given by:

$$\phi_{\max}^{2D} = \frac{\pi R^2}{2\sqrt{3}R^2} = \frac{\pi}{2\sqrt{3}} \tag{1.4}$$

The demonstration in volume relies on similar geometrical arguments. However, creating a regular dense packing in a volume requires the piling of dense packing in a plane. And we have just proved there is only one such dense packing. Hence, even though there are an infinite number of volumic dense packings [5], they all result from the arrangement of the same dense planes. On Fig.1.8, two iconic volumic dense packings used in crystallography.

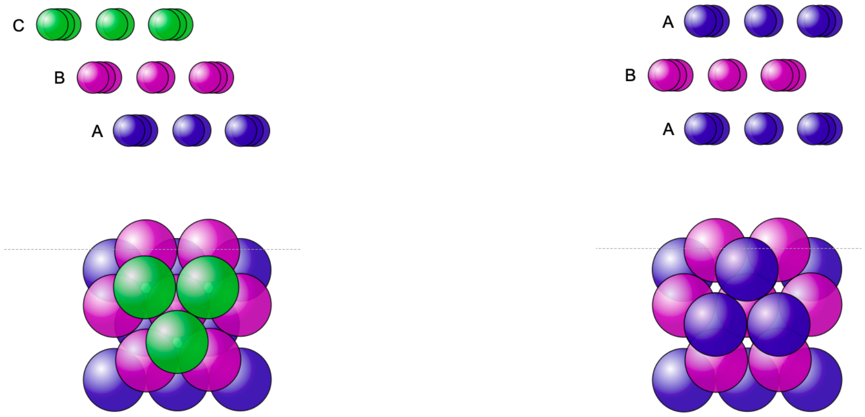

(a)

(b)

Figure 1.8 – (a) Face centered cubic (fcc). (b) Hexagonal close packed (hcp). Photos taken from Wikipedia, credit to Christophe Dang Ngoc Chan.

1.2.2 A range of packing densities

During the experiments led by Bernal, Scott and Kilgour [10, 113, 114], a wide range of packing densities has been discovered, from 0.52 for the loosest arrangement up to 0.64 for the densest. Actually, the experiment that defined the value of the random close packing was performed by Scott and Kilgour in 1969 [114]. They poured thousands of ball bearings into a large container, then vertically vibrated the system to achieve an assumed maximum density. In order to eliminate finite-size effects, they extrapolated the bulk packing density value. Besides obtaining the desired value of the random close packing, they showed that a sphere packing had many different metastable states. Going from one of this metastable state to another requires a certain amount of energy and the denser the packing the less probable it is to attain the next metastable state as Fig.1.9b demonstates. An example would be a sand heap on a flat surface. Indeed, its stable configuration would be a single layer of grains but reaching this state would require, for instance, kicking the flat surface for a certain amount of times.

It turned out that the density of a sphere packing has a wide range of values and is extremely dependent on the protocol used to create the packing. This even remains true for a simulated sphere packing, that is algorithm-dependent [82].

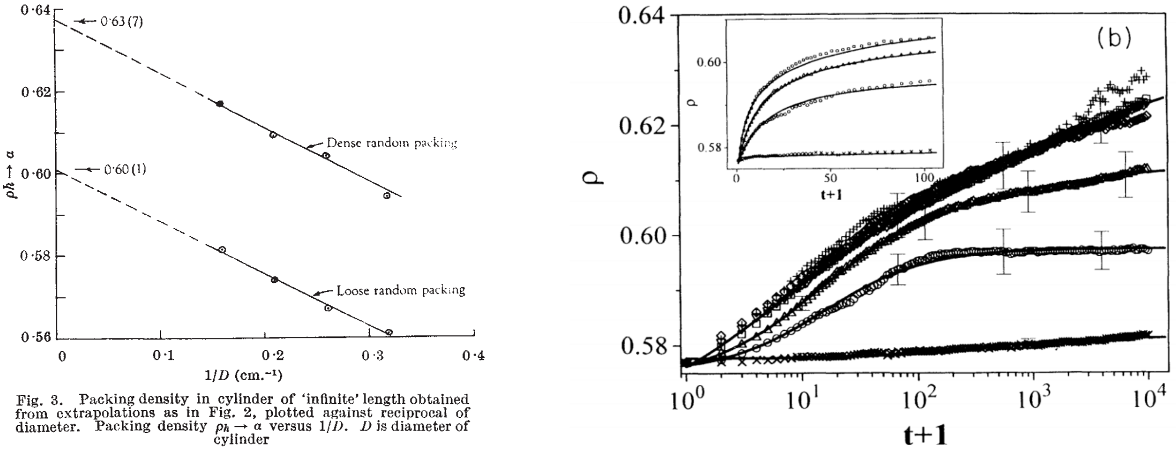

(a) (b)

Figure 1.9 – (a) Evolution of the packing density with the container size [113]. (b) Time evolution of the density of a shaken packing, from [70].

1.2.3 Jamming instead of packing

An interesting feature in the packing of granular matter is the transition from scattered and mobile particles to a coherent solid-like assembly while increasing the density of particles. This phenomenon has been named *jamming* and it has become trendy enough to even reach the biological realm. Some would use the concept of jamming to describe an assembly of cells forming a tissue while others would be reluctant about this usage[3].

While random close packing was introduced to describe liquid structure, scientists, notably in the field of granular matter, did not agree with this definition, stating that it was ill-defined [121]. A better suited definition would rather be built on mechanical properties, stability. The quantities of interest are still the mean packing fraction but also the contact/force networks. It must be noted that contact and force networks are distincts because not all contacts will transmit forces. There have been attempts to model it as a percolation phenomenon [97]. Experimental observation of these networks is rather challenging. An astute use of photoelasticity has allowed to directly see these chains forces in 2D but, for 3D assemblies the only observations are obtained from simulations. From the figure 1.10a it is clear that not all contacts transmit forces. Figure 1.10b shows that there is a large distribution in the number of contacts between grains. From this distribution, the most probable value appears to be 6 while there is no occurence of 12 contacts which corresponds to the densest crystalline packing. The few particles with less than 4 contacts are called rattlers.

A packing is said jammed when the particles and their nearest neighbours are in contact in such a way that mechanical stability is conferred to the packing. Then, a difficulty arises when the particles are frictional. Indeed, friction is an entire sector of research in itself. One way to determine if a packing is statically stable is to count on one hand the

---

[3] At least Pascal Damman

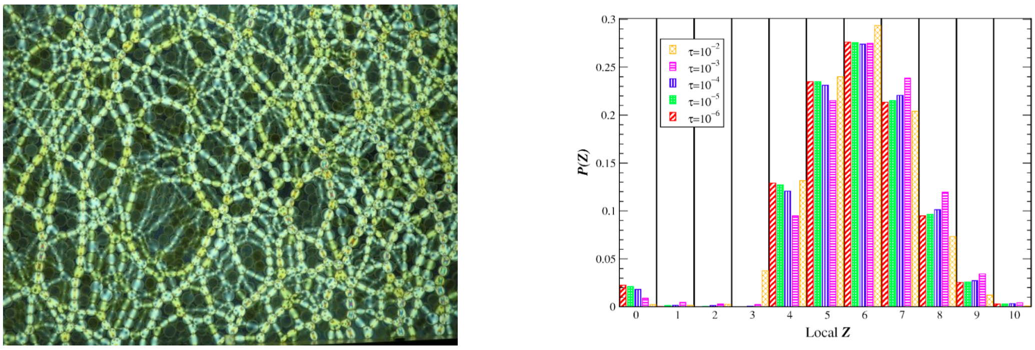

(a) (b)

Figure 1.10 – (a) Force chains, taken from Bob Behringer's home page [7]. (b) Distribution of contact number, taken from [33].

number of equations from force and torque balances per grain and on the other hand the unknowns derived from the contact forces. If there is a perfect match between these two numbers, the packing is said isostatic. Otherwise, it is either hypo or hyper static [91, 120, 128]. If the grains are frictionless, the torque balance equations are satisfied and the constraints of force balance yield d equations per grain in d dimensions. Denoting the mean contact number by z, there are thus $z/2$ unknowns per grain since each contact force is shared by two grains. Since there are only few rattlers, a packing is mechanically stable if all grains are mechanically stable, this leads to:

$$z \leqslant 2d \tag{1.5}$$

For frictional grains, this method of counting mechanical equations and contact unknowns can be extended by including the torque balance conditions and by defining the fraction of contacts that are fully mobilized. This yields an upper and a lower bound:

$$(d+1) \leqslant z \leqslant 2d \tag{1.6}$$

In spite of intensive research, hard-particle jamming is still not fully understood [8] and yet the actual Graal quest is to unify all the "glassy systems" under the same framework. A unified jamming diagram has been proposed by Liu and Nagel with temperature, packing fraction and shear stress as parameters [77].

It is indeed tempting to draw parallels between an athermal assembly of spheres and a thermally equilibrated one. An analogy may even be displayed with density playing qualitatively the same role as inverse temperature. Indeed, while slowly compressing a monodisperse hard-sphere fluid leads to a crystal phase – corresponding to the closest packing –, rapid compression rates yield random jammed packings – with densities depending on the compression rate.

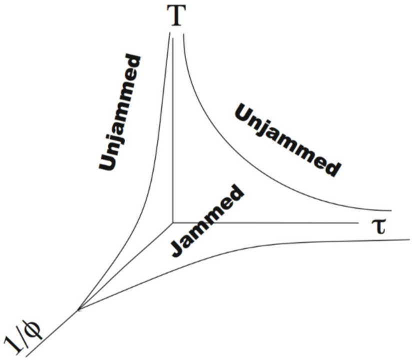
T
Unjammed
Unjammed
Jammed
τ
1/φ

Figure 1.11 – Unified jamming diagramm, with T the temperature on an axis, τ the shear stress on a another axis and the inverse of Φ, the packing fraction, on the last axis. Therefore, increasing one parameter while keeping the other two fixed leads to an unjamming transition. Taken from [77].

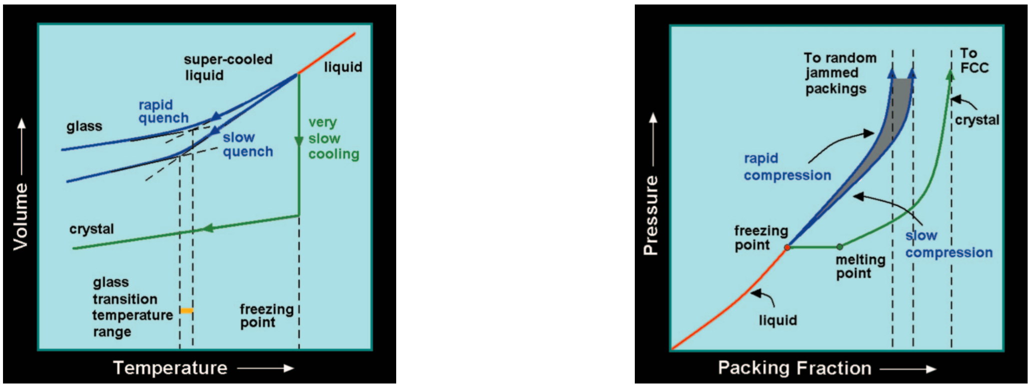
super-cooled liquid
liquid
rapid quench
glass
slow quench
very slow cooling
Volume
crystal
glass transition temperature range
freezing point
Temperature
To random jammed packings
To FCC
crystal
rapid compression
Pressure
freezing point
slow compression
melting point
liquid
Packing Fraction

(a)

(b)

Figure 1.12 – (a) Archetypal Volume/Temperature diagram showing the transition point between solid (glass & crystal) and liquid. (b) Pressure/Packing fraction diagram also exhibiting the transition between solid and liquid but for an assembly of spheres. In both cases, the solid state is made from two different branches. Taken from [121].

1.2.4 The conjecture of Edwards

The development of statistical mechanics was driven by the need of characterizing fluctuating properties. One could then think that since granular matter is not subjected to thermal fluctuation, the local properties would not fluctuate much but one would be strongly mistaken. Indeed, thermal fluctuations actually smooth inhomogeneities out. Statistical mechanics would thus be a great tool to modelize granular matter. However, because friction is highly non linear, the forces are not solely dependent on the positions of the grains. New statistical ensembles should be imagined and Edwards and Oakeshott pioneered this framework. Because particles interactions do not conserve energy, Edwards and Oakeshott [39] propose to use volume instead of energy in the derivation of the entropy. The underlying assumption being that in a given volume all configurations of grains positions and orientations are equally probable.

1.3 The packing of non spherical particles

So far, we have only considered spherical shapes for its convenient simplifications. Actually, using spherical shape for every other shape is source of scientific humor as in the article Fig.1.13.

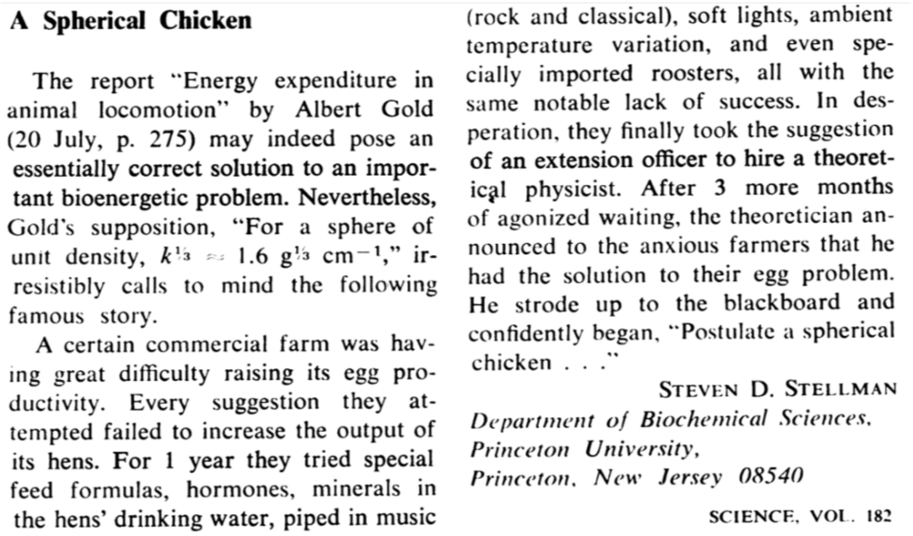

A Spherical Chicken

The report "Energy expenditure in animal locomotion" by Albert Gold (20 July, p. 275) may indeed pose an essentially correct solution to an important bioenergetic problem. Nevertheless, Gold's supposition, "For a sphere of unit density, $k^{1/3} \approx 1.6$ g$^{1/3}$ cm^{-1}," irresistibly calls to mind the following famous story.

A certain commercial farm was having great difficulty raising its egg productivity. Every suggestion they attempted failed to increase the output of its hens. For 1 year they tried special feed formulas, hormones, minerals in the hens' drinking water, piped in music (rock and classical), soft lights, ambient temperature variation, and even specially imported roosters, all with the same notable lack of success. In desperation, they finally took the suggestion of an extension officer to hire a theoretical physicist. After 3 more months of agonized waiting, the theoretician announced to the anxious farmers that he had the solution to their egg problem. He strode up to the blackboard and confidently began, "Postulate a spherical chicken . . ."

STEVEN D. STELLMAN
Department of Biochemical Sciences,
Princeton University,
Princeton, New Jersey 08540

SCIENCE, VOL. 182

Figure 1.13 – An article in Science 1973 [115].

Even though it may be seen as a drastic approximation, it is the most commonly made. Especially in granular matter where it is near impossible to take into account the infinite variety of grains' shapes. Nonetheless, for example in the case of granular flow, it has been shown that adjusting the rolling and sliding friction coefficients is pertinent to describe grains with peculiar shapes [44].

In some instances, however, the spherical symmetry is actually a singularity !

1.3.1 Direct observation of deviation

It is visually obvious that a stack of non spherical particles differs from a stack of spherical particles. If the particle shape only mildly deviates from the sphere, the heaps remains alike. That is heaps of spheroid particles, say rice or gravels, spontaneously adopt the typical pyramidal shape, as in the left side of Fig.1.14. A contrario, the stack becomes completely different if the particles largely deviate from the spherical shape. For instance, non-convex particles like staples or stars produce stable columnar stacks, totally impossible to observe in assemblies of spheres. Even more, these heaps formed from non-convex particles remain stable for very low packing fractions, see for instance the bottome right structure in Fig.1.14.

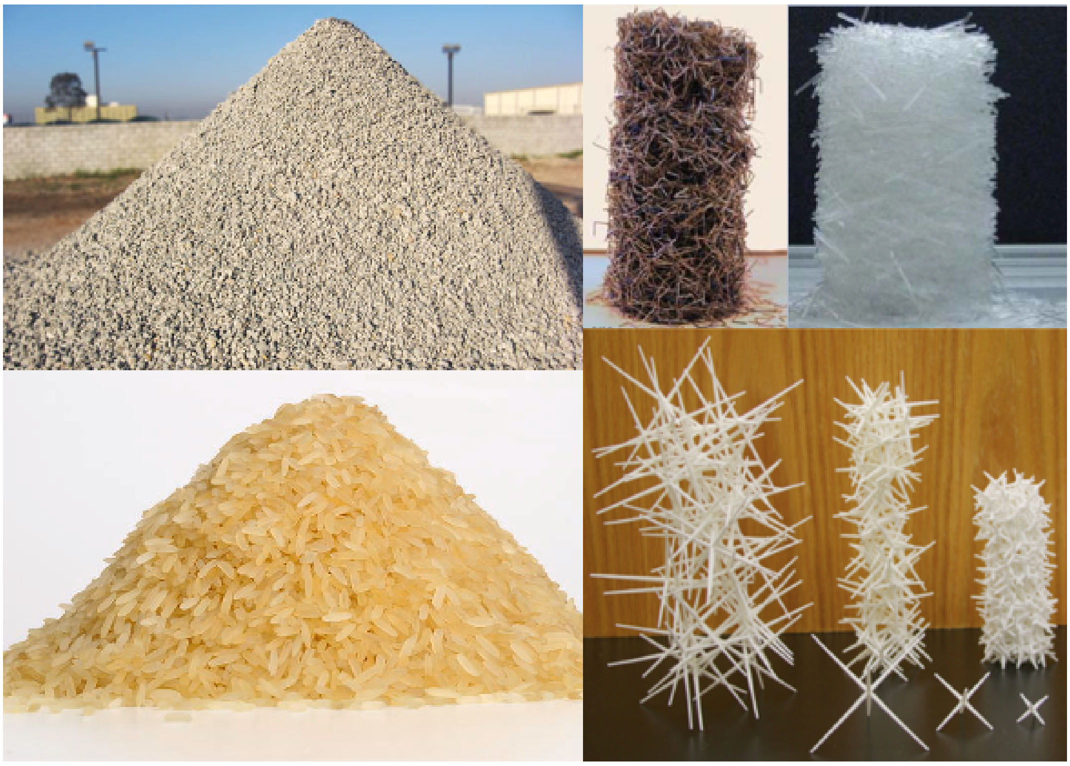

Figure 1.14 – On the left column, heaps of rather spherical particles – photos taken from the internet. On the right, column-like stacks of staples, rods and stars, photos taken from [121, 122, 49].

1.3.2 The sphere, the exception rather than the rule

To understand these different shapes of stacks, one may appreciate nonsphericity by introducing additional rotational degrees of freedom hence modifying the previous derivations about the mean number contact needed for mechanical stability.

In an article from 2004 [34], Donev *et al.* studied objects with shape gradually deviating from the sphere. It turns out that the sphere is actually the exception rather than the rule. Perfect spheres allow to achieve assemblies with low random-close-packing fractions and the lowest mean number of contacts.

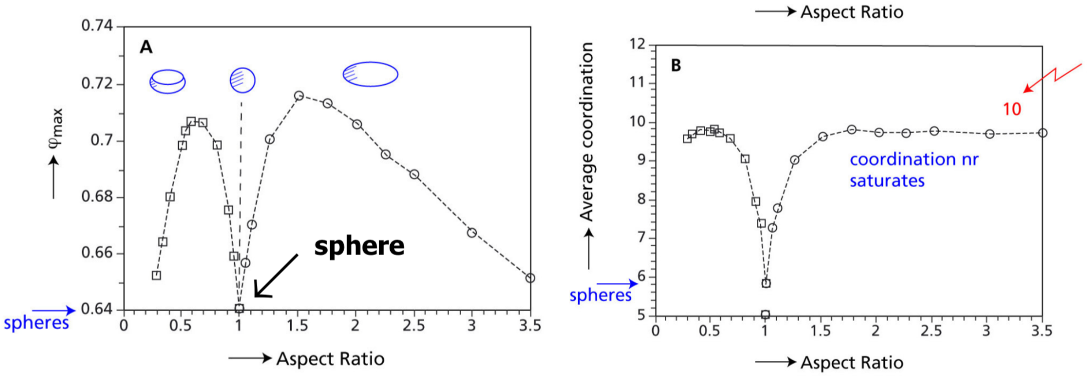

(a) (b)

Figure 1.15 – (a)Volume fraction and (b) coordination number against aspect ratio, both exhibiting a particuliar behaviour for the sphere shape. Adapted from [34].

The difference is even more drastic when the objects are rod-like or non-convex since mechanically stable structures are achieved with very low packing fraction. In 1996, Philipse *et al.* [104] proposed a model to account for the relation between packing fraction and aspect ratio for rod-like particles. The main assumption is that, unlike sphere packings, where contact correlations extend up to several neighbouring particles, the contacts between rods are uncorrelated. Thus, a relation may be drawn between the contact probability and the particle density. This relation, on one hand, involves the mean contact number and, on the other hand, an excluded volume. Expressing this excluded volume as a function of the particle aspect ratio and for very slender rods, this relation simply yields that the packing fraction is inversely proportional to the aspect ratio and the mean contact number:

$$\phi \simeq z\left(\frac{L}{D}\right)^{-1} \tag{1.7}$$

where ϕ is the packing fraction, z the mean contact number, L the length of the rod and D its thickness.

Their model is in good agreement with their experimental data as well as the ones in the litterature with a mean contact number of $z \simeq 5$.

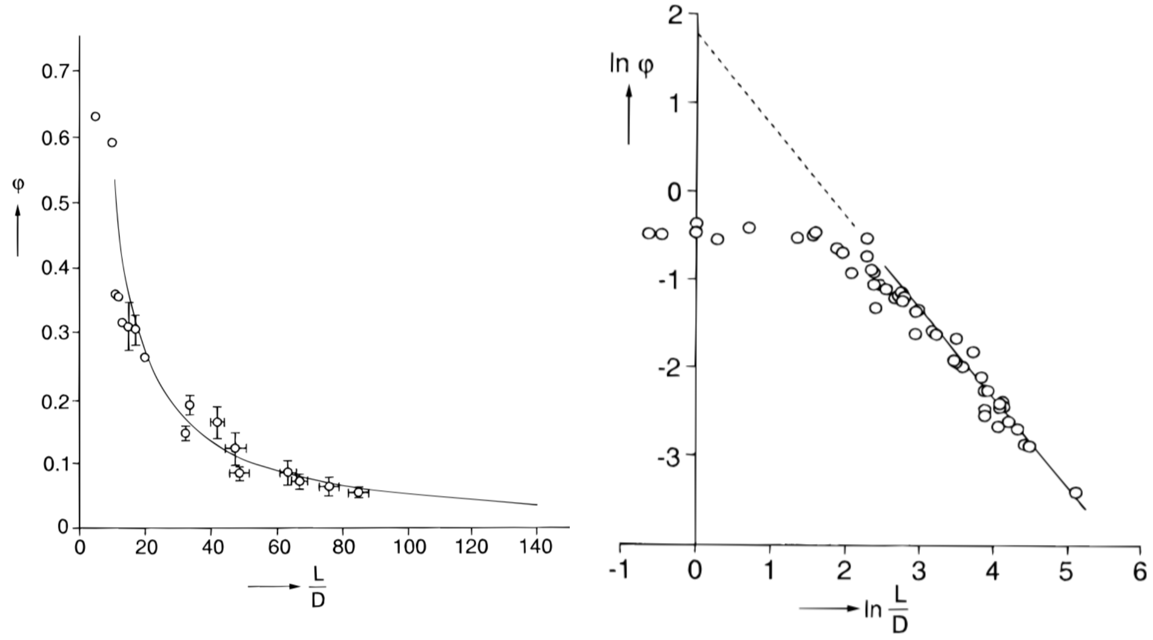

Figure 1.16 – Packing fraction against aspect ratio for rod-like particles. On the left, the data are plotted with a linear scale while on the right the same data are represented in a log-log graph. The solid curve corresponds to the theoretical expression given by Eq.1.7, in good agreement for great aspect ratios. Taken from [103].

1.4 The packing of granular-chains

Granular chains are made of connected spherical beads. They depart from the sphere shape thanks to these bonds while keeping flexibility. To some extent, they can be considered as the macroscopic equivalent of polymer chains.

1.4.1 Table-top observation

The unexpected behaviour of the granular-chain packing appears quite naturally when we put them on a table. If one puts short chains, *e.g.*, three monomers long as in the top left part of Fig.1.18, on a table, they will make a heap looking like classical sand heaps. However, if the chains used are gradually longer, the pile's shape changes. With long chains, say thirty monomers long as in the bottom right part of Fig.1.18, the stack no longer looks like a heap with a tilted surface but becomes a stable column alike stacks of non-convex particles.

In comparison with the spherical shape, we may sayt that the dynamics of compaction remains still very slow but the densest achievable state is lighter. Furthermore, the density depends on the chain length in an undefined manner. We may be able to propose a toy model to account for the packing fraction of granular chains by connecting two limit cases. Indeed, if a chain is short enough, we may visualize it as a rod while longer chains are akin to ropes. This difference in behaviour is related to the ability of the chain to make

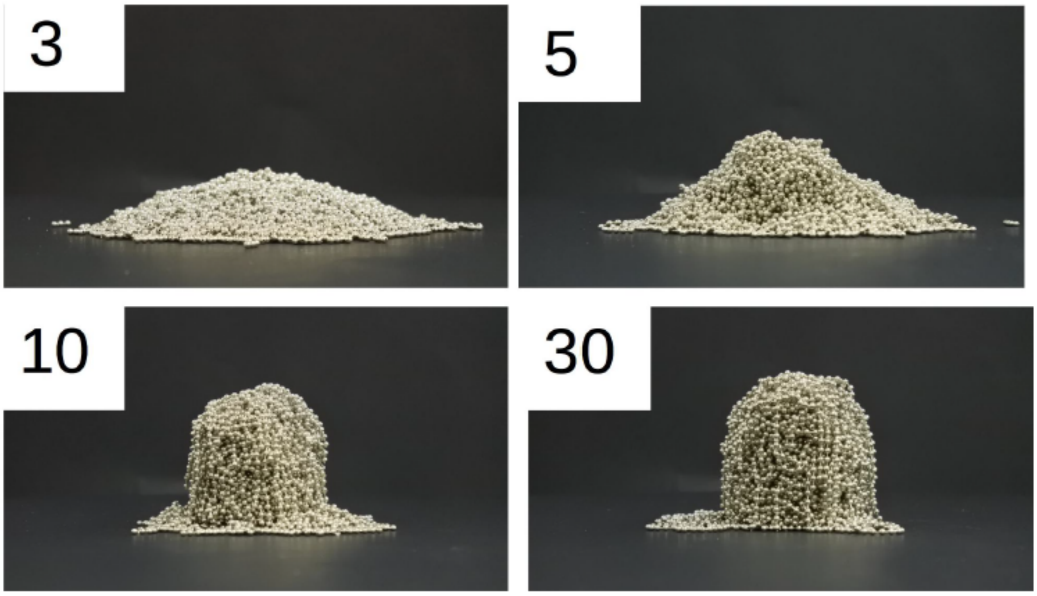

Figure 1.17 – Pile of granular-chains, with lengths of 3, 5, 10 and 30 monomers as indicated in the upper left corner of each photo. Taken from our work [37].

a loop. This minimum loop size, typically consisting of around ten beads in our case, may be seen as a persistence length.

On one hand, if we were to consider a chain as a rod whose aspect ratio is directly given by the number of beads N, we would have, assuming that we may use the relation developped by Philipse in [103], $\phi_{\text{spheroid}} \simeq Z/N$.

On the other hand, if we were to pack a chain as a rope, loops would appear. These loops may be seen as hollow spheroids that can be partially filled by other hollow spheroids. Hence, the maximal packing fraction of granular chains would be a fraction of the maximum packing fraction of spheroids. Numerically, since $\phi^{\text{max}}_{\text{spheroid}} \simeq 0.7$ and $\phi^{\text{max}}_{\text{chain}} \simeq 0.4$, this fraction would be approximately 0.6, which is not unrealistic.

Our experimental data, along the ones available in the litterature, are in a qualitative agreement with the proposed toy model.

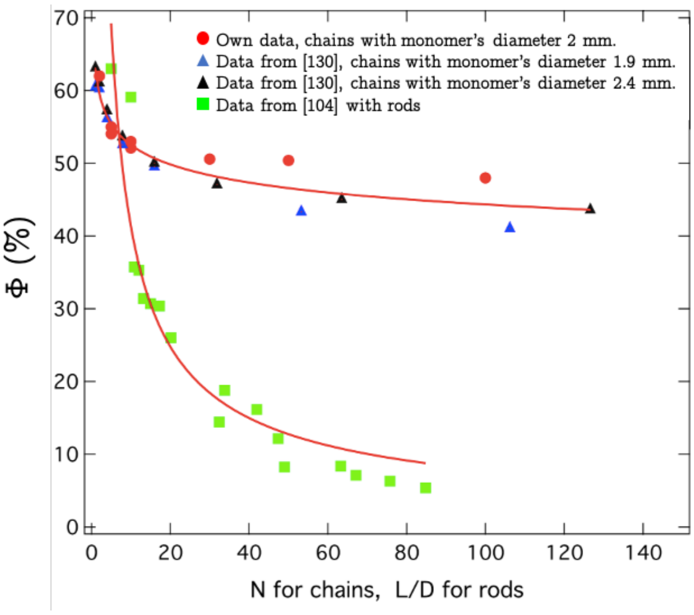

Figure 1.18 – Densest achievable state for stacks of chains with different lengths N and stacks of rods with different aspect ratios length over diameter L/D. The solid red curves correspond to the function $f : x \to 1/x$. Data reproduced from [130] and [104].

1.4.2 Direct method of investigation

We were not the first to be intrigued by the striking mechanical behaviour of granular-chain stacks. In 2012, Brown *et al.* [17], studied the stress response of granular-chain packings under uniaxial compression, see Fig.1.19a. From the stress-strain curves recorded for different chain lengths, *cf.* Fig.1.19b, they observed a transition at a precise chain's length. They attributed this transition to the persistence of the chain through the existence of a minimal loop size, see Fig.1.19c. They considered that the strain stiffening should be related to entanglements. Chains smaller than the minimum loop size cannot entangle and exhibit poor mechanical stability while long chains are strongly entangled. We note however that the observed dependance of the stress-strain relationships with the chain length above the threshold cannot be explained from this picture.

To confirm their hypothesis, they tried to directly observe the internal structure of the packing to prove the occurence of entanglements. They performed extensive X-ray tomography and recorded the precise positions of each bead and link in three dimensions, see Fig.1.20. Then, via computational operations and ”string-knotting analysis”, they analysed the entanglements and concluded that the longer the chain, the more entanglements there are.

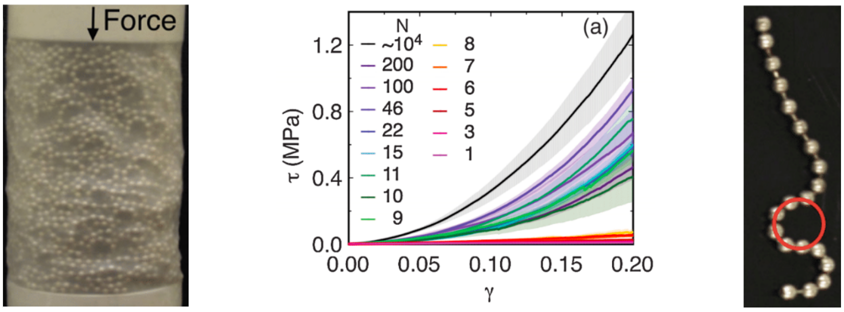

(a) (b) (c)

Figure 1.19 – (a) Uniaxial compression test. (b) Stress strain curves. (c) Definition of a loop. Taken from [17].

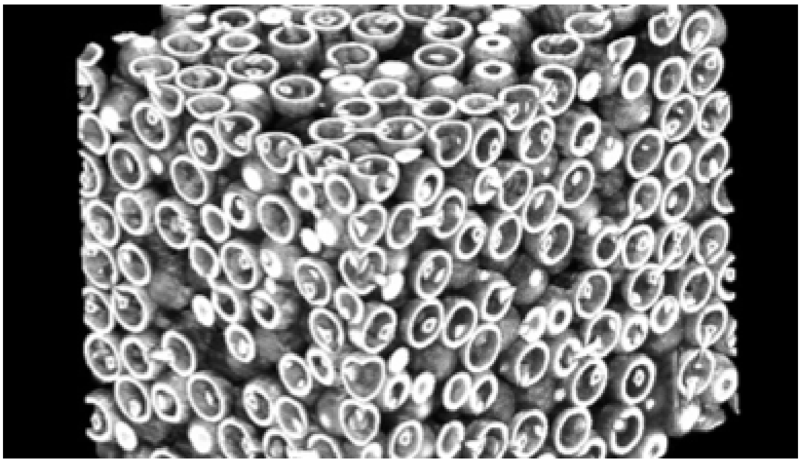

Figure 1.20 – Image reconstructed from the X-ray tomography of a chain packing. Taken from [75].

Chapter 2

Indirect method of investigation

To study the internal structure of a stack of granular chains, we have not used the previously described direct method of investigation based on X-ray tomography. In fact, this experiment requires very high intensity X-ray sources produced by synchrotrons and the results of Brown *et al.* [17] are not conclusive, in regards to the impressive experimental efforts required.

For these reasons, we have decided to investigate the internal structure with an indirect method. A collection of equal-length chains is placed in a flexible container and indented with a steel probe while measuring the force response.

2.1 Experimental setup

The experimental setup is based on the ProbeTack, an apparatus used in the food industry to quantify the texture of aliments. It consists in a steel probe that can be vertically driven, a stress gauge and a flexible container filled with granular chains, see Fig. 2.1.

2.1.1 Parameters of the experiments

Granular chains

For us, a granular chain is a set of metallic beads that are linearly connected via metallic rods along which they can rotate and translate. Because the particles we use are not point-like, the accessible volume of a bead connected to another is a cone given by an angle of approximately forty-five degrees. To some extent, the granular-chains behave as a conventional polymer chains with excluded volume interactions.

The used granular chains are industrially manufactured with only have minor deviations in their properties. Hence, we will discard any fluctuations and consider only averaged values (Tab. 2.1 and Fig. 2.2). We have investigated the behaviour of chains of various lengths, ranging from single beads to chains of fifty monomers long.

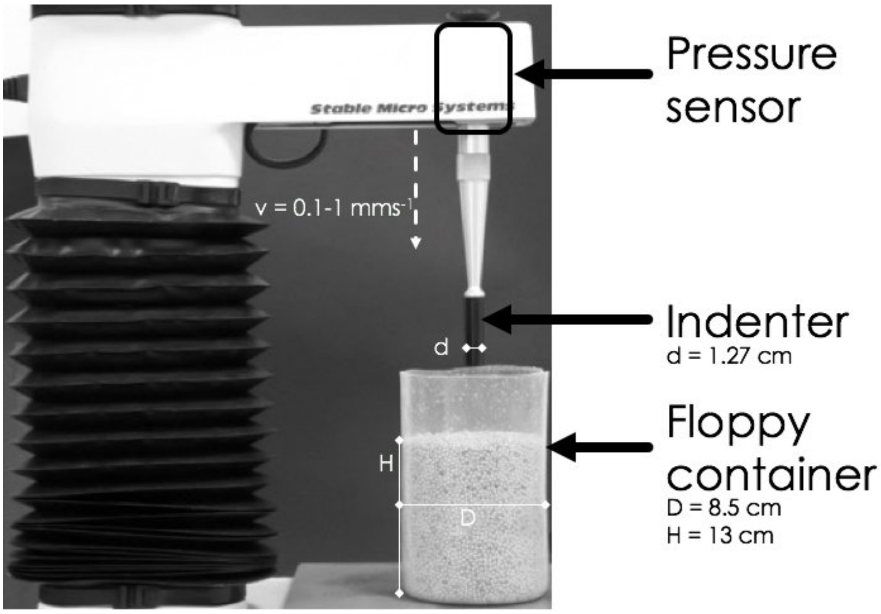

Figure 2.1 – Vertical indentation setup we used to measure the mechanical response of a stack of chains.

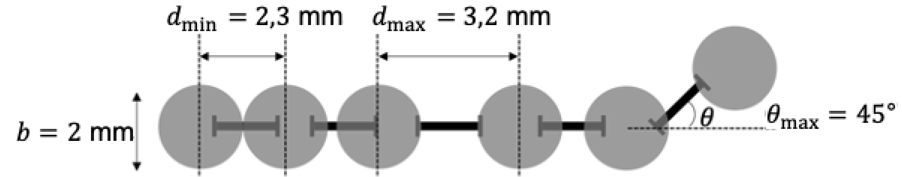
d_{min} = 2,3 mm
d_{max} = 3,2 mm
b = 2 mm
θ
θ_{max} = 45°

Figure 2.2 – Modelisation of the granular chain.

Container

For matter in grains, the container can play a major role, essentially through the solid friction at the walls. The clogging during the discharge of granular matter from a silo is a canonical example of this role. In fact, the contacts between solid grains produce chain forces at the origin of arches that lean against the walls. These arches can ultimately completely block the flow of grains. Because this effect is not intrinsic to the internal structure, but related to the existence of walls, we have tried to lessen it as much as possible, even though it cannot be fully eliminated. To reduce the formation of arches pushing on the walls, we used containers made of soft crosslinked Sylgard. Due to the elastic deformation, the walls are not able to sustain friction forces. We finally chose containers with a diameter of almost nine centimeters. Figure 2.3 shows the measured resistive force of granular-chain stacks under vertical indentation for different types of containers. We can see that if the container is wide enough, the stress curves exhibit similar behaviours whether its walls are hard or soft. In contrast, for small containers, the rigidity of the wall materials becomes very important. Measurements with soft-wall containers are alike the

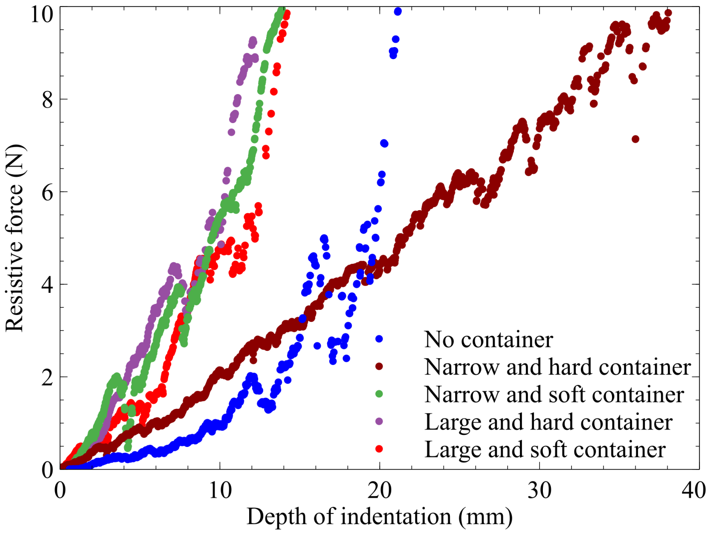

Figure 2.3 – Measured resisitive force against depth of indentation for different types of container.

previous ones, while a strong deviation is encountered for small hard-wall containers. Finally, we also perform the indentation experiments with no container at all, *i.e.* the chains are directly placed under the indenter in a pile-like stack. The measured resistive force is similar to the one obtained with soft walls. To avoid any problem of reproducibility mainly related to avalanches on the sides of the pile during indentation, we decided to use a soft container.

Indentation probe

To measure the stress during indentation, we chose a cylindrical probe of 40 mm height and 12, 7 mm of diameter. To make that choice we considered two conditions. First, the indenter should have a diameter bigger than the size of a chain's bead, or else the probe would penetrate the stack without inducing a resistive force related to the internal structure of the chains. Second, the indenter should be much smaller than the diameter of the container, otherwise friction at the wall would play an important role in the stress response.

Speed of indentation

The last parameter in our experiments is the speed of indentation. While the dynamics of the chain relaxation is not considered here, there are practical reasons for considering low indentation speeds. The stress gauge has a constant acquisition rate, hence the indentation speed must remain sufficiently low so that there are enough data points. On Fig. 2.4, it is clear that, for a given experimental configuration, increasing the indentation velocity leads to less data points. The indentation velocity should also be low enough to allow for the reorganisation of chains, in order to stay in a quasi-static regime. Considering the free falling of a single bead on its own diameter, we get the limiting velocity $\sim$ 100 mm/s. Considering these two limitations, we finally restrain the indentation speed at 0.1 mm/s.

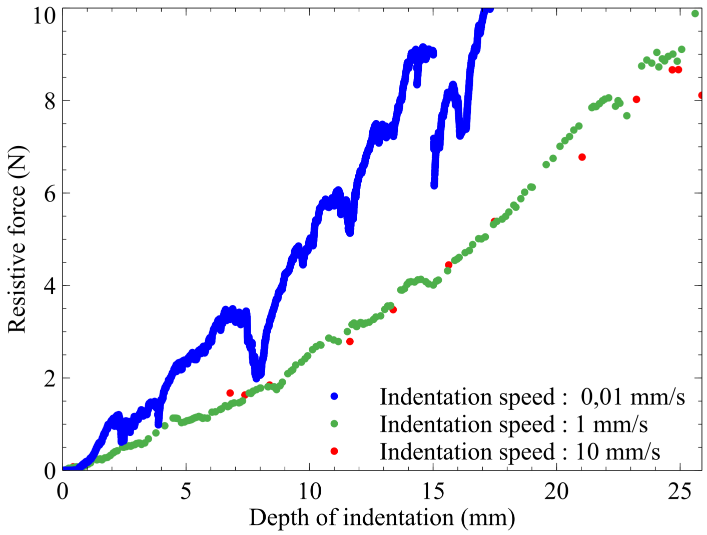

Figure 2.4 – Measured resisitive force against depth of indentation for different indentation speeds.

Recapitulative tables

Indenter	
Material	Delrin
d_{prob}	12,7 mm
v_{prob}	0.1 mm/s

Beads	
Material	Glass
ρ_{beads}	2.8 g/cm^3
Φ_{beads}	2 mm

Container	
Material	PDMS
D_{cont}	8.5 cm
H_{cont}	13 cm

Chains	
Material	Steel
ρ_{mono}	4.5 g/cm^3
b	2.4 mm
$\mathcal{N}$	$\in [2,3,5,10,30,50]$
d_{min}	2,3 mm
d_{max}	3,2 mm
θ_{max}	45°

Table 2.1 – Experimental parameters.

2.2 Preliminary observations

2.2.1 Experiments with glass beads

Before studying the resistive force of granular-chain assemblies, we performed indentation measurements for a container filled with glass spheres of identical diameter than the chain beads. This gives a starting point to test the role played by the connectivity.

In the literature, there have been several attempts to describe the behaviour of granular matter under vertical indentation, *e.g.* [52]. The main result is that, at first-order, there is a linear relationship between resistive force and indentation depth. This linearity arises from the hydrostatic pressure through the friction force required to move a grain over a depth z. In this case, the indentation force is given by the friction force $F_f = \mu\rho g z$, where μ, ρ are the friction coefficient and density, respectively, and g stands for gravity. As shown in Fig. 2.5b, the first-order approximation rapidly fails. In fact, the complex contact network between grains tend to scatter the stress in all directions along the force chains. The evolution of indentation force with depth should thus be given by the continuous reorganisation of this network during the probe motion. These force chains can be easily visualized with photo-elastic grains, Fig. 2.5a. Figure 2.5b represents three experiments of vertical indentation in a container filled with glass beads. The experimental data almost overlaps and can be described by the power law $F \propto z^{3/2}$.

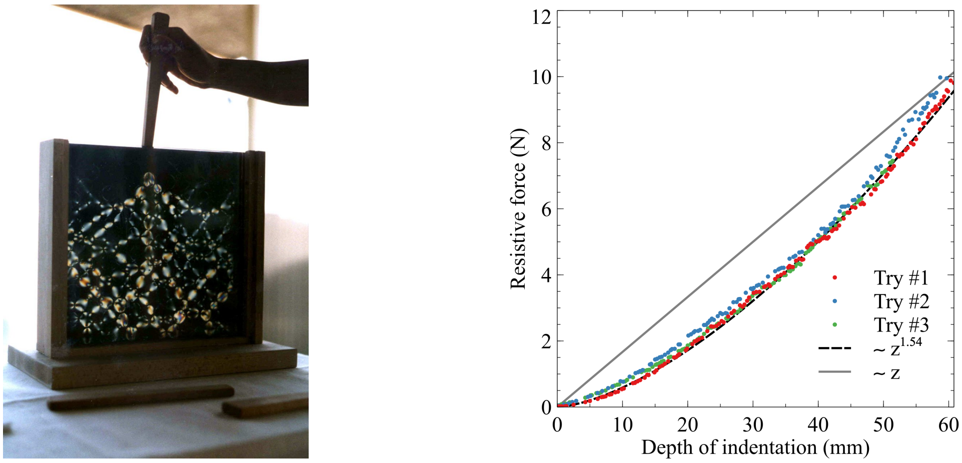

(a) (b)

Figure 2.5 – (a) Force chains are visible thanks to the photoelasticity of the grain material [3]. (b) Measured resisitive force against depth of indentation for unconnected beads.

2.2.2 Experiments with granular chains

Fig. 2.7 shows that the resistive forces measured for unconnected beads and a stack of 10 monomers chains are drastically different. While the resistive force for simple beads follows the $z^{3/2}$ power law, the indentation force is amplified for the stack of chains. For the first ten millimeters of indentation, both curves superimposed however. At the bead/monomer length-scale, both stacks are indeed loose, the indenter just compacting the first few layers. But while the probe further indents the system, *cf.* Fig. 2.6a, it cannot penetrate at all into the stack of granular chains, see Fig. 2.6b. Even with forces of several hundreds of Newton, the probe barely progresses of a few centimeters in the structure. It is clear that because of the connectivity between the monomers there is a global response from the granular-chain stack that qualitatively and quantitatively differs from the one for simple beads.

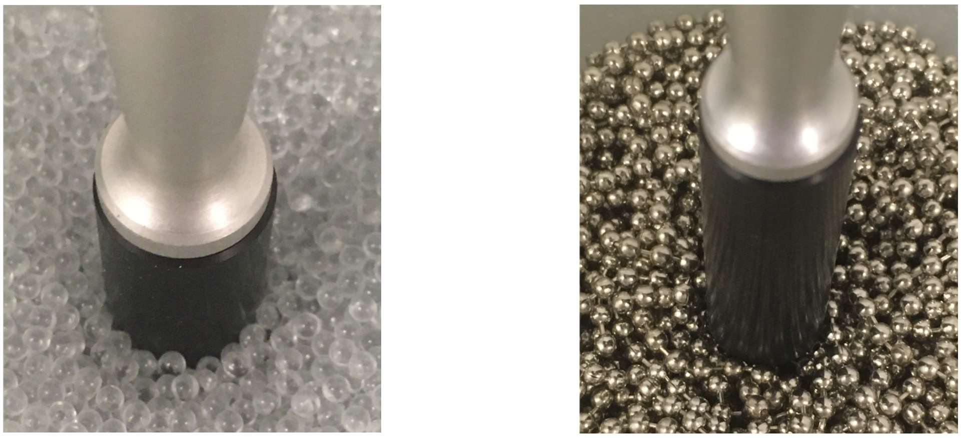
(a) (b)

Figure 2.6 – Zoom on the indenter when in (a) beads and (b) chains.

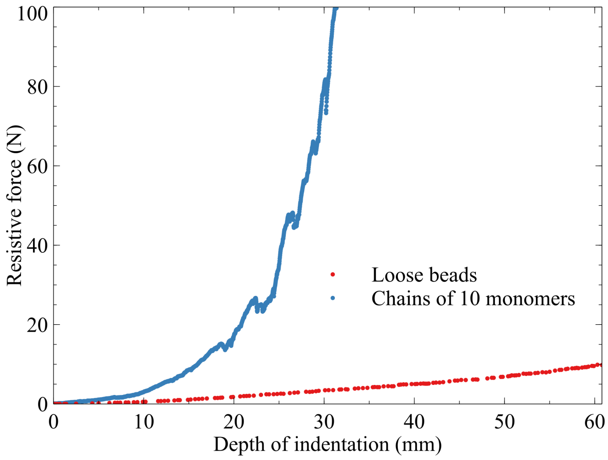

Figure 2.7 – Experimental curves of resisitive force against depth of indentation for simple beads and chains of 10 monomers.

Interestingly, as shown in Fig. 2.8a, the length of the granular chain strongly influences the resistive force. The longer the chain is, the steeper is its response to indentation.

Another noticeable feature of these experimental curves is the avalanche-like events happening all along the indentation. As one can see in Fig. 2.8b, details of the force-depth curves slightly differ from one experiment to another. All these avalanche events show similar trends: a rapid increase in the resistive force followed by an abrupt drop. These events may be viewed as local plastic rearrangements of the internal structure adopting a solid like behaviour until some failure happens.

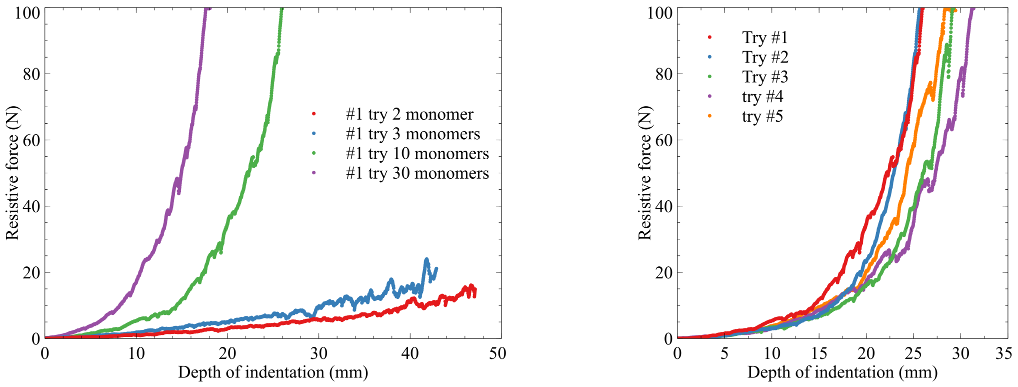

(a) (b)

Figure 2.8 – Measured resisitive force against depth of indentation for granular chains for (a) different lengths and (b) chains of 10 monomers.

In the following, we will address these two properties. We will start by studying the avalanche events. Secondly, we will rationalize the evolution of the resistive force against indentation depth and length of chain by inferring the internal structure of the stack thanks to tools from polymer physics.

Chapter 3

Avalanche dynamics

Since our granular chains assembly can sustain a certain mechanical stress, we may view it not as a collection of chains but as a solid. Moreover, we may consider it as an amorphous solid. Even though being a rather very broad category, amorphous solids share similar features in their response to mechanical stress. There is indeed consensus that plasticity in amorphous solids is related to local reorganizations [45]. One key point still debated is the universality class of the plastic yielding transition. This plastic yielding happens via pontaneous strain localization, intermittent dynamics and power-law distributed avalanches.
The first works on avalanches are rather related to earthquakes and are due to Gutenberg and Richter in the 50's [58, 56, 57]. They proposed a scaling law to link the apparition frequency of an earthquake n_s to its size s:

$$n_s \propto s^{-1-b} \tag{3.1}$$

It turns out that the parameter b is universal and was determined via the seismic surveys of Harvard. Its value is estimated to be $b \simeq 0.5$.

Plasticity of amorphous solids is beyond the scope of our research, thus we will restrict ourselves to present evidences that our experimental data could be related to plastic yielding.

3.1 Definition of an event

As for earthquakes, the properties of avalanches are usually studied from a plot of frequency versus the size of the local plastic events. In the experimental curve of the vertical indentation of a stack of granular chains, sudden drops in the resistive force are observed. These rapid variations may be explained by the failure of a given blocking point created by a given configuration of the force-chain network or by entanglements in the case of granular chains. After the failure, the released energy is redistributed over the rest of the structure, reaching another stable configuration. The structure is then able again to sustain an increase in force until another failure happens. We define an event by its amplitude s as defined in Fig. 3.1.

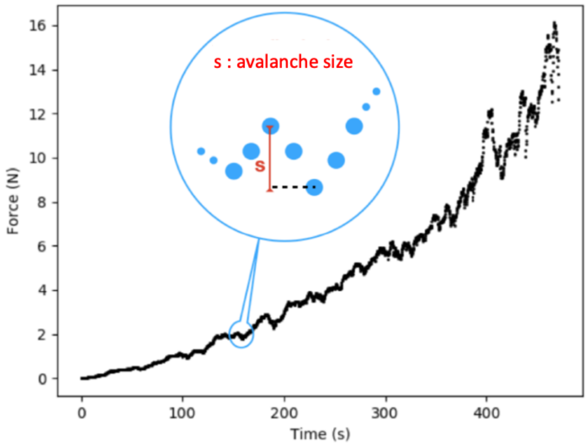

Figure 3.1 – Typical indentation curve and definition of an avalanche size. Blue dots in the inset are figurative for data points.

3.2 Cumulative distribution of event sizes

Instead of looking directly to the distribution of event amplitudes, we focus on the cumulative distribution. The idea is to not consider event by event but the ensemble of events with amplitude bigger than a certain limit. Considering the Richter-Guntenberg relation, this distribution becomes:

$$C_s = \int_0^s x^{-1-b} dx = \frac{1}{b} s^{-b} \tag{3.2}$$

Fig. 3.2 shows average cumulative distributions for stacks of granular chains of different length (2-10 monomers). The classical behavior of plastic events is observed: a decrease of the frequency following a power law coupled to a cut-off for large size events. A transition seems to emerge from the results. For short chains with $N \leq 3$, the cumulative distribution follows the power law $C_s \propto s^{-1/2}$, which means $n_s \propto s^{-3/2}$. This result strongly suggests that short chains behave as single beads, recovering the "classical" scaling for avalanches described in Eq.3.1.

For longer chains with $N \geq 5$, the cumulative distribution follows a different power law $C_s \propto s^{-3/2}$, which yields $n_s \propto s^{-5/2}$ for the bare distribution.

We may consider this change in the power-law exponent as an effect of the change in the internal structure of the granular-chain stacks. Indeed, the number of large events decreases more rapidly for the long chains than for the short chains because the network of blocking point becomes more dense.

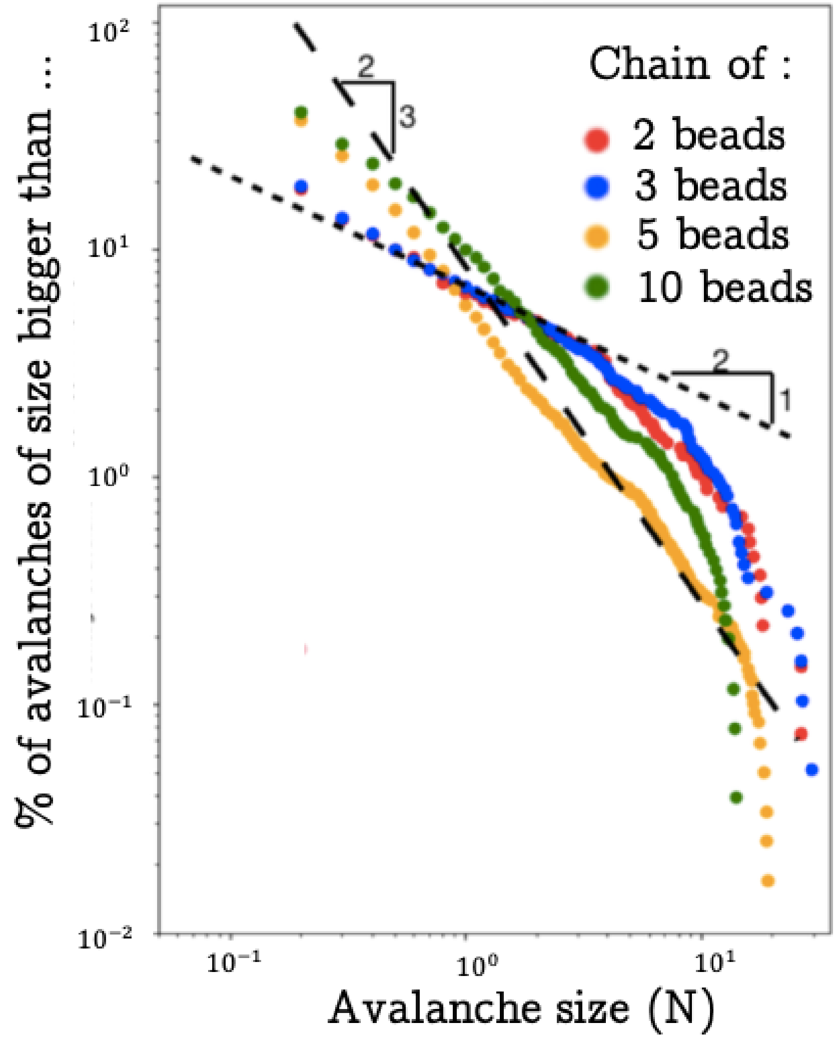

Figure 3.2 – Mean cumulative size of avalanches. The dashed and the finely dashed lines are guide to the eye for power laws $x^{-3/2}$ and $x^{-1/2}$ respectively.

Chapter 4

Mean behaviour

To rationalize the experimentally observed indentation curves with models from statistical physics of polymer, we look at their mean behaviour instead of focusing on the details of the random avalanche events (see previous Chapter). As shown previously, the key difference between molecular and granular matters relies on the balance between thermal and gravitational forces. At the molecular scale, thermal forces dominate and the particles undergo Brownian motion, while at the macroscopic scale gravity prevents any thermal motion. In the latter case, the studied systems usually called athermal do not explore their phase space anymore, hindering the use of statistical physics to describe their macroscopic behaviour through ensemble averaging over all accessible microscopic configurations.

The main question thus becomes: *How could we perform average estimation of variables for athermal systems ?* According to the conjecture proposed by S.A. Edwards [39], statistical tools may be used for athermal problems as long as we perform enough experimentations to test the different configurations of our ensemble of particles. The measurement by time average is replaced by averaging over a large number of experiments.

To this end, we have performed a large number of indentation runs for each chain length. In order to get rid of the possible metastable initial state, the system has been put as close as possible to its random close packing by shaking the assembly before each run.

4.1 Role of indentation depth

The average curves obtained for the different chain lengths are given in Fig. 4.1a (for comparison, Fig. 2.8a shows single experimental realizations). Whatever the length of the chain, the resistive force again grows rapidly with the indentation depth but this increase is now firmly rooted in statistical meaning.

We have already stated that the power-law resistive behaviour of single beads is reminiscent of the hydrostatic pressure $\sim z$ and force chains network $\sim z^{3/2}$. However, as soon as two monomers are linked together, the dependance between the indentation force

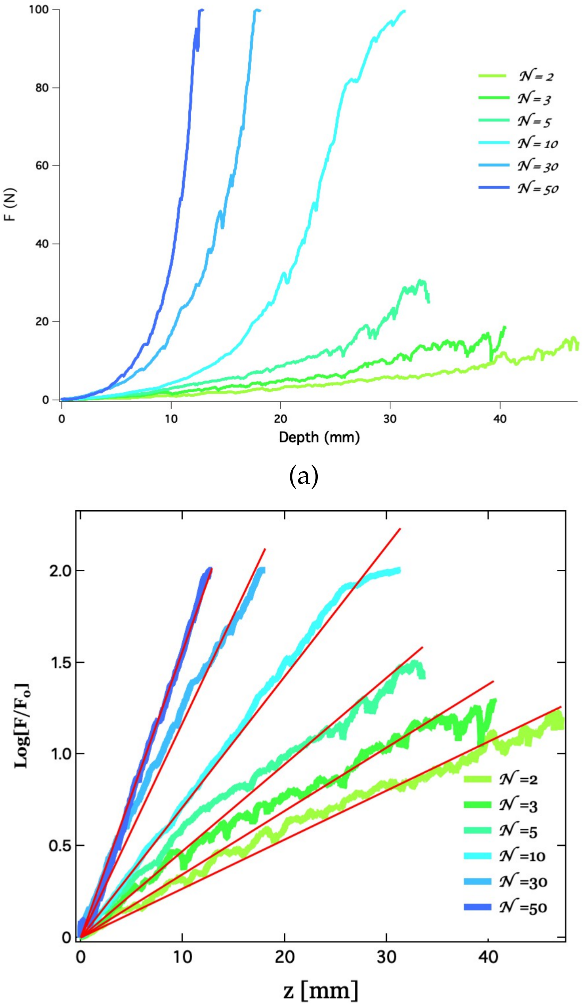

(a)

(b)

Figure 4.1 – (a) Mean resistive force F and (b) logarithm of the ratio F/F_0 against indentation depth z for different chain lenghts $\mathcal{N}$. The red curves are linear guides for the eye.

and depth is no longer described through a power law. Actually, in Fig. 4.1b, we have plotted the logarithm of the resistive force normalized by the quantity F_0. This quantity is arbitrary and chosen to be $F_0 = 1N$.

Figure 4.1b shows that the resistive force increases exponentially with the indentation depth.

4.2 Role of chain size

The resistive force grows exponentially with the indentation depth but from Fig. 4.1b it is clear that the length of the chain has a drastic impact on the structure's resistance. In order to quantify this effect, we use the slopes corresponding to the linear best fits of the $\log(F/F_0)$vs z curves of Fig. 4.1b. These slopes, mathematically equal to $d\log(F)/dz$, are plotted against the chain length on Fig. 4.2. Their evolution is best described by the power law $\sim \mathcal{N}^{0.46}$ with $\mathcal{N}$ the number of beads in the chain. From our indentation experiments on granular chains, two things stand out. There is a non-linear strain stiffening with the depth of indentation and the longer the chains the stiffer the response of the assembly. All experimental curves can be described by the law:

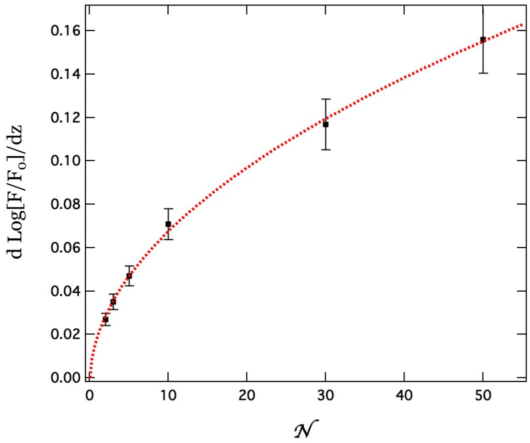

Figure 4.2 – Rate of the exponential increase of the resitive force $d\log(F)/dz$ againts the chain's length $\mathcal{N}$. The red dashed curve corresponds to the best power law fit $\sim \mathcal{N}^{0.46}$.

$$F(z) = F_0 \exp\left[\mathcal{N}^{0.46}\left(\frac{z}{a}\right)\right] \tag{4.1}$$

where a is the size of a single monomer.

The dependance of the resistive force on the chain's length strongly indicates that pieces of information about the internal structure of the granular chains assembly could be obtained from these experiments.

4.3 Self-amplification of friction

Before tackling the issue of the internal structure, we explore the origin of the very strong resistive force exhibited by granular chains assemblies. The answer should be related to friction. To convince oneself of this assertion, a simple experimental thought is needed. If one imagines the same assembly but with no friction between the chains, the indenter would meet no resistance. To borrow a polymer-like analogy of this frictionless assembly, imagine to push your finger inside a bowl of very oily spaghettis. However, knowing that the resistance comes from friction is not a final answer because friction is still to this day a subject of intense research. From Leonard de Vinci in early XVI$^{\text{th}}$ century to Tabor in 1972 [105], only one major step understanding friction is the mechanism explaining the surface independent character of friction from details about the microstructure of the object. Nonetheless, friction is something humanity has been confronted to since the dawn of time. It can be harnessed to make fire, it is detrimental when it hinders the motion of our trains and it can also be amusing as with the Chinese Finger Trap. In some of these applications, it has also been observed that the resistive force exhibits an exponential growth.

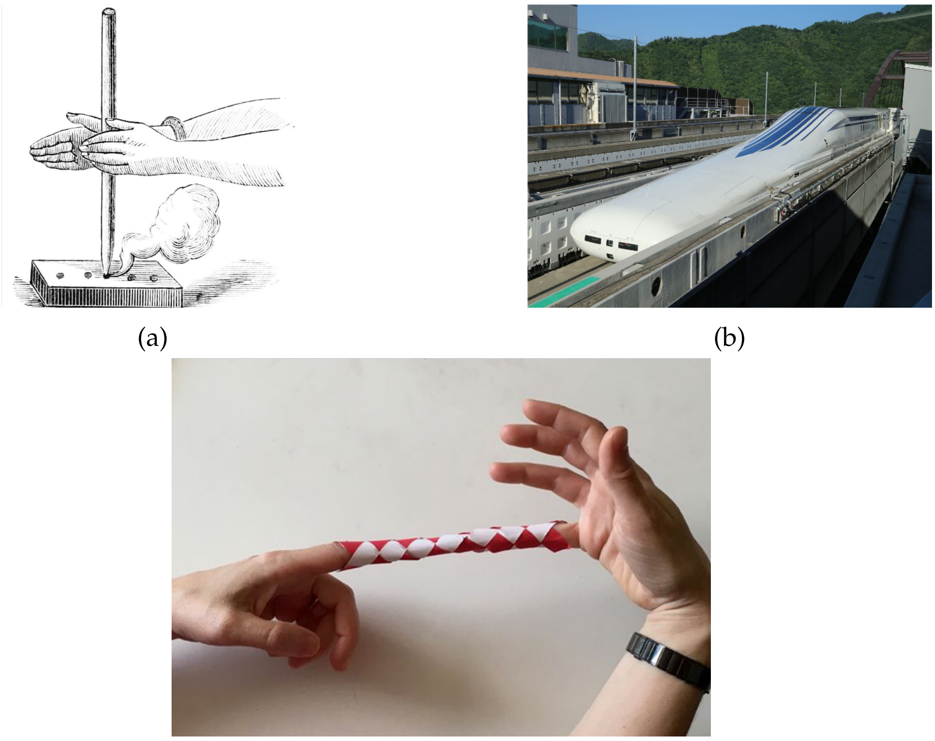

(a) (b)

(c)

Figure 4.3 – (a) Making fire with friction. (b) Avoiding friction with magnetic levitation. (c) The Chinese finger trap, images taken from Wikipedia.

We will briefly review two instances where this exponential behaviour is observed, the capstan and in interleaved books.

4.3.1 The capstan

The capstan is well-known to sailors and climbers. It helps the first ones hauling cables and the second ones as a life-safety system. The principle is rather straightforward and directly related to friction. By wrapping the rope around the capstan, a substantial part of the load is relieved through the fixing point of the capstan thanks to the friction with the rope. The rest of the load is supported by the person at the other end of the rope. The relation between load force and the hold force is given by:

$$T_{\text{hold}} = T_{\text{load}}\, e^{-\mu\phi} \tag{4.2}$$

The used notations are given in Fig. 4.4.

The person exerting the holding force sees a load force reduced by a factor that exponentially grows with the number of turns of the rope around the capstan ϕ, expressed in

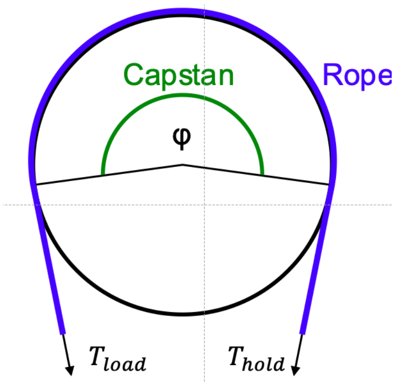

Figure 4.4 – Schematic of a capstan.

radian times the friction coefficient μ. A stunning numerical application of this formula is that one single kilogram is enough to support the weight of the Eiffel tower if one has wrapped a rope sixty-five times around a capstan, with $\mu = 0.25$.

4.3.2 Interleaved phonebooks

Recently, Alarcon *et al.* [1] have shown that the "magic" behind the resistive force exhibited by interleaved phonebooks can be rationalized by considering the friction between book pages and the complex geometry of the assembly.

The action of interleaving the pages actually causes a deformation from the rest position, represented by the angle θ_n in Fig. 4.5. This tilt of the leaves is enough to induce a normal compressive force when a force trying to pull apart the interleaved books is exerted. Since according to Amontons-Coulomb law, this normal compressive force generates a friction proportional to the pulling force, we get the self-amplification of friction !

The traction force needed to pull apart the interleaved phonebooks, given by Eq.4.3, grows exponentially with the so-called Hercules number α. This parameter takes into account the square number of pages M, the page thickness ϵ, the friction coefficient μ and the pages interleaving distance d. The total friction force reads:

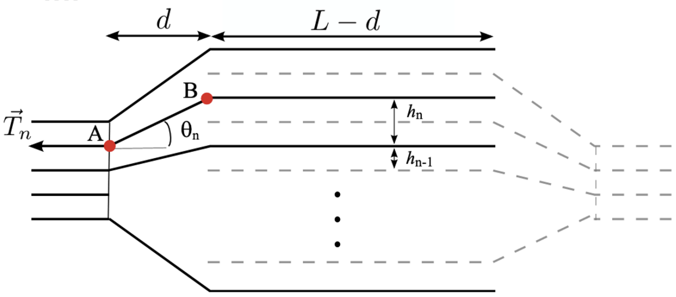

Figure 4.5 – Schematic of two interleaved sets of sheets, taken from [1].

$$T = 2MT^{\star}\sqrt{\frac{\pi}{4\alpha}}\, e^{\alpha}\, \mathrm{erf}(\sqrt{\alpha}) \tag{4.3}$$

where $\alpha = 2\mu\epsilon M^2/d$.

There are many videos on the internet of people trying to pull apart two interleaved phonebooks [29]. Spoiler alert: they never pull apart, the failure comes from the binding.

4.3.3 Typical equation governing self-amplification

Whatever the experimental system, wrapped rope or interleaved pages, the underlying physical principle remains the same. Self-amplification of friction happens when a feedback loop is created. To better visualize it, let us consider the well known toy Chinese finger trap[1]. This game consists in inserting a finger at each end of the tube, as in Fig. 4.3c. If the tube was rigid, friction between the tube and the finger would very slightly prevents the finger from exiting the tube. It would yet be easy to pull the finger out of this trap. For flexible tubes, the pulling force coupled to friction will stretch the tube to give it a hyperboloid shape at the origin of the feedback loop. Indeed, the slope of the hyperboloid generates a compressive force proportional to the pulling force in a similar way as interleaved books. The more one pulls, the more trapped one is. The general relations that translate this feedback loop are given by:

$$\frac{dF}{dz} = \mu \frac{F}{b} \tag{4.4}$$

$$F = F_0\, e^{\mu z/b} \tag{4.5}$$

where b a typical length scale in the problem.

4.4 Interlocking points

The exponential growth of the indentation force observed for granular chains in Fig. 4.1 strongly suggests that a self-amplification mechanism is at work ! The strain stiffening of granular-chain assemblies should thus be described with an equivalent of Eq. 4.5. To use this relation, we have to determine the typical length-scale in our problem. The self-amplification stems from blocking points between chains, i.e. entanglements. Thus the typical length scale would simply be the mean distance between two blocking points. Hence, we would expect in our case:

$$\frac{dF}{dz} = \mu M_z F \tag{4.6}$$

where M_z is the density per unit length of blocking points, $M_z = N_{\text{block}}/z$.

To estimate the density in blocking points, we use the Edwards conjecture by considering that the average internal structure of a stack of granular chains is equivalent to the structure of thermally equilibrated chains. In other words, the internal structure of a stack of granular chains would be analogous to a polymer melt !

---

[1] which is Chinese only by its name

Polymer – Theoretical background

A polymer is a succession of units, called monomers, bonded by covalent interactions. Even though a polymer may be branched or ring-shaped, we will restrict ourselves to linear chains. A polymer can either be in a solution or in a melt (Fig. 4.6). Depending on the polymer concentration/volume fraction, we may distinct two cases, dilute and semi-dilute. The transition occurs at a threshold in volume fraction, $\phi^* \sim N^{1-3\nu}$, where ν determines the type of solution, and the size of the chain through its average end-to-end radius $R \sim N^\nu b$. For very low concentrations, such that $\phi \ll \phi^*$, the chains are isolated and do not interact with each other. For a concentration greater than the threshold, *i.e.* $\phi > \phi^*$, the chains start to interpenetrate.

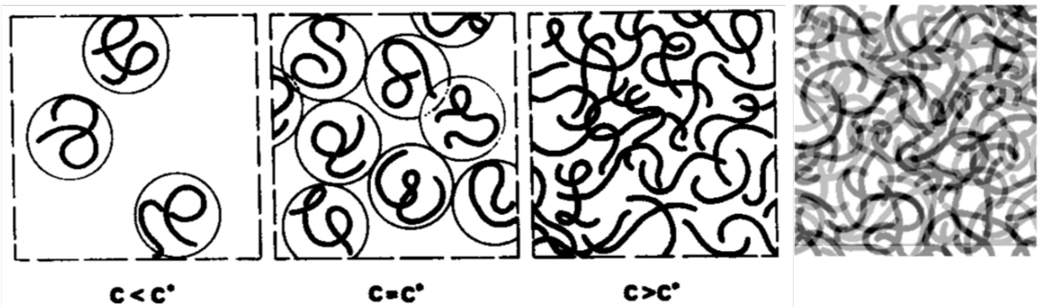

Figure 4.6 – Schematic view of the internal structure of polymer solution and melt, taken from [53].

Before defining how two chains interact, we introduce the interaction between two non-bonded monomers. This interaction is attractive at long distance and repulsive at short distance. From the Mayer function and the virial expansion, a volume that quantifies the antagonism between repulsion and attraction can be defined. This excluded volume depends on the temperature and is given by:

$$v(T) = \int \left(1 - \exp\left[V(r)/k_\mathrm{B}T\right]\right) \mathrm{d}r^3 \tag{4.7}$$

where r is the distance between two monomers and $V(r)$ the interaction potential between them.

With respect to temperature, this excluded volume can be negative or positive. When it is negative, the polymer tends to collapse on itself and this situation is related to a bad solvant. When it is positive the polymer tends to swell: the solvant is called good solvant. Finally, there exists a critical temperature, called Θ, for which this excluded volume is null. For a solution at this temperature, the chain is considered ideal. We will restrict our discussion to good solvants.

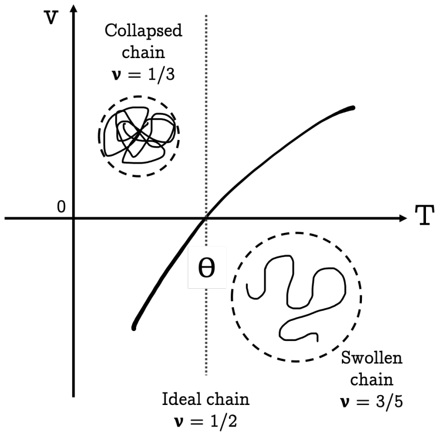

Figure 4.7 – Evolution of the excluded volume with temperature: v is negative for $T \leq \theta$ and positive for $T \geq \theta$. Taken from [16].

Since polymer chains are microscopic objects, they are subject to thermal fluctuations, each monomer fluctuating randomly. Within this frame, one may visualized the succession of monomers of a polymer as a random walk of N steps (the step size being the length of a monomer). In ideal condition, the chains are adequately described with pure random walks, while self-avoiding random walks are expected when excluded volume interactions are present. This distinction has to be made because while it is easy to derive the mean end-to-end distance of a random walk, there is no exact solution for a self-avoiding random walk. The average end-to-end distance of a random walk of N steps, of step size b, is given by:

$$R \sim b\sqrt{N} \tag{4.8}$$

For the good-solvant case, Flory has derived a clever way to obtain this quantity by minimizing the free energy of a chain [48]. Indeed, on one hand, the excluded-volume interaction tends to swell the polymer and on the other hand the monomers are bonded creating an entropic cost to swell the chain. Balancing these two terms leads to:

$$R \sim bN^{\nu} \tag{4.9}$$

where ν is the Flory exponent.

To derive ν for a self-avoiding chain, Flory first estimated the entropic term related to the chain elasticity. The free energy F_e is derived from the partition function Z via the Boltzmann constant k_B: $F_e = -k_B T \ln Z$. If the chain is ideal, we have $Z \sim \exp\Big(-R^2/Nb^2\Big)$ which finally yields:

$$F_e \simeq k_b T \frac{R^2}{b^2 N}$$

Regarding the excluded volume interactions, the decrease in configurational entropy can be written as $Z \sim (V - Nv)^N$ (where $v = b^d$ is the excluded volume in d-dimension).

The associated free energy is:

$$F_v \simeq -Nk_bT\ln(V - Nv) \simeq F_0 - k_bT\frac{N^2b^d}{R^d}$$

Minimizing the total energy $F_e + F_v$ yields a relation between the number of monomers and the end-to-end distance:

$$R \sim bN^{3/(2+d)} \equiv bN^{\nu} \tag{4.10}$$

As a last point, it turns out that a polymer in a melt has the same mean size than an ideal chain due to the screening of monomer-monomer interactions [53].

Derivation of the indentation force from blocking points density

With the analogy between a stack of granular chains and a polymer melt, the length-scale determining the density of blocking points is given by the chain size R (Eq. 4.8). We assume that every monomer of a chain can be a blocking point. Their density per unit length and per chain is given by the ratio of the number of monomers $\mathcal{N}$ over the size of the coil R:

$$M_z \sim \frac{\mathcal{N}}{b\sqrt{\mathcal{N}}} \sim \frac{\sqrt{\mathcal{N}}}{b} \tag{4.11}$$

Inserting Eq. 4.11 into Eq. 4.6, we get after integration:

$$F \sim F_0 \exp\left[\mu\sqrt{\mathcal{N}}\,\left(\frac{z}{b}\right)\right] \tag{4.12}$$

This theoretical expression of the evolution of the resistive force based on the polymer analogy is in good agreement with the empirical relation describing the experimental data, $F/F_0 = \exp\left[\mathcal{N}^{0.46}\,(z/b)\right]$.

4.4.1 A semi-dilute regime for self-amplified friction

We have derived a model that fits the experimental observations on the basis of an adventurous analogy between granular matter and real polymer chains subjected to Brownian motion. Alas, it is difficult to definitely prove that this assumption is valid. However, this theoretical frame predicts other behaviours that can be experimentally investigated. Indeed, between dilute and melt states, there exists a semi-dilute regime that should strongly impact the indentation response of granular-chain assemblies.

In the semi-dilute regime, the previously derived length-scale fixed by the coil radius breaks down. Nonetheless, P.-G. de Gennes has introduced the concept of blob to overcome this problem. The chains interact with each other and with solvant molecules, thus there are subparts of a chain that only interact with the solvant. The blob is this – maximal – unperturbed subpart of the chain. Within this theoretical framework, a chain of $\mathcal{N}$ monomers becomes in the semi-dilute regime a chain of $\mathcal{N}/g$ blobs. These blobs

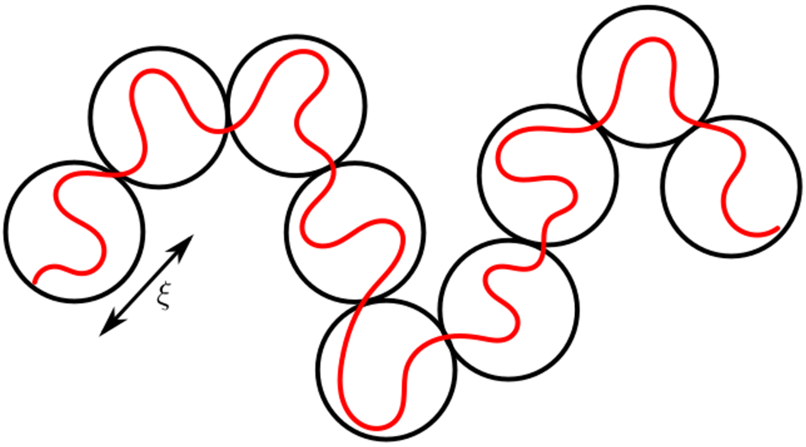

Figure 4.8 – Blob picture: the chain, in red, can be seen as a chain of blobs, black circles, of size ξ.

each contain g monomers and are unperturbed by the interaction with other chains. The polymer solution is now viewed as a blob-chain melt ! With this new entity, a new length scale appears: the size of the blob ξ, given by Eq. 4.9 in a good solvant, $\xi \sim bg^{\nu}$. For such a melt of blob chains, the chain size is given by Eq.4.5:

$$R \sim \xi \sqrt{\frac{\mathcal{N}}{g}} \tag{4.13}$$

To derive the interlocking density, we also consider that blocking points cannot be assimilated to the number of monomers anymore. Many of them are unperturbed, we should instead consider the number of blobs in a single chain. Hence, the density of blocking points becomes,

$$M_z \sim \frac{\mathcal{N}/g}{\xi\sqrt{\mathcal{N}/g}} \sim \frac{\sqrt{\mathcal{N}}}{b} g^{-\nu-\frac{1}{2}} \tag{4.14}$$

We have now to determine the relation between g and the volume fraction to obtain a testable expression for the indentation force in semi-dilute regime. In a blob of size ξ there are g monomers of size b, we thus have:

$$\Phi = \frac{gb^3}{\xi^3} = g^{1-3\nu} \tag{4.15}$$

Inverting Eq.4.15 and inserting it in Eq.4.14, we finally obtain an experimentally testable relation:

$$M_z \sim \frac{\sqrt{\mathcal{N}}}{b}\, \Phi^{(1+2\nu)/(6\nu-2)} \tag{4.16}$$

Considering the Flory exponent $\nu = 3/5$ valid for 3D chains, Eq. 4.16 becomes:

$$M_z \sim \frac{\sqrt{\mathcal{N}}}{b}\Phi^{\frac{11}{8}} \tag{4.17}$$

This expression for the density of blocking points is consistent with the previous one since when $\Phi = 1$ we recover the expression for a pure melt, see Eq. 4.11.

Finally, the resistive force of granular-chain assemblies in a semi-diluted regime is obtained by inserting Eq. 4.17 into Eq. 4.6. Integration of the resulting equation yields:

$$F \sim F_0 \exp\left[\mu\sqrt{\mathcal{N}}\left(\frac{z}{b}\right)\,\Phi^{\frac{11}{8}}\right] \tag{4.18}$$

This relation can be tested experimentally by diluting the granular-chain assemblies with simple beads in given proportion. Practically, it has been challenging to homogenize the blends that exhibit a severe tendency to spontaneously segregate. We have performed the same indentation experiments, for a chain of thirty beads and for a range of volume fractions. Figure 4.9 shows that the effect of dilution is clear. The more diluted the system is the more it tends to follow the behaviour of simple beads. As expected, the dilution leads to a decrease in the resistive force. Figure 4.9 shows the evolution of $\mathrm{d}\log(F/F0)/dz$ slopes with the volume fraction.

The black dashed line corresponds to the best fit $\sim \Phi^{1.1}$ while the red solid line follows the theoretically law of Eq. 4.18 derived from the semi-dilute polymer analogy. The agreement between predictions and experimental data is convincing.

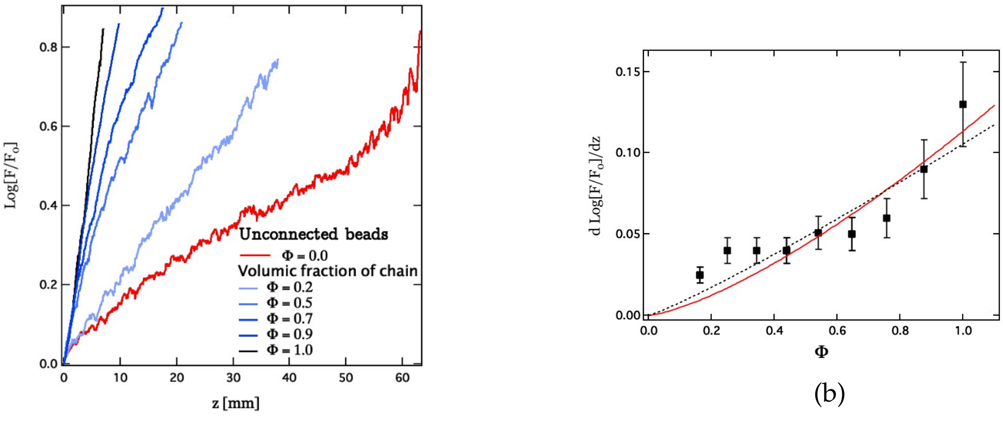

(a)

(b)

Figure 4.9 – (a) Effect of dilution on the resistive force. (b) Evolution of the slope of (a), $d\log(F/F_0)/dz$, with the volume fraction of chain.

4.4.2 Master curve

Finally, the collapse of all indentation curves in melt and semi-dilute regimes shown in Fig. 4.10 substantiates the proposed model for the resistive force and thus the granular chain–polymer analogy.

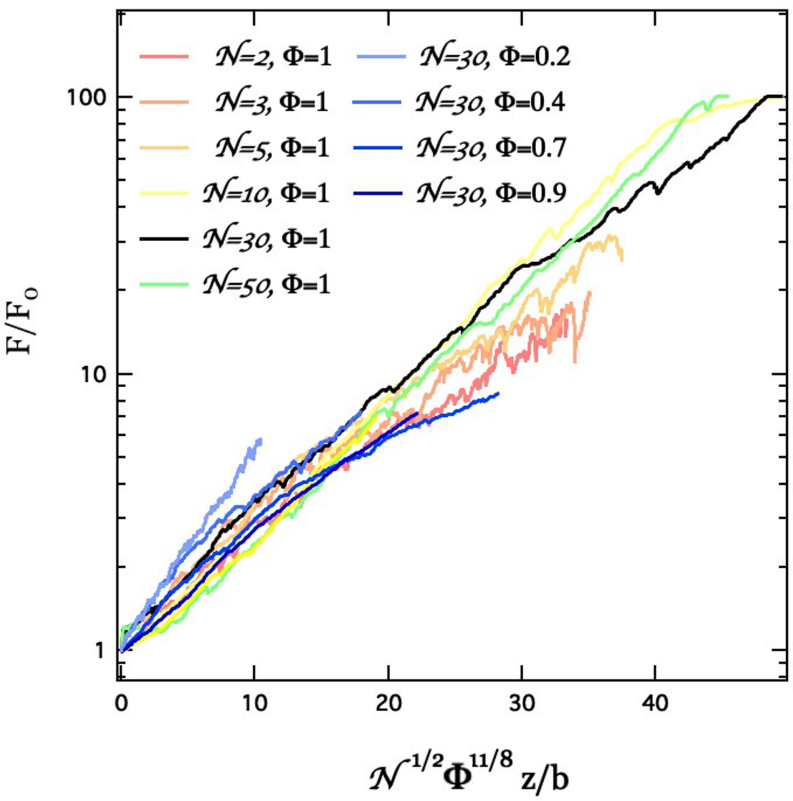

Figure 4.10 – Comparison between the measured resistive force and the theoretical expectation from Eq.4.18 for the two investigated cases: melt ($\Phi = 1$) and semi-dilute.

In conclusion of this first part, the emergent strain-stiffening behavior in granular-chain assemblies, as observed through indentation experiments, seems to originate from a self-amplification of friction due to polymer-like interlocking contacts. Interestingly, this system exhibits a new self-amplification exponent (1/2, in chain length) with respect to previous exponents for a capstan (1, in angle) [118] and interleaved books (2, in number of sheets) [1]. However, even if the developed interlocking model seems to capture well the experimental data, we stress that it implicitly assumes sufficiently long chains for proper conformational statistics to be achieved, which is only approximate in our experiments. Also, we assumed the use of these statistical tools to be allowed in the sense of the conjecture of Edwards.

These observations clearly support the idea that a granular-chain assembly has an internal structure which is not so far from the average internal structure of classical polymer chains.

Part II

Can a vibrated system be described by statistical physics ?

> *Fire and heat provide modes of explanation in the most varied domains, because they have been for us the occasion for unforgettable memories, for simple and decisive personal experiences. Fire is thus a privileged phenomenon which can explain anything. If all that changes slowly may be explained by life, all that changes quickly is explained by fire. Fire is the ultra-living element. It is intimate and it is universal. It lives in our heart. It lives in the sky. It rises from the depths of the substance and offers itself with the warmth of love. Or it can go back down into the substance and hide there, latent and pent-up, like hate and vengeance. Among all phenomena, it is really the only one to which there can be so definitely attributed the opposing values of good and evil. It shines in Paradise. It burns in Hell. It is gentleness and torture. It is cookery and it is apocalypse. It is a pleasure for the good child sitting prudently by the hearth; yet it punishes any disobedience when the child wishes to play too close to its flames. It is well-being and it is respect. It is a tutelary and a terrible divinity, both good and bad. It can contradict itself; thus it is one of the principles of universal explanation.*
>
> Gaston Bachelard, *Psychoanalysis of fire*, 1938 [4]

Part introduction

Fire and heat or temperature and energy are physical notions that have pervaded in the everyday life in such a way that we are accustomed with them while they are actually intricated notions. Temperature can be defined in two overlapping ways. First, in thermodynamic sense, the temperature of a system is the inverse of the variation of the system's entropy with energy. Second, a more accessible definition of temperature is its relation to the mean square velocity of the particles. Besides, temperature being a relative concept, the absolute zero of the measure of temperature has been set as the point where all particles are motionless. It is however crucial to point out that the definition of temperature only holds for equilibrated systems. In other words, for systems in which the concept of entropy has a meaning and equipartition of energy is true. This is actually a great restriction since out-of-equilibrium situations are rather the rule than the exception. Yet, even though out-of-equilibrium thermodynamics is nowadays making progresses, a dedicated theoretical framework is still lacking and one has to envision out-of-equilibrium systems with the tools developed for equilibrated systems.

A telling example of such approaches has been used in the previous part. Leaning on Edwards' conjecture, we studied the internal structure of an assembly of granular chains as a thermally-equilibrated system, in spite of it being static. This was possible because we examined the mean behaviour of an ensemble of different granular chains piles. In this case we somehow explored the phase space by repeating the experiments and thus generating new conformations. Yet, to study at a macroscopic scale the dynamical processes that can be observed at a microscopic level, we have to inject energy to counteract gravity. Alas, one critical difference between particles at the microscopic and the macroscopic scale is the type of interactions between grains. At the macroscopic scale, interactions are inelastic and at each collision energy is lost. A clear example of this phenomenon is the several bounces of a single marble dropped onto a plate while a bag, filled with the same marbles, dropped in the same fashion would not bounce at all. Energy conservation cannot thus be used to produce a theoretical framework, unlike for ideal gases. Since at the macroscopic scale the relevant energy scale is the potential energy and not the thermal energy, the common thermodynamic arguments break down. For instance, while based on entropic considerations mixing of an ensemble of particles is favored, vibrated or rotated granular materials tend to be segregated according to their size [32, 20]. This effect is part of everyday life when big chunks of cereals are at the top of the box and smaller chunks at the bottom, a phenomenon commonly known as the Brazil nut effect.

For macroscopic systems, the notion of temperature as energy input is unsound but fundamental to draw an analogy with microscopic systems. We will see that producing an effective definition of temperature is challenging.

Chapter 5

How to thermostatize an experiment with vibrations ?

As demonstrated by the beautiful experiments of Jean Perrin about sedimentation of colloids, it is clear that to overcome gravity, we have to inject energy, playing the role of a ″reservoir temperature″ in our system. This energy input will have to allow our system to explore phase space so that the notion of ensemble average becomes meaningful.

5.1 The experimental setup

There are several possibilities to inject energy into a macroscopic system by either shearing, rotating or vibrating the particles. Since we study quasi 2D systems, we choose vibration as the energy input. An electrodynamic shaker is used to generate an uniaxial vibration. Even though this apparatus has been used prior to 2015, a detailed study of the parameters of this apparatus is provided in [62]. In the following, we will only highlight the key features of this setup.

5.1.1 The apparatus

The experimental setup is rather straightforward, see Fig. 5.1. A uniaxial motion is produced by an electrodynamic shaker, that can be controlled by a frequency generator coupled to a power amplifier in such a way that the peak to peak motion is periodic with a given amplitude. This motion is transmitted to the test plate via a coupling rod whose diameter is thin enough to act as a fuse in case of a mechanical failure. An air bearing carriage helps to ensure the uniaxiality of the motion. Finally, the motion of the objects set on the test plate is monitored by a camera. The images thus acquired are afterwards processed by home made codes in Python. A critical aspect in these types of experiment lies in the perfect levelling of the test plate. Indeed, any minute tilt of the plate leads to drift and, since the test plate has a rather limited area, the boundaries are rapidly reached by the particles. There are two ways to face this problem : perfectly levelling the plate,

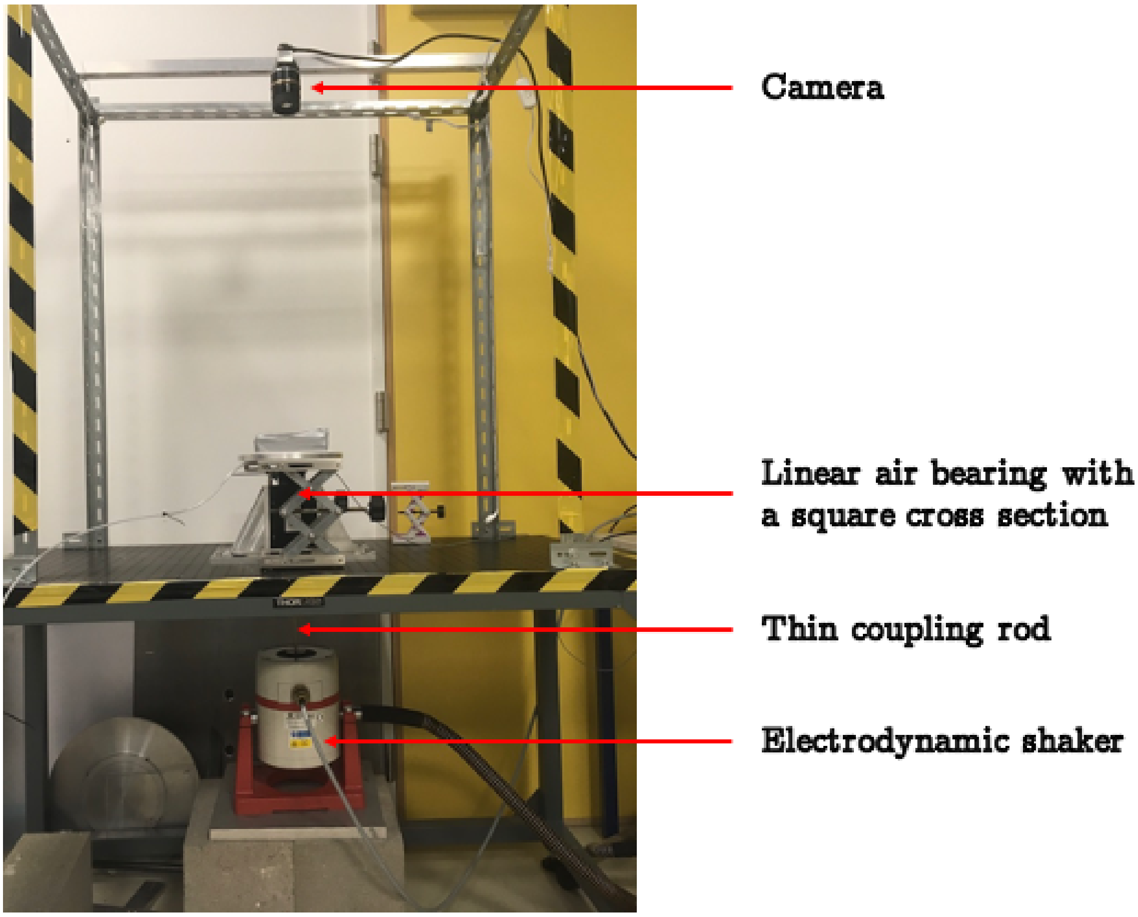
Camera
Linear air bearing with a square cross section
Thin coupling rod
Electrodynamic shaker

Figure 5.1 – Setup we used to perform vibrated experiments.

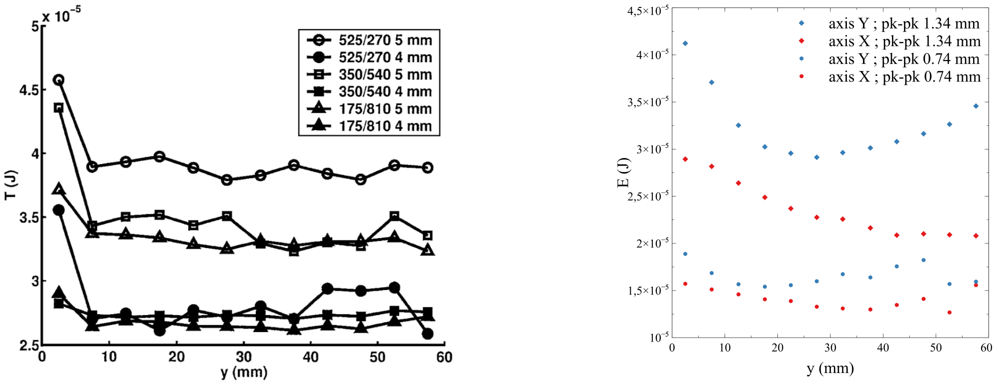

(a) (b)

Figure 5.2 – (a) Evolution of the temperature T, measured as a kinetic energy, with y the depth, measured for a binary mixture of particles of radii 5 and 4 mm, taken from [127]. (b) Evolution of the temperature E, measured as a kinetic energy, with y the depth, on two different axis, adapted from [126]. For both graphs, the measure of depth is opposite to gravity.

which is near impossible, or tolerate the drift. Per se, the drift is not a problem because assuming the motion is linearly composed of a drift part and a Brownian part we may afterwards subtract the drift. The real issue is the finiteness of the test plate. To overcome this, we may design a specific test plate, say a harmonic potential, so that the motion is confined away from the boundaries. Hence, the motion would be composed of three parts : drift, harmonic and Brownian.

5.1.2 Granular temperature

With the proposed experimental set-up, we are now able to inject energy in our system. However, does this mechanical energy input act in a similar way as thermal energy ? This question is actually hard to answer.
Regarding kinetic energy, a granular temperature may be estimated by studying the fluctuations of the particles' velocity. However, because a significant part of the kinetic energy is lost through dissipation by friction and inelastic collisions, unexpected phenomena arise. For instance, it has been found, see Fig. 5.2a, that a fluidized granular system in 3D composed of two different species relaxes towards a state with two separate and yet coexisting granular temperatures [127]. Another discrepancy between the temperature experienced by microscopic and macroscopic grains is the anisotropic behaviour for the latter because of the influence of gravity [126, 129, 28], as in Fig. 5.2b.

It is thus clear that the energy input of the vibrating experimental setup, that we may define via the amplitude and the frequency of the vibration, could not directly be compared to a universal temperature. Two types of in situ "thermometer" have been studied [28, 25], the first one comprising a torsion oscillator immersed in a vibrofluidized ensemble of particles and the second one consisting in measuring the position probability distribution of a single particle on an inclined plane. It would be interesting to test if, given the same energy input, these thermometers would yield the same result. In the following, we will study a single particle in interaction with a thermostating bath and show that the fluctuations of the particle's velocity depend on both the energy input and the bath's characteristics. Hence while the energy input is adjusted from the frequency and amplitude of vibration in our set-up, we will not claim to any universality.

5.2 A thermostating bath

As for the question of the internal structure of matter, the question of motion has deep historical roots. Interestingly enough, these two notions huddle together at the beginning of the XX$^{\text{th}}$ with what is now known as the Brownian motion.

What is motion and what is driving it ? Empirically, we may describe the motion of an object as the time evolution of its position because its velocity is different from zero at a given time. As to what initiates and stops motion, we may simply state that it is due to an increase of its energy and its dissipation, respectively. A picture of this behaviour may be laid out through the billiard game prism where to set a ball in motion the player has to strike it with its cue, then the ball may hit another ball or bounce off a wall. In any case, part of its momentum is loss. The ball also loses its initial energy by friction on the cloth of the pool table as well as friction with air. Eventually, all of the initial energy is dissipated and the ball stops. As to the ball's trajectory, it can be easily understood and predicted in terms of Newtonian equations. What would happen if the player hits the ball again and again ? And what if each time, this player hits it in a random direction ? Obviously, keeping tracks of all the previous plays, the ball's trajectory could be afterwards accounted for by Newtonian equations. However, it would be impossible to predict the future positions of the ball, which is the very purpose of a model. This thought experiment of billard's ball random motion was actually what many botanists of the mid XIX$^{\text{th}}$ century and before had observed under their microscope. Even though several scientists have written on these observations before Robert Brown, this name has been preserved by posterity. Surely because Brown thouroughly studied and reported his observations without giving in any a priori as to the origin of the erratic motion of the particles under microscope. We may summarize all these microscopic observations as in [18] :

- The motion is very irregular, composed of translations and rotations, and the trajectory appears to have no tangent.
- The motion of a particle is independent of other particles, even when two approach one another to within a distance less than their diameter.
- The motion is more active the smaller the particles.
- The motion is independent of the composition and density of the particles.
- The motion is more active the less viscous the fluid.

- The motion is more active the higher the temperature.
- The motion never ceases.

Among these observations, the first one implying that the notion of velocity is mathematically not attainable has prevented the scientists at that time to conclude on this erratic motion. We may even borrow the words of Stephen G. Brush in [18] to summarize this situation, *three-quarters of a century of experimentation produced almost no useful results, simply because no theorist had told the experimentalists what quantity should be measured!*

It is indeed only in 1905 when Albert Einstein [42], while working on the existence of atoms and postulating that this erratic motion could be actually observed given sufficiently small particles, proposed the first theoretical framework to study Brownian motion. Einstein and Schmolukovski's equations express two key features. First, on average, the square of the displacements is proportional to time. Second, displacements are not time correlated and they follow a Gaussian distribution. This mathematical object, being a continuous yet random time function with independent increments, has been developed first by Norbert Wiener [125] and furthermore studied by Paul Lévy [81].

In parallel, Paul Langevin [76] devised a different theoretical approach, starting from the Newton's equation stating that the acceleration of a particle is proportional to the force exerted on it. Neglecting gravity, the exerted force is composed of a dissipation term due to the viscosity of the particle's environment and a force X due to collisions of the molecules surrounding the considered particle.

$$m\dot{v} = -m\gamma v + X(t) \tag{5.1}$$

where m is the mass of the particle, v its speed and γ the friction coefficient.
This force X is random and, at the time of Langevin, mathematically ill-defined. It is the work of J.-L. Doob [35] that gave a sound mathematical description of this approach.

5.2.1 The generalized Langevin equation

Equation 5.1 proposed by Langevin on physical grounds, may be developed in a broader context, see e.g. [131, 106, 123]. If we consider $N+1$ particles in interaction and only one is of interest, we may want to eliminate the degrees of freedom coming from the N other particles, which correspond to a "thermal bath". The Hamiltonian of the system can be written as

$$\begin{aligned} H_{\text{system}} &= H_{\text{particle}} + H_{\text{bath}} && (5.2)\\ &= \Big(\frac{p^2}{2m} + V(q)\Big) + \Big(\sum_{i=1}^{N} \frac{p_i^2}{2m_i} + U_{\text{bath}}(q, x_1, ..., x_N)\Big) && (5.3)\end{aligned}$$

where q is the generalized coordinate of the particle of interest, p its conjugate momentum with m the particle's mass and $V(q)$ the potential energy associated ; x_i, p_i, m_i and U_{bath}

are similarly defined for the particles constituting the bath.
In the Caldeira-Legget model, the particles of the bath are harmonic oscillators [19]. They fluctuate, yet not diffuse, around an equilibrium position, the particle of interest being linearly coupled to the bath particles. The potential energy of the bath may be written as

$$U_{bath} = q \sum_{i=1}^{N} g_i x_i + \frac{1}{2} \sum_{i=1}^{N} m_i \omega_i^2 x_i^2 \tag{5.4}$$

where the first term of the right hand side of Eq.5.4 is the coupling between the bath and the particle of interest while the second term is purely related to the bath.
Finally, the Hamiltonian of the system becomes

$$H_{system} = \frac{p^2}{2m} + V(q) + \sum_{i=1}^{N} \frac{p_i^2}{2m_i} + q \sum_{i=1}^{N} g_i x_i + \frac{1}{2} \sum_{i=1}^{N} m_i \omega_i^2 x_i^2 \tag{5.5}$$

which leads to

$$m\ddot{q} = -d_q V - \sum_i g_i x_i \tag{5.6}$$

$$m_i \ddot{x}_i = -m_i \omega_i^2 x_i - g_i q \tag{5.7}$$

A Laplace transform of Eq.5.7 allows to turn this differential equation into an algebraic one which can be solved. After an inverse Laplace transform, we obtain the solution

$$x_i(t) = x_i(0) cos(\omega_i t) + \frac{\dot{x}_i}{\omega_i} sin(\omega_i t) - \frac{g_i}{m_i \omega_i^2} \left(\Big[q(t) - q(0) cos(\omega_i t) \Big] - \int_0^t cos\Big(\omega_i (t-\tau)\Big) \dot{q}(\tau) d\tau \right) \tag{5.8}$$

Using Eq.5.8 in Eq.5.6 finally yields the generalized Langevin equation[1]

$$m\ddot{q} = -d_q W - \int_0^t \mu(t-\tau) \dot{q}(\tau) d\tau + X(t) \tag{5.9}$$

where

$$\begin{cases} W(q) = V(q) - \sum_{i=1}^{N} \frac{g_i^2}{m_i \omega_i^2} q^2 \\ \mu(t) = \sum_{i=1}^{N} \frac{g_i^2}{m_i \omega_i^2} cos(\omega_i t) \\ X(t) = -\sum_{i=1}^{N} g_i \Big[\Big(x_i + \frac{g_i}{m_i \omega_i^2} q(0) \Big) cos(\omega_i t) + \frac{p_i(0)}{m_i \omega_i} sin(\omega_i t) \Big] \end{cases} \tag{5.10}$$

and where $X(t)$ is called the random force and $\mu(t)$ the friction kernel.

One may show that the random force and the friction kernel are related in what is called the second fluctuation dissipation theorem [74]

---

[1] Usually shortened as GLE

$$\langle X(0)X(t)\rangle = k_B T \mu(t) \tag{5.11}$$

The friction kernel is also usually called memory kernel because it depends on the knowledge of q at all times before t. Physically, the motion of the particle of interest impacts the particles of the bath, driving them in an out-of-equilibrium state which then needs a finite time to relax. This lag in the response of the bath to the motion of the particle subsequently affects the motion of the particle. From the fluctuation dissipation theorem, it is clear that the correlation time of the random force determines the decay time of the memory kernel. In the Ohmic model, the memory kernel is given by

$$\mu(t) = \frac{m\gamma}{\tau_c} e^{-t/\tau_c} \tag{5.12}$$

where τ_c is the correlation time of the random force.
The equation developed by Langevin corresponds to the limiting case of a free particle with a vanishing correlation time $\tau_c \to 0$:

$$\begin{cases} W(q) = 0 \text{ (free particle)} \\ \mu(t) \xrightarrow[\tau_c \to 0]{} m\gamma\delta(t) \text{ (Dirac delta function)} \\ \int_0^t \mu(t-\tau)\dot{q}(\tau)d\tau \xrightarrow[\tau_c \to 0]{} m\gamma\dot{q}(t) \end{cases} \Rightarrow m\ddot{q} = -m\gamma\dot{q}(t) + X(t) \tag{5.13}$$

5.2.2 Different possible baths

For vibrated particle experiments, all previous observations report a deviation from the Maxwell-Boltzmann distribution for the particle velocity, see *e.g.*[78, 96, 109] and Fig.5.3. This deviation is reflected in an overpopulation for high velocities. The tail of the distribution seems to scale as a stretched exponential with exponent $-3/2$. We have recalled how the interactions between the bath and the particle of interest are key to its motion. The design of the bath should thus be made with great care in our experimental set-up to ensure a proper thermalization of macroscopic objects.

In the literature, two studies exhibit enhanced Gaussianity in the velocity distribution thanks to two different means. The first one, proposed by Baxter *et al.* [6] see Fig.5.3b, consists of two layers of different particles. The bottom layer is composed of heavy metallic dimer particles and the top one by lighter plastic particles, so that the lighter particles are always on top of the dimer layer. While deviation in the velocity distribution tail is found for the dimers, the lighter particles do not exhibit such deviations. In [108], Reis *et al.* rendered the bottom plate of the test area rougher, this roughness helped randomizing the particle's velocity.

The first 2D design that comes in mind because of its similarities to the microscopic world, would be a single large and heavy bead surrounded by smaller/lighter beads. We

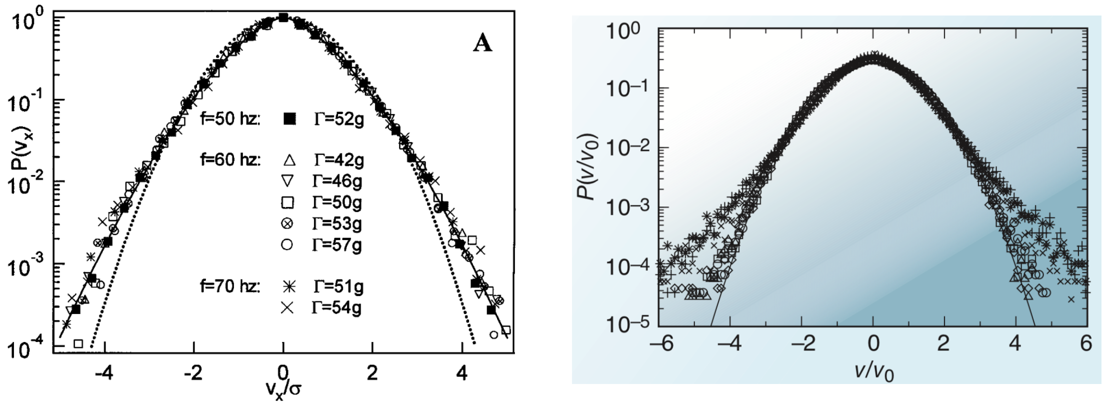

(a) (b)

Figure 5.3 – (a) Observed deviation from Maxwell-Boltzmann distribution in vibrated particle experiments in [109]. (b) The use of a dimer bath negates these deviations, taken from [6].

have tested such a design, as shown in Fig.5.4a, where one metallic bead of 4.5 mm diameter is immersed in a bath of plastic beads of 1 mm diameter. A second type of bath, midway between the first design and the one proposed in [6], has been implemented. That is, a metallic bead of 4.5 mm diameter surrounded by metallic dimers of 2 mm diameter, see Fig.5.5a. A final design similar to the set-up used by Reis *et al.* [108], consists in rendering the bottom plate of the test area rougher in order to improve the randomizing of the velocity of a steel sphere. Roughness were achieved by either glueing plastic beads on the bottom plate see Fig.5.6a, or directly 3D-printing the experimental arena with a pattern of embedded beads see Fig.5.6b.

Experimentally, we compared these three different designs through the prism of the one step increment probability distribution (equivalent to the velocity distribution). We tracked the position $x(t)$, along both axis, of the black metallic bead and derived the one step increment $\Delta x = x(t+\delta t) - x(t)$. This one step increment density is naturally related to the average velocity by $v = \Delta x/\delta t$. The distribution computed for each design comes from the recordings of three 30 minute long trajectories at a rate of 30 images per second, for a total number of 162000 frames. In each case, the same shaker parameters were used: a frequency of 30 Hz and an acceleration of 24m.s^{-2}.

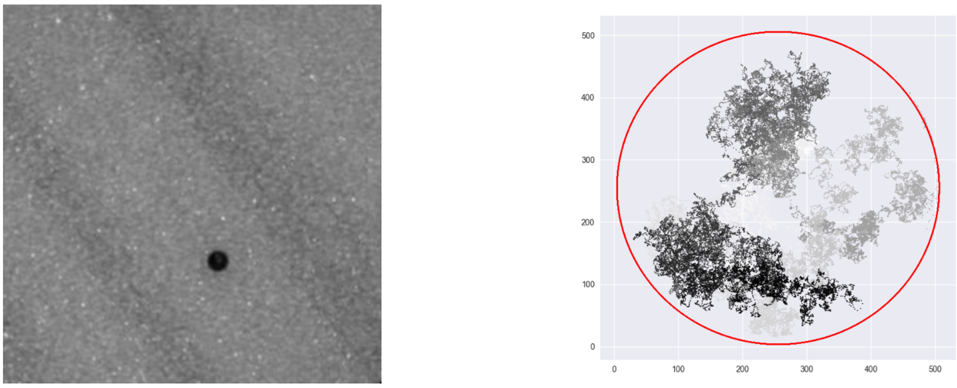

(a)

(b)

Figure 5.4 – (a) Black metallic bead (diameter 4.5 mm) immerged in a layer of small plastic beads (1 mm diameter) and (b) part of the trajectory of the black bead during an experiment with a shaker excitation frequency of 30 Hz and acceleration of 24 m.s^{-2}. The grey nuances are an indicator of the course of time.

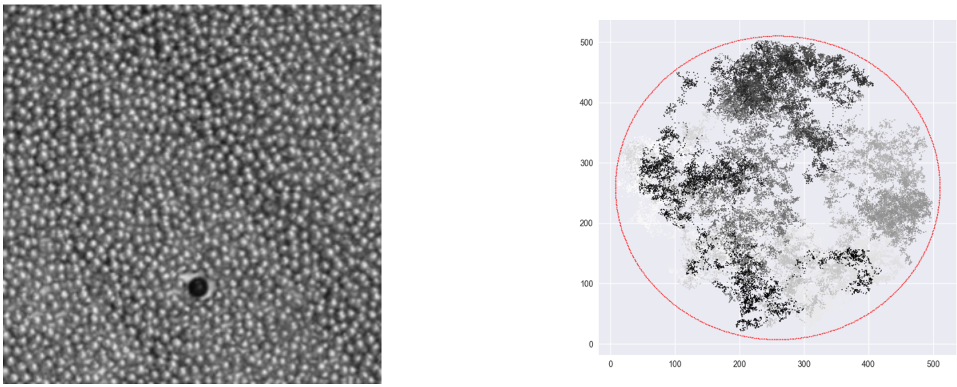

(a)

(b)

Figure 5.5 – (a) Black metallic bead (diameter 4.5 mm) immerged in a layer of metallic dimers (2 mm diameter) and (b) part of the trajectory of the black bead during an experiment with a shaker excitation frequency of 30 Hz and acceleration of 24 m.s^{-2}. The grey nuances are an indicator of the course of time.

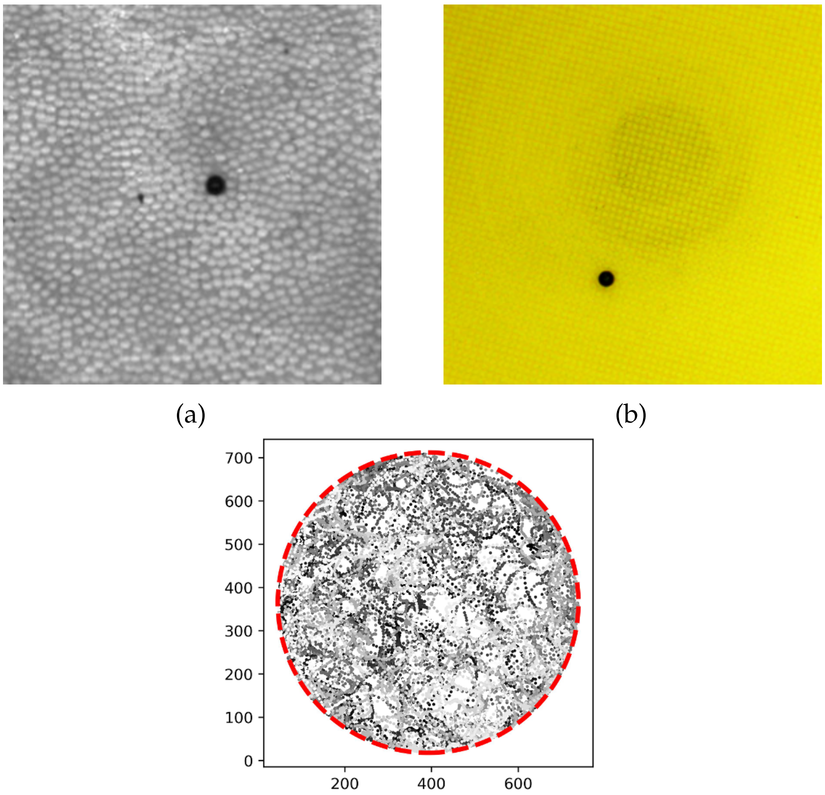

(a) (b)

(c)

Figure 5.6 – Black metallic bead (diameter 4.5 mm) on top of (a) a glued layer of plastic beads (2 mm diameter) and (b) the 3D-printed arena. In (c) part of the trajectory of the black bead during an experiment with a shaker excitation frequency of 30 Hz and acceleration of 24 m.s^{-2}. The grey nuances are an indicator of the course of time.

Having tracked the positions of the metallic bead over time, it is rather straightforward to get the one step increment probability distribution. In Fig.5.7, we can clearly see that this distribution is centered around 0 in each case and that its variance depends on the design. We observe large deviations from the Gaussian distribution for large velocities when the design includes a bath of explicit particles – plastic beads or metallic dimers, see Figs.5.7a and 5.7b. However, when the solvant is replaced by a layer of glued beads, the one step increment distribution is well fitted by a Gaussian function. The fact that a layer of glued beads behaves as a thermal bath may strike as surprising. Indeed, why would a layer of identical beads, glued on a plate and thus moving in a perfectly correlated way, randomize the motion of a particle on top of it ? One would even guess the opposite given possible correlations between subsequent collisions. Nonetheless, evaluating the velocity autocorrelation function (VACF) confirms the strong randomization produced by the glued beads, see Fig.5.8.

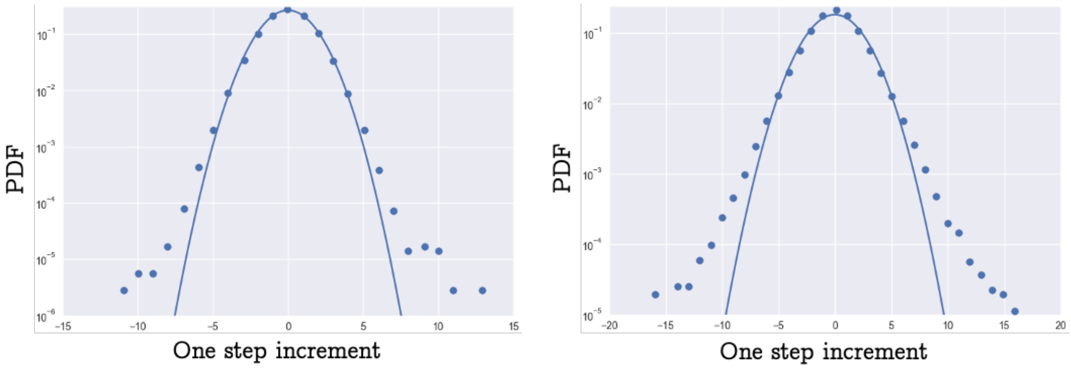

(a) $\sigma = 1.51$

(b) $\sigma = 2.18$

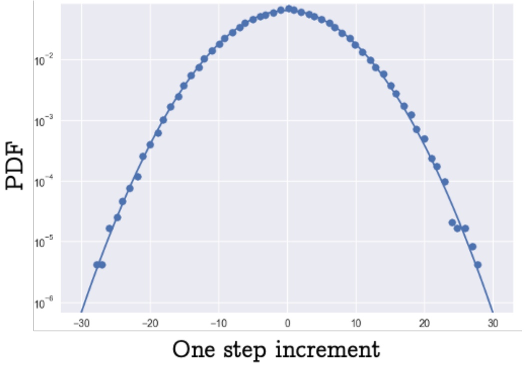

(c) $\sigma = 6.27$

Figure 5.7 – Probability density function (PDF) of the one step increment Δx for different solvant bath (a) small plastic beads (b) dimers (c) glued beads. The solid blue lines represent a Gaussian fit with σ as the standard deviation of the distribution.

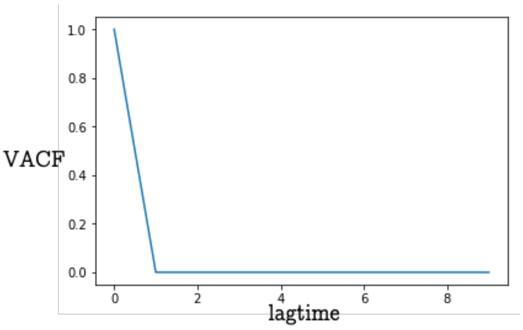

Figure 5.8 – VACF of the metallic bead moving on top of the glued beads layer. Just the first lagtimes are represented here.

Chapter 6

A macroscopic Brownian particle in a double well trap

We have seen that our experimental setup enables us to perform equilibrated stochastic experiments with a single particle at the macroscopic scale. Furthermore, we can 3D-print any desired arena shape in which the particle will evolve. We hence capitalized on this aspect to investigate a macroscopic analogue of the problem of the harmonic trap. We actually designed a double-well trap (Fig. 6.1).

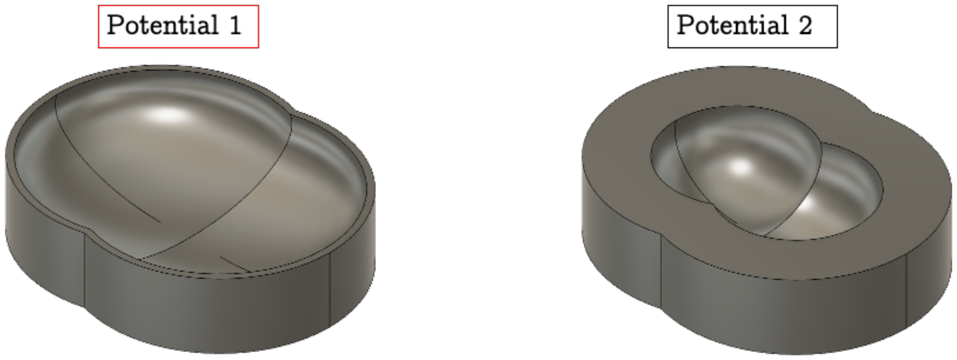

(a) (b)

Figure 6.1 – (a) and (b) Perspective views of the two different potentials we used.

6.1 The double-well arena

We tested two double-well arenas of two different stiffnesses. Each arena is defined by two identical and intersecting spherical caps. These spherical caps intersect in such a manner that the particle has to get over a peak of height z_i in order to move from one well to the other, as shown in Fig.6.2. The potential 2 (Pot. 2) is stiffer than the potential 1 (Pot. 1). For each arena, the results for a given shaker acceleration γ, with a fixed frequency $f = 30$ Hz, come from the realization of six 10 minute long runs, recorded at

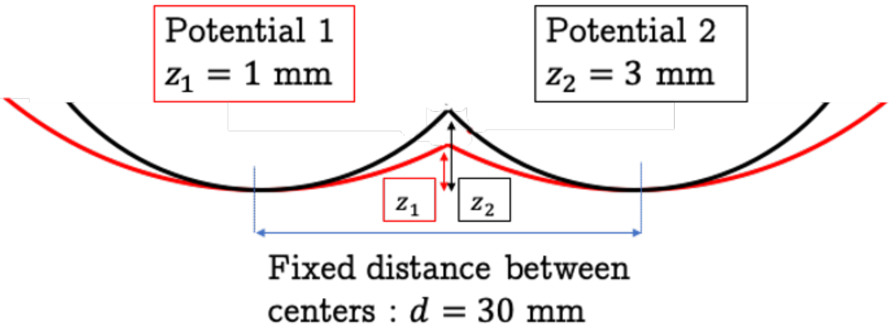

Figure 6.2 – Schematic side view of the potentials with barrier heigths $z_1 = 1$ mm (Potential 1) and $z_2 = 3$ mm (Potential 2).

a frame-rate of 30 images per second. This leads to a total number of 108000 recorded particle's positions. An example of the trajectory of a particle in our double-well arena is represented in Fig.6.3.

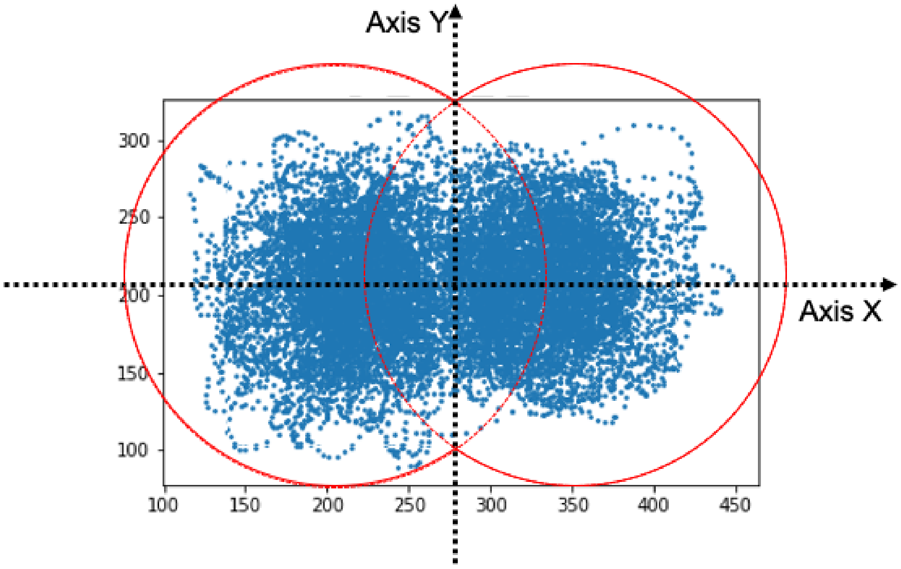

Figure 6.3 – Example of a trajectory in a double well trap. The red finely dashed lines correspond to the shapes of the well. The X-axis is defined as the line joining the centers of the well.

6.2 Particle's positions

Since we can track the particle's positions, we may compare their probability distributions to the ones expected for a Brownian particle trapped in a harmonic potential:

$$\Pi(x) = \sqrt{\frac{k}{2\pi D}} \exp\left(-\frac{k}{2D}(x-\mu)^2\right) \tag{6.1}$$

where k is the potential stiffness, D the diffusion coefficient and μ the origin of the potential.

In Fig.6.4, we have represented the position's probability distribution on the X-axis and the Y-axis separately. The experimental distributions are fitted with a Gaussian function:

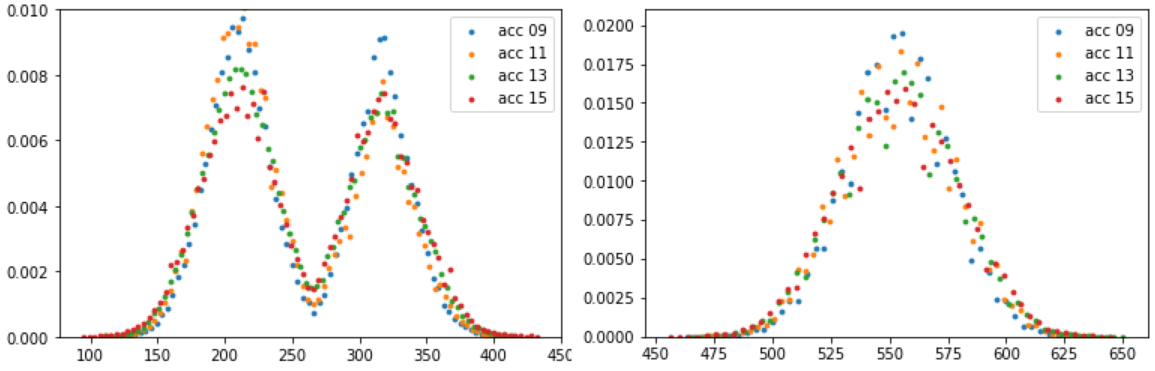

(a) (b)

Figure 6.4 – Example of the position probability on (a) the X-axis and (b) the Y-axis for four accelerations "acc": $\gamma = 9, 11, 13$ and $15\ \mathrm{m.s^{-2}}$.

$$P_G(x) = \alpha \exp\left(- \frac{(x-\mu)^2}{\tau} \right) \tag{6.2}$$

On the X-axis, it is actually a sum of two identical Gaussian functions. The results are displayed in Fig.6.5 (the data point were omitted for clarity) and we clearly see the difference between the well stiffnesses along the effect of the shaker's acceleration. Indeed, the potential 2 is stiffer than the potential 1 and the associated probability distribution is narrower, on each axis, than the one for the potential 1. Also, the greater the shaker's acceleration the wider the distribution becomes. We have thus studied the evolution of the fitting parameters α and τ with respect to the shaker's acceleration γ. From Eq.6.1,

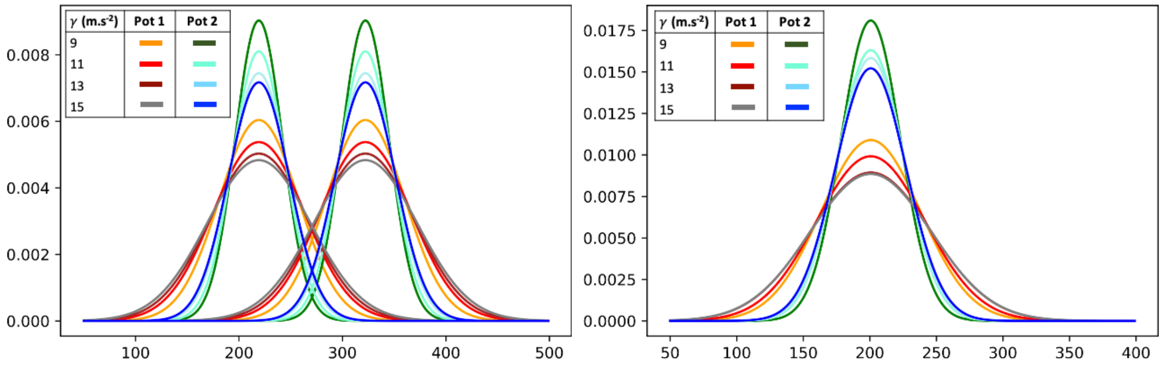

(a) (b)

Figure 6.5 – Position probability distributions modelled by Gaussian functions for the different potentials and accelerations on the (a) X-axis and (b) the Y-axis.

we expect the following dependencies:

$$\begin{cases} \alpha \sim D^{-1/2} \sim T^{-1/2} \\ \tau \sim D \sim T \end{cases} \tag{6.3}$$

where we have used the fluctuation dissipation relationship between D and T, the temperature. As detailed in the first chapter, a consistent definition of a granular temperature is beyond the scope of our work, so we will only rely on the assuption that increasing the shaker's acceleration also increases the granular temperature linearly. We thus expect:

$$\begin{cases} \alpha \sim \gamma^{-1/2} \\ \tau \sim \gamma \end{cases} \tag{6.4}$$

From our results, the fitting parameters α and τ do satisfy the previous relations, as shown in Fig.6.6.

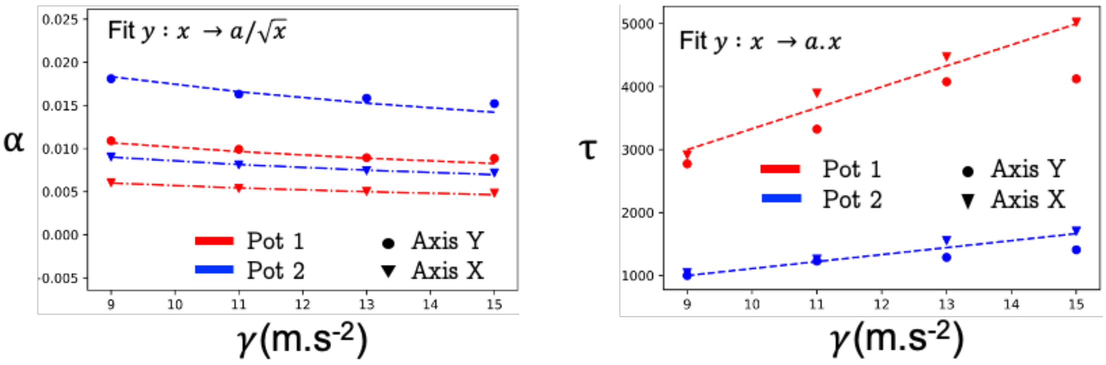

(a)

(b)

Figure 6.6 – Evolution of the fitting parameter (a) α and (b) τ with the shaker's acceleration γ.

To finally conclude on the parallel between our double-well arenas and the harmonic potential trap, we can verify that $(\alpha^2\tau)^{-1} = \pi$. While this is true on the Y-axis, this relation breaks down on the X-axis, which can be understood since on this axis the particle is not trapped in a single potential but may jump between two harmonic traps.

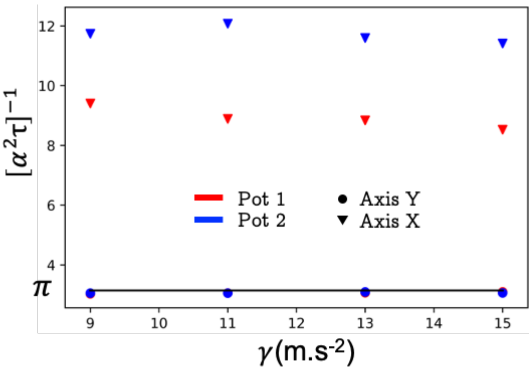

Figure 6.7 – Evolution of the produt $\alpha^2\tau$ with the shaker's acceleration γ.

6.3 Mean escape time

The double-well arena also enables us to measure the mean escape time from an harmonic trap. On the X-axis, the particle is either located in the left well or in the right well. We may, besides, verify that the probability for the particle to be in the left well or in the right one is 1/2, see Fig.6.8a. According to Kramer's expression, see [73], the mean escape time depends on the energy difference ΔE, between the escape point and the bottom of the potential well, and the temperature T as:

$$\tau_{\text{escape}} = \tau_0 \exp\left(\frac{\Delta E}{k_B T}\right) \tag{6.5}$$

In Fig.6.8b, we have plotted this mean escape time against the shaker's acceleration γ and we fitted our experimental data points by $a.\exp(b/\gamma)$. All these observations clearly state that the proposed setup induces a thermalization of the macroscopic particles and that the acceleration of the shaker determines the temperature of the system.

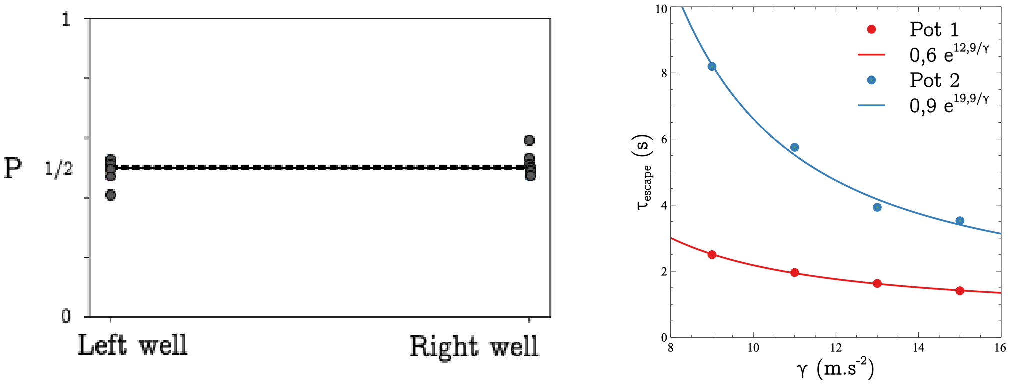

(a) (b)

Figure 6.8 – (a) Probability for the bead to be located in the right or the left well. The black dashed line correponds to the probability 1/2. (b) Mean escape time from a well. The solid lines are best fits to $a.\exp(b/\gamma)$.

Part III

How is a long chain translocating ?

Today, thanks to the ingenious work of biologists, mainly of geneticists, during the last thirty or forty years, enough is known about the actual material structure of organisms and about their functioning to state that, and to tell precisely why present-day physics and chemistry could not possibly account for what happens in space and time within a living organism. The arrangements of the atoms in the most vital parts of an organism and the interplay of these arrangements differ in a fundamental way from all those arrangements of atoms which physicists and chemists have hitherto made the object of their experimental and theoretical research. Yet the difference which I have just termed fundamental is of such a kind that it might easily appear slight to anyone except a physicist who is thoroughly imbued with the knowledge that the laws of physics and chemistry are statistical throughout. For it is in relation to the statistical point of view that the structure of the vital parts of living organisms differs so entirely from that of any piece of matter that we physicists and chemists have ever handled physically in our laboratories or mentally at our writing desks. It is well-nigh unthinkable that the laws and regularities thus discovered should happen to apply immediately to the behaviour of systems which do not exhibit the structure on which those laws and regularities are based. [...]
I propose to develop first what you might call "a naive physicist's ideas about organisms", that is, the ideas which might arise in the mind of a physicist who, after having learnt his physics and, more especially, the statistical foundation of his science, begins to think about organisms and about the way they behave and function and who comes to ask himself conscientiously whether he, from what he has learnt, from the point of view of his comparatively simple and clear and humble science, can make any relevant contributions to the question.

Erwin Schrödinger, *What is life*, 1944 [112]

Part introduction

For a long time, Biology and Physics were two separate branches of science on the ground that the laws governing inanimate matter could not be the same for living matter. Hence, biophysics is rather young in comparison with other sciences and still bears the stigma of this prolonged separation. These stigma are that often a researcher in biophysics is litterate in either biology or physics but rarely both. Thus the same problem is differently investigated depending on one's background, which may lead to a certain antagonism or, quoting P.-G de Gennes, *Physicists and physico-chemists have displayed imperialism and arrogance towards biology.*, who first hand could appreciate this phenomenon when changing his physical research topics for biological ones :
When I moved in the Institut Curie, I was very surprised to see how difficult it was to discuss about cellular adhesion. When we, physicists, studied this process, we considered a minimal model with few adjustable parameters, maybe one chemical addition but no more, and we tried to observe if a very simple phenomenon would emerge. Since it was very simple, we could not be too wrong – while, to reveal how a fibroblast moved, biologists had involved an extremely complex set of chemical reactions. In order to know if a mechanism is relevant, they inhibit many others. This leads to a more cumbersome labour of testing and validation than we physicists are used to.
Having received a cursory education in life sciences, we are partial to the physics side. Hence we will tread cautiously with biological issues and we will adopt the approach described by Schrödinger, that is *a naive physicist's ideas about organisms*. We will also not claim any conclusive remarks on biological issues, our interest here is the study of a phenomenon that has biological roots.
This phenomenon is polymer translocation. In physicists terms, it is very simple to describe because it simply consists in the crossing of a polymer from one medium to another. However, once this physical definition is enunciated we have to amend it by all its biological ramifications.

Chapter 7

A first approach to translocation

7.1 Biological context

A cell, whether prokaryotic or eukaryotic, may be visualized as a production unit with inputs and outputs with its inside being separated from the outside medium by a phospholipidic membrane. The set of chemical reactions happening inside the cell is known as the metabolism. The regular behaviour of the outer membrane is to let the required inputs enter and to block the rest.

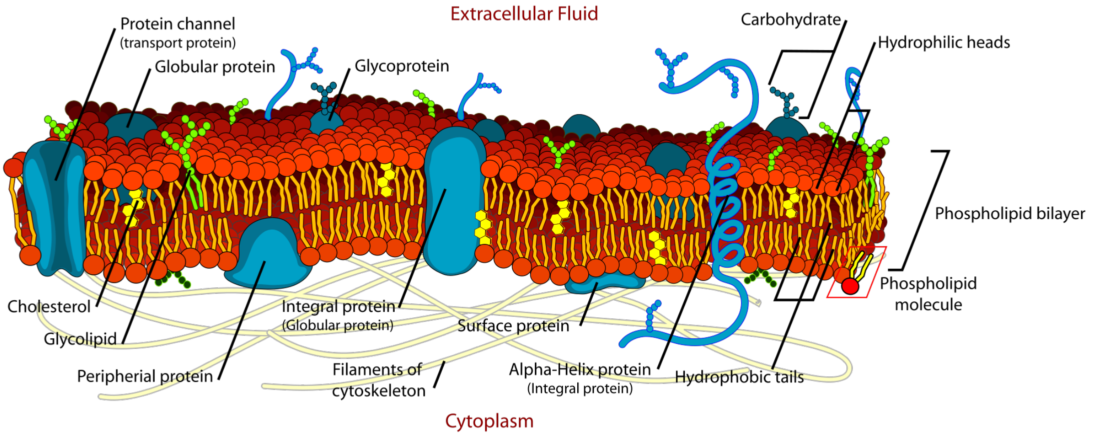
Extracellular Fluid
Protein channel
(transport protein)
Globular protein
Glycoprotein
Carbohydrate
Hydrophilic heads
Phospholipid bilayer
Phospholipid
molecule
Cholesterol
Glycolipid
Peripherial protein
Integral protein
(Globular protein)
Surface protein
Filaments of
cytoskeleton
Alpha-Helix protein
(Integral protein)
Hydrophobic tails
Cytoplasm

Figure 7.1 – Schematics of the architecture of the cell membrane. Taken from Wikipedia, credit to Mariana Ruiz.

There are three principal ways of passing through the membrane. It may be by diffusion, endocytosis or through a pore crossing the membrane. Diffusion happens for small, uncharged molecules such as oxygen and carbon dioxyde and also for hydrophobic molecules like lipids. Endocytosis consists in engulfing the outside material by the membrane which then forms into a vesicle that separates from the membrane and circulates inside the cell. The last manner, that interests us primarily, is through a pore in the membrane, which is the case for instance for water molecules. The pore is in fact a protein complex, whose structure and composition render it more or less selective. As an example of a pore membrane, we may cite the aquaporin. Aquaporin is a protein complex forming the pores for water molecules. Actually, in mammals, there is not one but four different aquaporins based on different protein structures. These different structures may allow for different selectivities in what may pass through the channel. The aquaporine channel may also respond to stimuli from external hormones or other molecules, leading to different rates and directions of water transport. In fact, on the cell membrane, these four aquaporin channels associate with each other so that in one location there are four possible passageways for water to move through the cell membrane. Also, it is generally assumed that the crossing frequency of water molecules through one pore is close to $10^9 s^{-1}$.

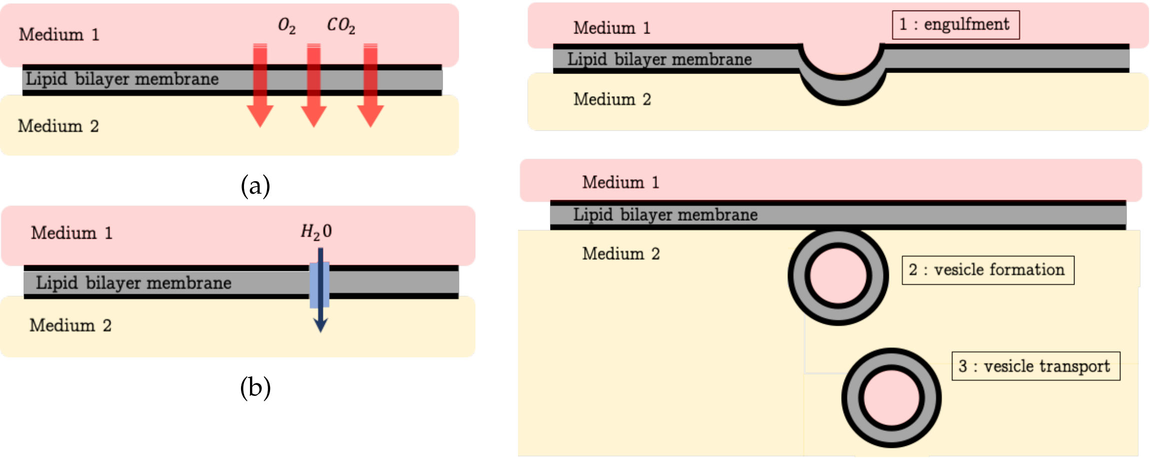

(a)

(b)

(c)

Figure 7.2 – Three pathways across the cell membrane, by (a) diffusion or (b) through a membrane pore (b) and (c) via endocytosis.

For eukaryotic cells, that is most of the cells of the human body, there is a second level of architecture within the cell. Indeed, the eukaryotic cell is constituted, besides its outer membrane, of a cytosol, a cytoskeleton and different organelles. In a few words, the cytosol is the internal fluid, the cytoskeleton is a network of tubules spanning the whole cell interior and the organelles are membrane bounded structure, *e.g.* the nucleus. A chemical reaction may be achieved in the membrane as well as in the cytosol or in an organelle. This chemical reaction may require reactants coming from either outside the cell or from another reaction that may have happened at a different site or not, while the products of this reaction may participate in another reaction or move outside the cell. This leads to an intense traffic within the cell as well as with its outside. This traffic is performed via two different types of motion [9], on one side diffusion in the cytosol and on the other side along the cytoskeleton network thanks to Brownian motors. Also, since the membrane bounded organelles participate in this set of chemical reactions, translocation of molecules through pores is thus required.

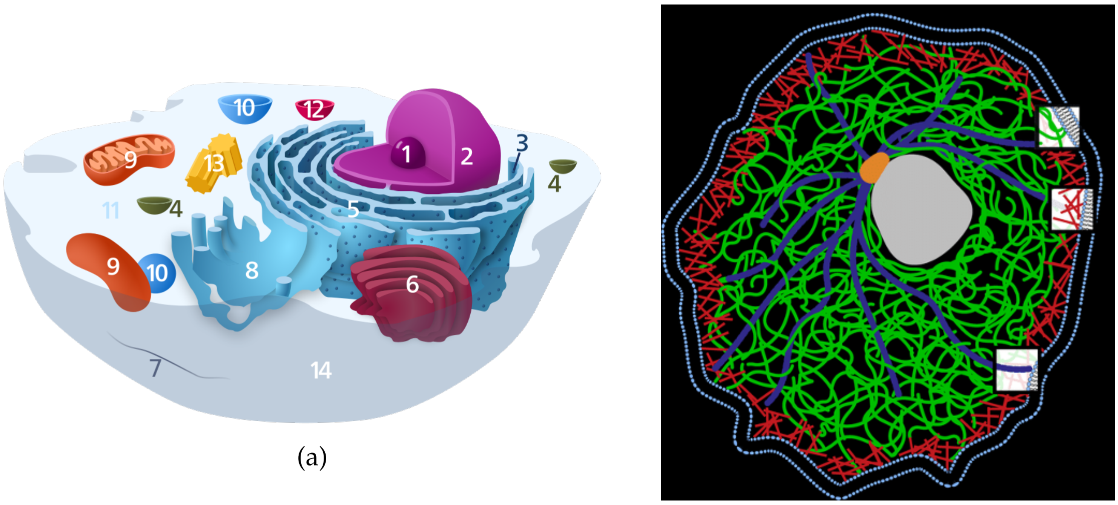

(a)

(b)

Figure 7.3 – (a) The internal structure of a prototypal animal cell: (1) Nucleolus (2) Nucleus (3) Ribosomes (4) Vesicle (5)Rough endoplasmic reticulum (6) Golgi apparatus (7) Cytoskeleton (8) Smooth endoplasmic reticulum (9) Mitochondrion (10) Vacuole (11) Cytosol (12) Lysosome (13) Centriole (14) Cell membrane. Taken from Wikipedia, credit to Kelvinsong. (b) A schematic of the cystoskeleton; in blue are the microtubules, in green intermediate filaments and in red actin filaments. Taken from [92].

Virus infection is another instance of translocation occurring in a cell worth mentionning. Indeed, a virus, in order to replicate itself, injects its genetic material inside a cell to highjack the cellular replication machinery[1]. To do so, there are two possibilities, either by endocytosis or through a pore in the membrane. While most of the viruses enter the cellular target by endocytosis, a certain type of virus, named bacteriophage for it infects bacteria, has evolved to use a special organelle, called a 'tail', for host recognition, attachment and genome delivery into the cell. We will discuss the case of the bacteriophage in a more detailled manner as an example and because it is considered to be the most numerous replicating biological entity on earth. Their number is estimated to be on the order of 10^{31}. Although most of these bacteriophages are unknown to us, we may categorize them according to their genetic material, whether it is DNA or RNA. These two categories may then be subdivided into single stranded or double stranded and agagin subdivided into linear or circular genomes. A bacteriophage may or may not possess a membrane. Yet another sorting is the pathway of genome internalization. From these 10^{31} bacteriophages an incredible diversity exists and thus we will not review all the differences one may encounter but rather detail the known properties of one type of bacteriophage, without any claim of generalization. Amongst the most studied bacteriophages is the bacteriophage T4 that infects the Escherichia Coli bacteria.

---

[1] Machinery it is itself lacking.

The bacteriophage T4 has a total length of around 200 nm and width 90 nm for a structure mainly made up of four elements. First is the head, referred as the capsid, containing the genomic material among proteins. Second, a 1200 Å long and 250 Å wide contractile tail sheath through which the genomic material will pass during cell infection. Third, the baseplate, actually an extension of the tail tube, is a dome-like structure that attaches the phage particle to the cell surface and acts as a plug for the genomic material. There is, at the center of the baseplate, a 10.5 nm long and 3.8 nm wide needle-like structure. The fourth element are the six long tail fibers that interact with the cell surface receptors.

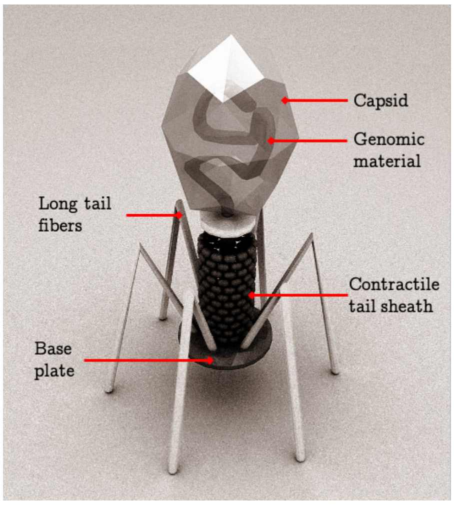

Figure 7.4 – Artistic rendering of the T4 architecture. Adapted from Wikipedia, credit to Oona Räisänen.

The common view on this bacteriophage infection is the following[2]. Once the virus is in contact with the bacteria, the long tail fibers interact with the cell surface receptors. These fibers bind and release randomly due to thermal fluctuations, leading to a walk of the virus on the outer bacteria membrane until a certain amount of them, thought to be three, are simultaneously bound. Thermal fluctuations are then ineffective to break the binding which becomes irreversible. Due to a conformation change in the long tail fibers or via thermal fluctuations, the baseplate reaches the bacterial membrane leading to a conformation switch from an hexagonal to a star conformation. Following this conformation change, the tail sheath contracts and drives the rigid tail tube through the membrane using the pointed needle that actually digests the peptidoglycan layer, creating an opening through which the tail tube can reach the cytoplasmic membrane of the host cell. The contact of the tail tube with the cytoplasmic membrane initiates the release of the phage DNA into the host.

---

[2] For more details, refer to *e.g.* [83, 95, 89].

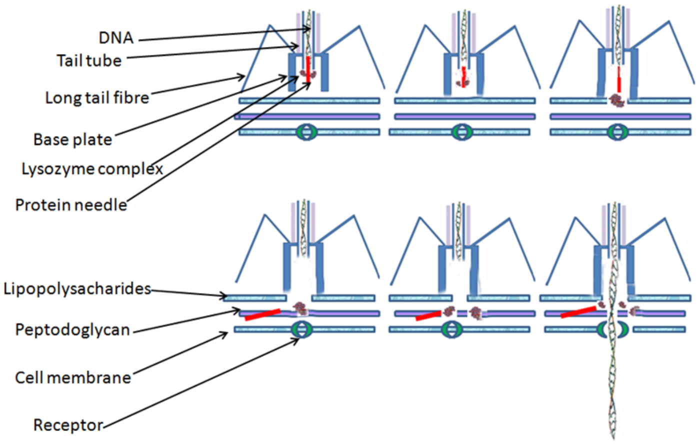
DNA
Tail tube
Long tail fibre
Base plate
Lysozyme complex
Protein needle
Lipopolysacharides
Peptodoglycan
Cell membrane
Receptor

Figure 7.5 – T4 injection into a cell. Taken from Wikipedia, credit to Dr. Graham Beards.

Once the genome of the virus inside the cell, its replication involves different parts of the bacteria as schematized in Fig.7.6.

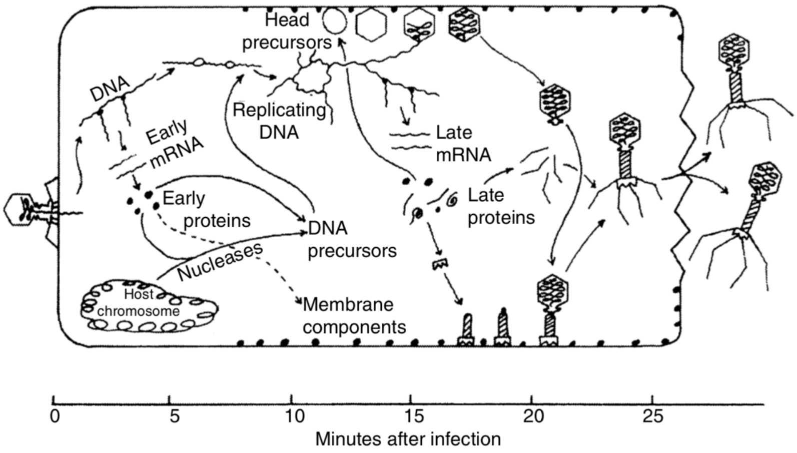
Head precursors
DNA
Early mRNA
Replicating DNA
Late mRNA
Early proteins
Late proteins
DNA precursors
Nucleases
Host chromosome
Membrane components
0
5
10
15
20
25
Minutes after infection

Figure 7.6 – T4 replication sequence. Taken from [83].

To summarize, polymer translocation is happening everywhere, at all times and in many different fashions.
As stated at the beginning of this introduction, our aim is not to study specific biological instances of polymer translocation but rather how a polymer translocates from a medium to another through a pore.

7.2 Experimental investigations of macromolecule translocation

Experimentally, measuring and observing translocation of macromolecules is rather challenging and demands very finely tuned equipment. In the 50’s, Coulter patented [24] a device to count the number of molecules in very dilute suspensions and estimate their size. This method of counting is based on the measure of the electric current resulting from an applied electric field between two chambers filled by an ionic solution and separated by a membrane. Hence, whenever a macromolecule is passing through the membrane, a drop in electrical current is measured, giving an indirect access to the molecule size and its translocation time, see Fig.7.7a. The device developped by Coulter was limited to particles of micrometric size but rapidly this technique was enhanced to be able to detect particles with sizes as small as dozens of micrometers [30]. Then, in the 70's, some teams were able to detect particles at the nanoscale and measure ionic flow across proteinic pores in synthetic lipid membranes [64] and biological membranes [94]. It is however only in the 90's, thanks to a Coulter-like device for molecular counting, see Fig.7.7b, that had been observed the first single-molecule[3] translocation [66].

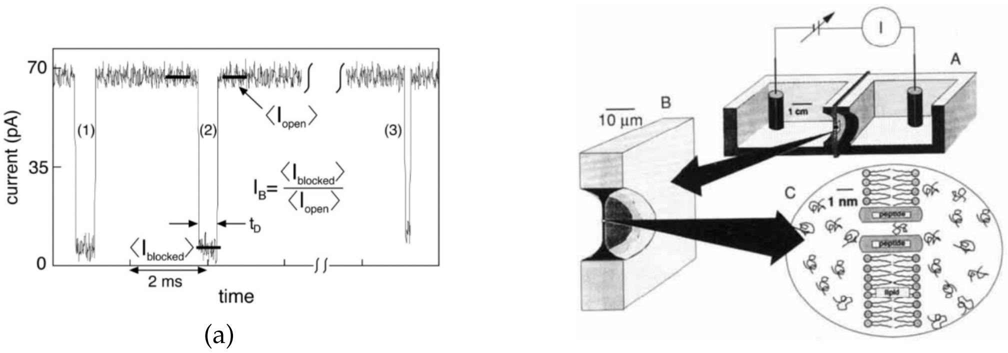
70
35
0
current (pA)
(1)
(2)
(3)
$\langle I_{open} \rangle$
$I_B = \frac{\langle I_{blocked} \rangle}{\langle I_{open} \rangle}$
t_D
$\langle I_{blocked} \rangle$
2 ms
time
I
A
B
C
10 µm
1 cm
1 nm
peptide
lipid

(a)

(b)

Figure 7.7 – (a) Examples of a "current blockade" caused by a polymer entering the pore and partly blocking the ions flows. Unsuccessful attempts of polymer translocation result in current blockades of very short durations see *e.g.* (3) as opposed to (1) and (2). Taken from [88]. (b) Schematic representation of the device allowing measurement of macromolecule translocation. Taken from [14].

7.3 Two modes of translocation

In our study, we focused on two types of translocation : free translocation, as in Fig. 7.8a & 7.8b, and translocation of a polymer confinemed in a cavity, Fig. 7.8c & 7.8d. We restrict our investigation of free translocation to a linear chain set halfway across a wall through an opening pore of size d smaller than two monomer diameters. This translocation is said free because the only interactions considered are between the monomers of the chain and the wall. In the case of a self-avoiding chain, we also consider interactions between monomers.

For the second case, a chain is confined in a cavity with an opening pore of the same size.

---

[3] In the case in point, a single stranded ARN and ADN molecules.

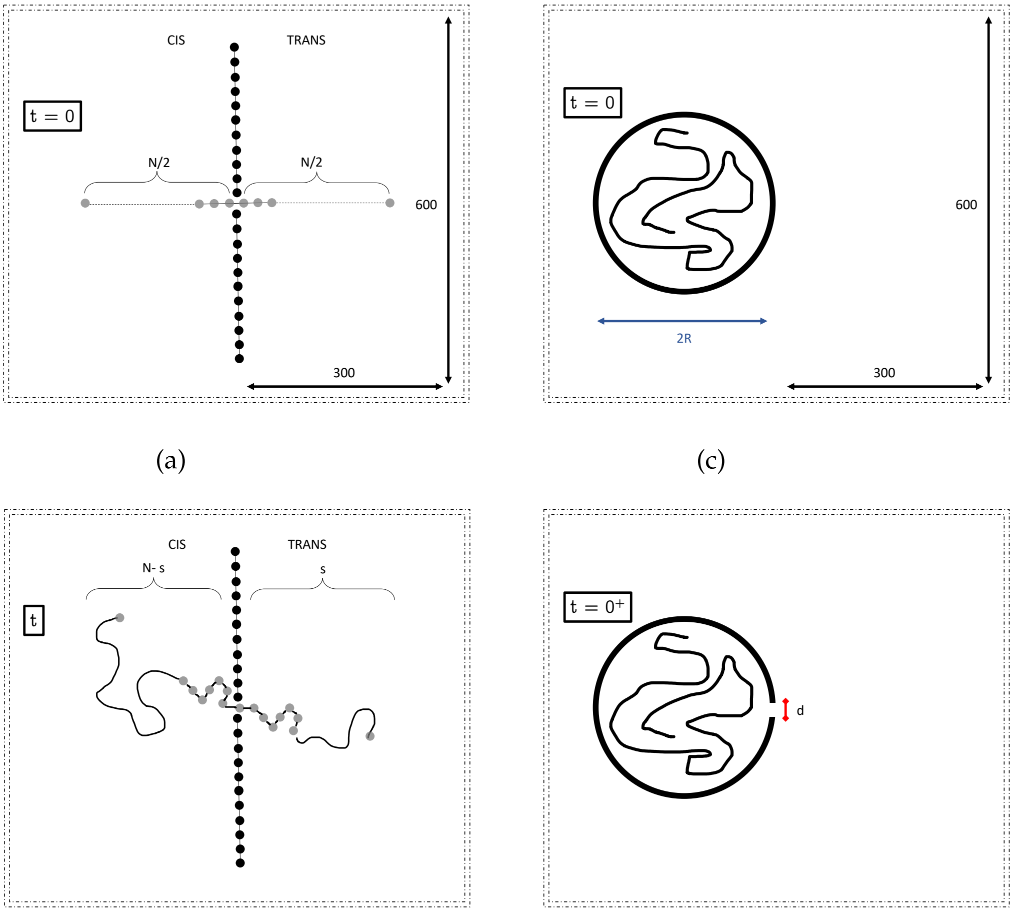

(a) (c)

(b) (d)

Figure 7.8 – Free translocation: (a) initial configuration and (b) at later times ; Translocation outside a cavity: (c) cavity initially closed until equilibrium is reached then (d) an opening is created.

7.3.1 Description of the simulation

The simulations are performed with LAMMPS, a classical molecular dynamics code. LAMMPS is the acronym for Large-scale Atomic/Molecular Massively Parallel Simulator. It is distributed as an open source code under the terms of the GPL by Sandia National Laboratories, a US Department of Energy laboratory. According to its developers, *LAMMPS has potentials for solid-state materials (metals, semiconductors) and soft matter (biomolecules, polymers) and coarse-grained or mesoscopic systems. It can be used to model atoms or, more generically, as a parallel particle simulator at the atomic, meso, or continuum scale.*
It is thus a very powerful tool.
In our case, the simulations are constrained to 2D. All the units are Lennard-Jones (LJ) units, defined from the LJ potential below. All distances are given compared to the size

of a particle, set to 1. The simulation box is a square of size 600 with periodic boundary conditions. The box is divided in two equal sub-boxes by a wall. This wall is made of frozen particles of size 1 that interact with the other particles in the simulation via a purely repulsive truncated LJ potential:

$$U_{LJ}(r) = \begin{cases} 4\epsilon[(\sigma/r)^{12} - (\sigma/r)^{6}] + \epsilon & \text{if } r \leqslant 2^{1/6}\sigma, \\ 0 & \text{if } r > 2^{1/6}\sigma, \end{cases} \tag{7.1}$$

where r is the distance between two particles, σ the diameter of the particle (in our simulation $\sigma = 1$) and ϵ is the parameter adjusting the depth of the potential (in our simulation $\epsilon = 1$).

The polymer is modeled as a linear bead-and-spring chain. To go beyond this modelization of an ideal chain, we add a repulsive LJ interaction between unconnected beads, as given by Eq.7.1,to take into account excluded volume interactions.

The pairs of beads are bonded by a finite extension nonlinear elastic (FENE) potential:

$$U_{FENE}(r) = -\frac{1}{2}kR_0^2 ln\Big(1 - \frac{r^2}{R_0^2}\Big) \tag{7.2}$$

where r is the distance between two bonded particles, k is the spring constant (in our simulation $k = 30$) and R_0 the maximum allowed separation between two bonded particles (in our simulation $R_0 = 1.5$).

To avoid an explicit description of the solvent molecules, the dynamics is obtained by solving the Langevin equations of motion for every beads in our chain:

$$m\ddot{r}_i = F_i^C + F_i^F + F_i^R \tag{7.3}$$

where m is the mass of the bead i (in our simulation $m = 1$), F_i^C is the resultant of conservative forces (LJ and FENE), $F_i^F = -\xi v_i$ is the dissipative force due to friction[4] (in our simulation $\xi = 0.5$) and F_i^R the random force whose first and second order moments are:

$$\begin{cases} \langle F_i^R \rangle = 0, \\ \langle F_i^R(t) F_i^R(t') \rangle = 6k_B T \xi \delta_{ij} \delta(t - t'). \end{cases} \tag{7.4}$$

where the amplitude of the second moment is provided by the fluctuation-dissipation theorem.

The results presented here are obtained from 500 runs; if occasionnaly fewer runs are performed then it is indicated.

---

[4] In our simulation, the solvent is said implicit because reduced to its mean effect.

7.3.2 Free translocation

The ″free translocation″ can be considered as a thought experiment. The chain is only subjected to thermal fluctuations, frictional drag, elastic forces from adjacent segments and interactions with the membrane/pore. Thus, if the chain is fully on one side of the membrane, the odds that it translocates across the membrane are very small. In our case, the initial configuration of the chain is mid-translocation. That is, if the chain consists of N monomers, there are $N/2$ monomers on one side and $N/2$ on the other side. This initial configuration is very unlikely to spontaneously happen. Actually, it has been shown [93, 54, 110], that the probability for an end monomer of a self-avoiding chain to enter the pore scales as $N^{-1.48}$, under the assumptions of equilibrium. It is therefore clear that for long chains this probability of introducing the first monomer inside the pore drastically drops to zero.
Usually, to distinguish the two sides, people call ″trans″ the side towards which the translocation is achieved and ″cis″ the other one. Even though in our case both sides are equivalent, the side on the left will be named ″cis″ and the one on the right ″trans″.
In the first set of simulations, the initial configuration was a straight chain as on Fig. 7.8a. Later on, because this might induce a bias, a second set of simulations was performed but with an initial configuration that was first equilibrated. This equilibrated configuration was obtained by blocking the monomer located at the middle of the chain for a time larger than the relaxation time, before releasing it. In comparing the two methods, no significant impact on the results has been measured.

Is translocation really happening ?

A first question we may ask is whether translocation is happening or not. Indeed, the chain may well be in a favorable configuration and mildly fluctuates halfway through the opening. Actually, the chain is translocating and we may see it in two distinct ways.
First and classically in this type of problem, the measured quantity is the index of the monomer that is located at the opening of the wall at any time. This quantity is, of course, equivalent to the number of monomers that are on the trans side, if the monomers are numbered in ascending order from trans to cis.
Figure 7.9a shows ten runs of the translocation for a $N = 54$ long chain. At time $t = 0$, the chain is halfway on both sides ($s = 27$) and at the end of the simulation the chain is either translocated on the cis side ($s = 0$) or the trans side ($s = 54$).
These curves are reminiscent of those of a $1D$ random walk with symmetric absorbing boundaries.

Another insight into the phenomenon of translocation is the probability distribution of the position of the chain's center of mass, as depicted in Fig. 7.9b. Indeed, if the chain was to be in a favorable configuration the distribution would be a Gaussian centered around the pore location. It turns out that for short times the chain is preferentially lo-

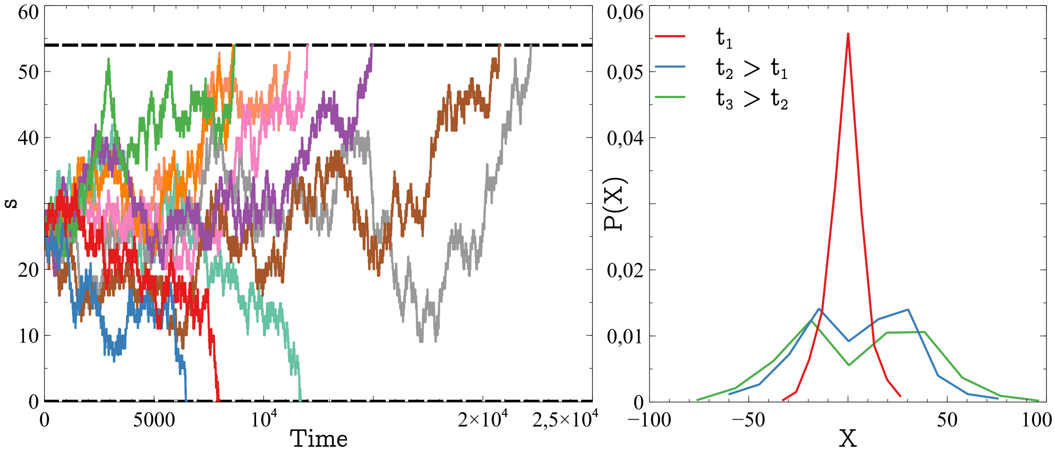

(a) (b)

Figure 7.9 – (a) Time evolution of the number of translocating monomers for a self-avoiding chain long of 54 monomers. Translocation ends when $s = 0$ or $s = 54$, figurated by the black dashed lines. (b) Probability distribution of the position of the center of mass of the chain at three different times for a self-avoiding chain long of 74 monomers. At first the probability is centered around the origin, then gradually a hole in the distribution appears at the origin, due to the translocation.

cated at the pore but for longer times, the chain leaves the pore to be on either side of the wall. This effect can be related to the entropic penalty of a constriction.

Translocation dynamics

As clearly noticeable in Fig. 7.9a, time averaging the previously defined quantity s would not yield any relevant outcome for two reasons. First because the chain translocates with equal probability on both sides of the wall, hence for an infinite number of runs the average would be half the length of the chain. Secondly, because each translocation process occurs with a different finite amount of time, the time averaging is inoperative. A workaround to this problem is to discretize time. To do so, we consider another quantity, the mean waiting time for a monomer. The waiting time corresponds to the total count of monomer crossings through the membrane. From the results displayed in Fig. 7.10, we recover the fact that both sides are equivalent, the waiting time being symmetric. Thus, we can, without any loss of generality, study the translocation of only half the chain. Also we may notice that this waiting time depends on the monomer position in the chain. The waiting time for the mid monomer is much longer than the one for an end monomer.

Finally, instead of looking at $s(t)$, the evolution of the number of monomers on one side with time, we are interested in $x(t) = s^*(t) - N/2$ where $s^*(t)$ is the inverse of the cumulative waiting times. The overall aspect of the curves for the ideal and the self avoiding chains in Fig. 7.11 is the same, even though we may notice that the process of translocation is slower for self-avoiding chains than for ideal ones.

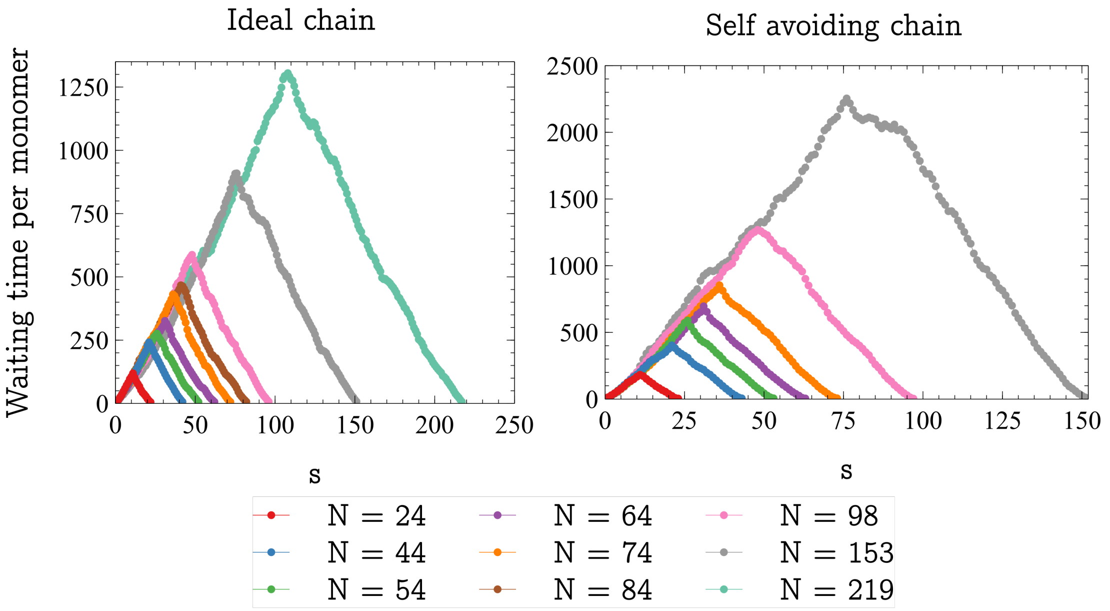

Figure 7.10 – Waiting time for ideal and self avoiding chains of different lengths. Whatever the chain length, the longest waiting time corresponds to the translocation of the mid monomer. For each chain length, the waiting time for an ideal chain is shorter than the one for a self-avoiding chain.

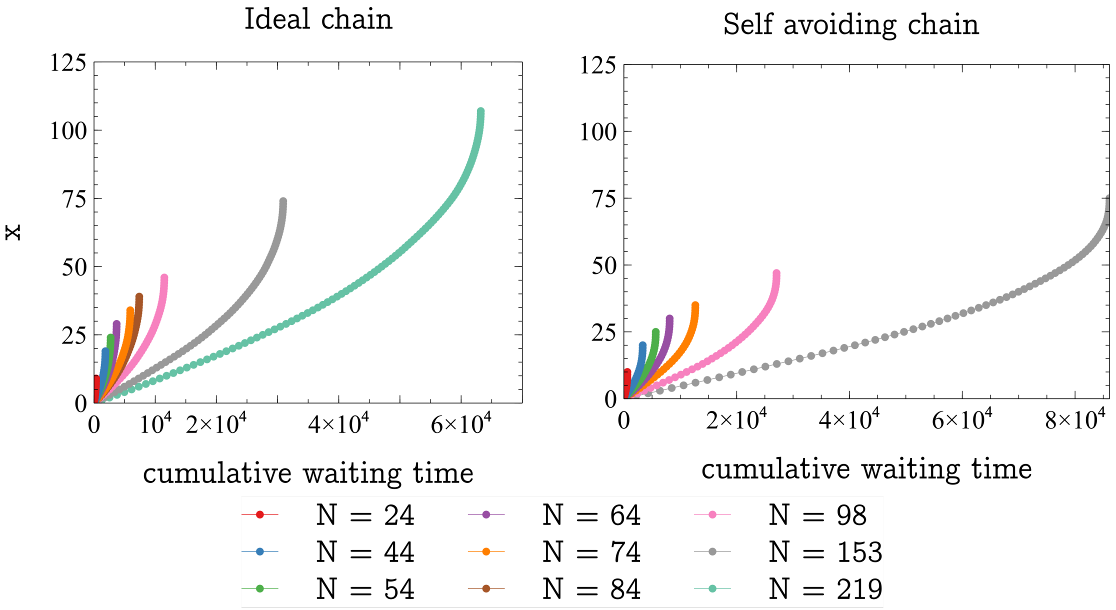

Figure 7.11 – Time evolution of the scaled monomer index $x(t) = s^*(t) - N/2$ in the pore for ideal and self-avoiding chains of different lengths.

Total translocation time

Another quantity of interest is the translocating time, whether on the trans or the cis side (the time required for the full chain to go through the membrane). Fig. 7.12a shows that the translocating time strongly depends on the index of monomers, following different power laws for ideal and self-avoiding chains.

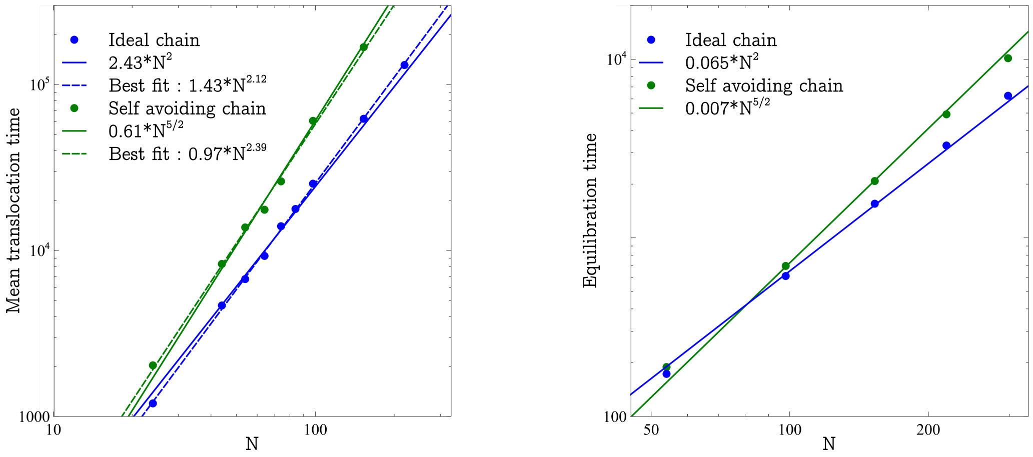

(a) (b)

Figure 7.12 – (a) Mean translocation time and (b) Mean equilibration time for ideal and self-avoiding chains of different lengths. The solid line curves are obtained via a power law best fit with the exponent already chosen while the dashed line curves corresponds to a power law best fit with the exponent as a fitting parameter.

The best fits with power laws yield exponents of 2.12 and 2.39 for ideal and self-avoiding chains, respectively. These values are reminiscent of the equilibration time of a chain in the Rouse model:

$$\tau_R \sim N^{1+2\nu} \begin{cases} N^2 & \text{ideal chain in 2D,} \\ N^{5/2} & \text{self-avoiding chain in 2D,} \end{cases} \tag{7.5}$$

where ν is the exponent giving the RMS end-to-end distance, $R \sim aN^\nu$ (1/2 and 3/4 for ideal and self-avoiding chains in 2D).

In spite of the exponent similarity, it is however odd to compare translocation times to the equilibration times of Rouse chains. Indeed, one might expect the former to be much longer than the latter due to the friction imposed by the pore in the wall. For comparison, simulations of bare chain relaxations are performed. The obtained Rouse times are shown in Fig. 7.12b. It turns out that the Rouse time, even though having the same scaling law, is indeed smaller than the translocation time by more than an order of magnitude (the ratio of both prefactors is approximately 50).

One might also question why the translocation time should be compared to the Rouse time at all. What is the connection between these two quantities, if any ? Furthermore, if we try to rescale the previously obtained time evolution of $x(t)$ to obtain a master curve, the outcome is not very satisfactory. The Fig. 7.13 represents the evolution of $x(t)/N$ with respect to time divided by N^{α} with $\alpha = 2$ for an ideal chain and $\alpha = 2.5$ for a self-avoiding one.

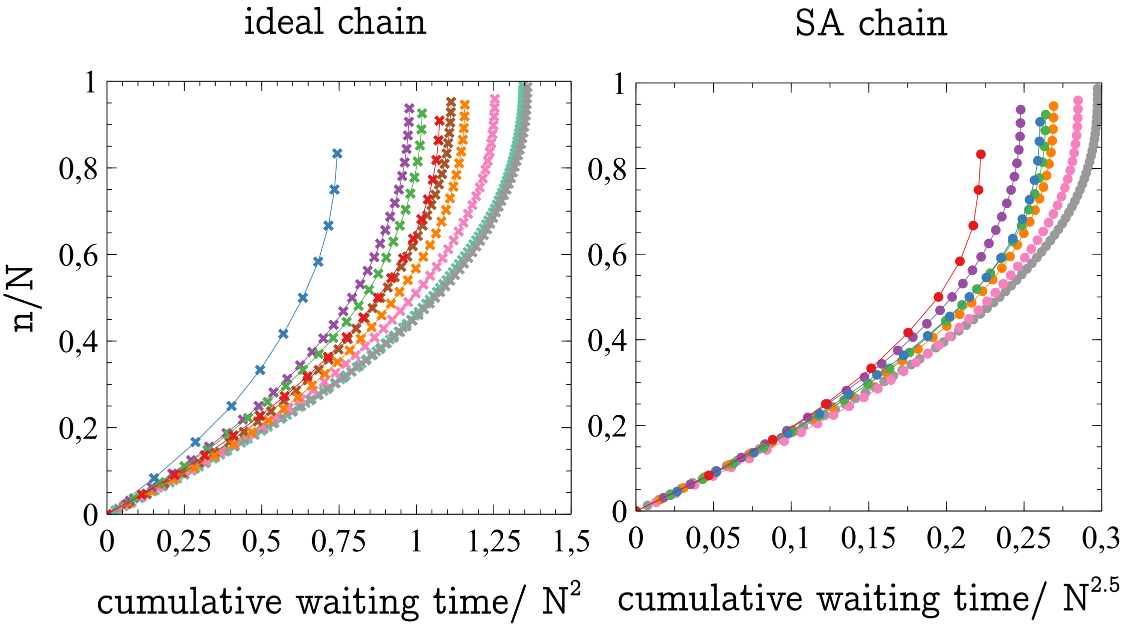

Figure 7.13 – Normalized time evolution of the rescaled monomer index in the pore for ideal and self-avoiding (SA) chains of different lengths.

Is this seemingly correspondance between the translocation time and the Rouse time just a coincidence ? In the literature, see Tab.7.1, one may find a rather wide range of power laws (still 2.5 in 2D for a self-avoiding chain) describing the mean translocation time.

According to:	α value	Model
[22]	2.5	2D MC
[79]	2.50 ± 0.01	2D BFM
[124]	2.51 ± 0.03	2D bead-spring MD
[65]	2.48 ± 0.07	2D FENE MD
[21]	2.5	2D BFM
[80]	2.44 ± 0.03	2D GROMACS
[101]	$2 + \nu = 2.75$	2D
[101]	$2 + \nu = 2.588$	3D
[80]	2.22 ± 0.06	3D GROMACS
[124]	2.2 ± 0.03	3D bead-spring MD
[36]	2.52 ± 0.04	3D FENE MD
[60]	2.516	3D FENE MD
[38]	2.516	3D FENE MD

Table 7.1 – Recapitulative table of the power law exponents in the litterature regarding the mean translocation time. Different models have been used: MC = Monte Carlo simulations; BFM = bond fluctuation model; bead-spring MD: molecular dynamics with bead-spring model for the bonds; FENE MD: molecular dynamics with FENE bonds; GROMACS: MD software.

Distribution of translocation times

Another way to look at these translocation times is to study their probability distribution. According to Chatelain *et al.* [21], with which our results on Fig. 7.14 agree, the exponential decay of the probability density function (PDF) for large translocation times T indicates that the translocation time cannot follow a power law nor a stretched exponential behavior.

This discussion on the distribution tails may be put into perspective with the Langevin formalism for a 1D random walk. Indeed, free translocation can be seen as a random walk with two absorbing boundaries and we can compare it to a random walk with only one absorbing boundary.
We performed numerical simulations of overdamped Langevin stochastic differential equations:

$$\xi \dot{x} = \eta(t) \tag{7.6}$$

where ξ is the damping coefficient and $\eta(t)$ the fluctuating force.
As shown in Fig. 7.15, completely different distributions are obtained for one and two absorbing boundaries. While a power law decay is observed for a single absorbing barrier, an exponential cutoff appears for the system with 2 symmetric absorbing barriers.

Let us derive an analytical expression of the distribution $P(T, L)$ for a random walker to reach the origin at time T, its initial position being L, in one dimension. To do so, we have to calculate the probability density $p(x, t|L)$ of the walker to be located at x after a time t, starting from the position L and under the absorbing condition $p(0, t|L) = 0$. This

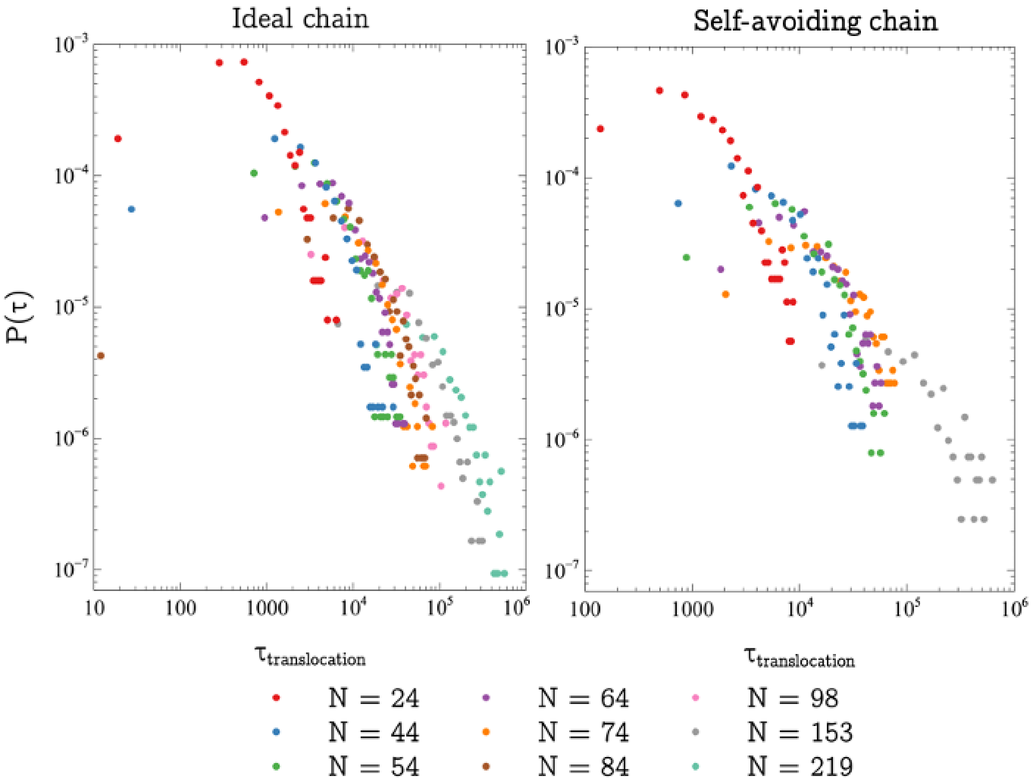

Figure 7.14 – Distribution of translocation times for ideal and self-avoiding chains of different lengths.

probability p actually verifies the diffusion equation:

$$\partial_t p(x,t) = D\partial_x^2 p(x,t) \tag{7.7}$$

with D the diffusion coefficient and the conditions:

$$\begin{cases} p(x,0|L) = \delta(x-L) & \text{initial condition} \\ p(0,t|L) = 0 & \text{boundary condition} \end{cases} \tag{7.8}$$

This can be solved using the method of images, which consists in considering a mirror particle initially located at $-L$ so that the conditions for the diffusion equation become:

$$\begin{cases} p(x,0|L) = \delta(x-L) - \delta(x+L) & \text{initial condition} \\ p(0,t|L) = 0 & \text{boundary condition} \end{cases} \tag{7.9}$$

Under these conditions, the probability density p is the combination of two Gaussian distributions:

$$p(x,t|L) = \Big(4\pi Dt\Big)^{-1/2}\Big(\exp(-(x-L)^2/4Dt) - \exp(-(x+L)^2/4Dt)\Big) \tag{7.10}$$

Finally, the target probability density P corresponds to the flux at the origin:

$$P(T,L) = D\partial_x p|_{x=0} = L\Big(4\pi D\Big)^{-1/2} T^{-3/2} exp(-L^2/4DT) \tag{7.11}$$

effectively yielding a power law decay at long times, which is recovered from our Langevin simulations, see Fig.7.15a.
To our knowledge, there is no exact derivation for the two absorbing boundary problem.

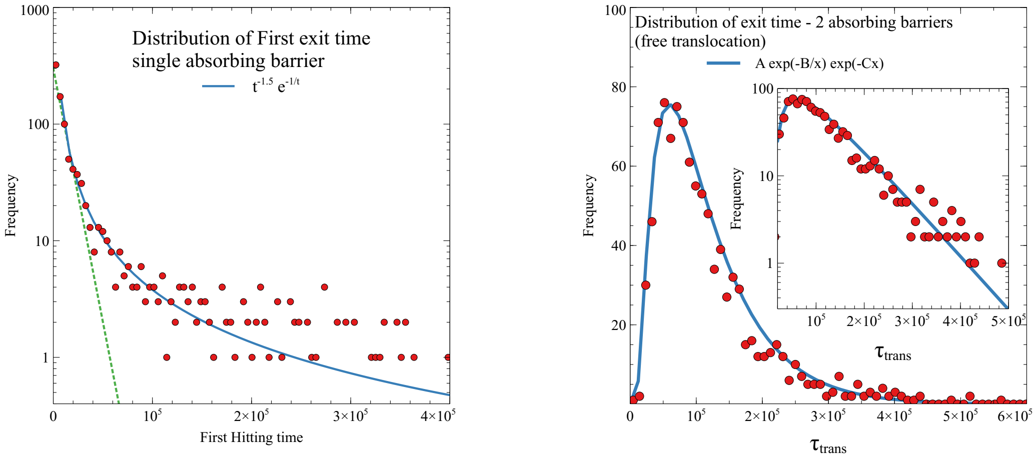

(a) (b)

Figure 7.15 – Results from numerical solutions of Langevin equations for a 1D random walk with (a) 1 or (b) 2 absorbing boundaries.

The observation of unusual distributions of translocation times with an exponential cutoff is therefore not a clue to understand the evolution of the translocation with the chain length.

Pore size effects

In our study, we limited ourselves to a single type and size of pore, set so that only one monomer can cross the wall at a time. We also chose to set the same interactions between the wall and the monomers as in between the monomers of the chain. Yet, in a broader context, the pore characteristics are bound to play a crucial role. In vivo, the careful design of the pore imparts its finely tuned selectivity toward chemical species. As to the comparison between the pore size and the monomer size, it has been shown in [59] that the pore size strongly affects the scaling exponent for the translocation time. Obviously, the bigger the opening the more there are monomers at a time in the pore and the previously used approach on the monomer index breaks down. When the pore size is much bigger than the radius of gyration of the polymer, bulk diffusion is expected.

7.3.3 Confined translocation

Another instance of translocation, related to ejection of genetic material from a bacteriophage to a cell, consists in a chain initially confined inside a circular cavity and translocating to an unlimited volume. In vivo, there can be multiple sources driving the ejection of the polymer chain outside the capsid ranging from osmotic pressure to bare hydrostratic pressure. However, since it is still unclear what the contributions of the different pressures to the overall mechanism of translocation are, we studied a simpler problem and only considered entropy-based pressure due to confinement. To tackle this question, we employed the same molecular dynamics simulations with the same parameters for the particles interactions except that we did not consider the case of an ideal chain.

Translocation dynamics

A confined chain faces two opposing traits. On one hand, the polymer pervaded volume is smaller than the equilibrated one, the chain is in an entropically unfavorable state. On the other hand, to escape this unfavorable state, one of the chain ends needs to ”find” the opening pore, a very low probability event. Even though the excluded volume interactions tend to make it more probable. Unlike free translocation, translocation of confined chains is bound to happen towards a single direction. The problem is not symmetric anymore and the number of monomers to be translocated corresponds to the total length of the chain. Also, the cavity radius over the radius of gyration determining the degree of confinement is the control parameter to consider. In order to describe the translocation process we may want to slice it into different parts. The first one being the time needed to find the opening pore and the second one the translocation itself. For now, we discard the problem of finding the hole by forcing the location of one chain end in the pore. In Fig. 7.16a, we can see that the dynamics of the translocation due to confinement greatly differs from free translocation. Indeed, while for free translocation we could see an acceleration of the process, confinement driven translocation is actually slowing as the chain gets outside the cavity. This could be interpreted as a consequence of the gradual decrease in effective confinement. Fig. 7.16a also shows the drastic influence of the radius of the cavity, i.e. the degree of confinement, on the mean translocation time.

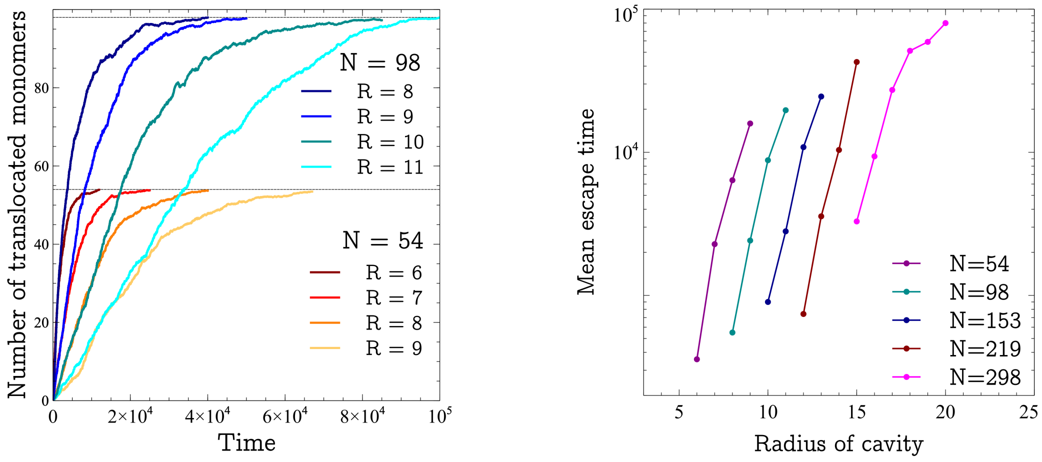

(a) (b)

Figure 7.16 – (a) Time evolution of the number of monomers translocating for two self-avoiding chains of different lengths and for different cavity radii. (b) Mean escape time of a self-avoiding chain, with different lengths, out of a cavity, with different radii.

Rescaled translocation time

The mean escape time should be determined by the number of monomers and the degree of confinement, $\tau \sim N^{\alpha}F(R/R_{\mathrm{F}})$, where F represent an unknown function. A natural rescaling of the mean escape time consists in dividing the radius of the cavity by the typical polymer size at equilibrium, $R_{\mathrm{F}} \sim aN^{3/4}$, as in Fig. 7.17a. The data remains however scattered since the dependence of the escape time in N is not considered yet. All the data collapse on a single curve by dividing the mean escape time by the number of monomers to the power 4, see Fig. 7.17b. The observed rescaling suggests that the mean escape time scales as $\tau \sim N^{4}F(R/R_{\mathrm{F}})$. The dependance in the degree of confinement, $F(R/R_{\mathrm{F}})$ seems to be complex and cannot be described with a simple power law.

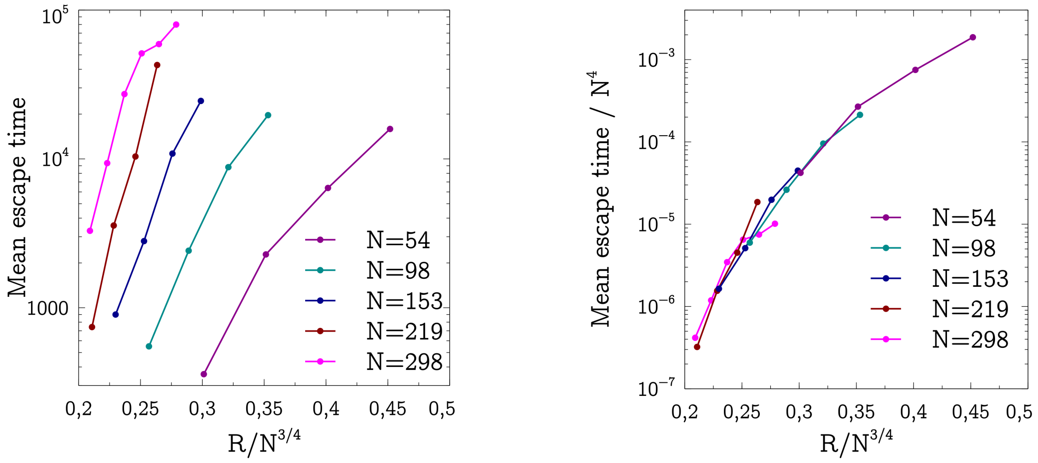

(a) (b)

Figure 7.17 – (a) Mean translocation time with respect to the rescaled radius of cavity $R/N^{3/4}$. (b) Empirical attempt to rescale the mean escape time by N^4.

Cavity shape influences

The shape of the cavity is a parameter not investigated in our work but still worth mentioning for practical applications. Even though many viruses have icosahedral enveloppes, there are instances where the capsid is elongated as a prolate, which is the case for bacteriophages, or even conical, as for the HIV capsid [89].
It has been shown in [2] that for flexible polymers a spherical shape of the capsid, compared to an ellipsoidal shape, leads to a quicker packaging of the genetic material inside the capsid but a slower ejection. However, for semi-flexible polymers such as DNA the spherical shape expedites both packaging and ejection. Ejection, being the inverse problem of translocation is another aspect not covered in our work however it is interesting for technological and biological purposes.

Chapter 8

Free translocation mechanisms

As outlined in the previous chapter, free translocation is determined by the number of monomers in the chain. In spite of a clear and reproducible power law dependency of the mean translocation time with the chain length, a consensus on the modelisation of this behaviour is still lacking in the literature. According to [102], this has led to *what is colloquially known to researchers in this field, "an exponent war"*. In the following two sections, we will describe the two main paths of modelisation and point out their respective strengths and shortcomings.

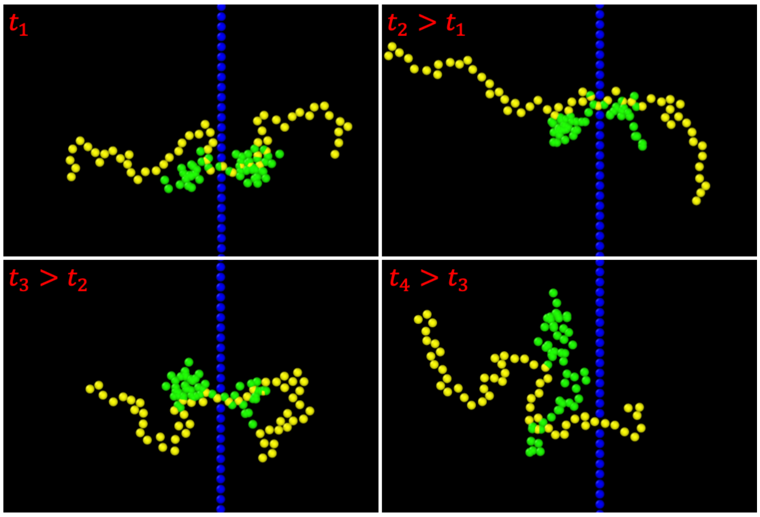

Figure 8.1 – Snapshots of the the translocation process of an ideal chain and a self-avoiding one as per our simulations. The blue beads stand for the wall particles, the green particles are related to the ideal chain and the yellow ones to the self-avoiding chain.

Let us recall one of the most important observations, the exponent describing the mean translocation time depends on the nature of the chains. An example is shown in Fig.8.1, where at time t_4 the ideal chain has already translocated while the self-avoiding one is still across the wall. Different exponents are reproducibly observed for ideal, self-avoiding 2D and self-avoiding 3D chains. These observations bring a drastic constraint on the translocation mechanisms since any valid theoretical model should thus be able to reproduce this behaviour.

8.1 Sung and Park's theoretical approach

The first approach, laid out by Sung and Park in [119], consists in a coarse-grained vision of the translocation process. Indeed, the single quantity of interest is the monomer located at the pore and the single interaction is the one between the monomers and the wall, which is purely repulsive. Therefore, the translocation problem is boiled down to a stochastic process of a particle crossing a free energy barrier and the translocation time is transcribed as the mean first passage time over this barrier.

8.1.1 Derivation of the potential – End-to-end distance distributions

The first step to get the entropic penalty on a translocating chain crossing a pore in a repulsive wall is to determine the associated conformation changes. Translocation is obviously an out-of-equilibrium process but an insight to this problem can be obtained from the MD simulation of a free chain and an equilibrated chain tethered to a surface, illustrated in Fig.8.2.

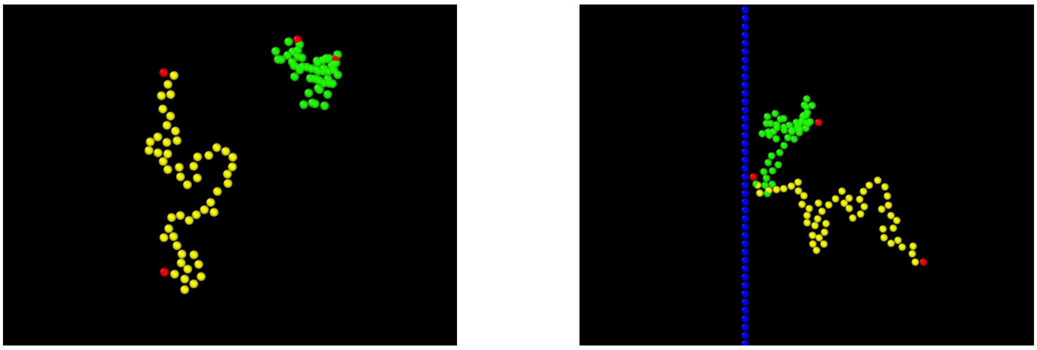
(a) (b)

Figure 8.2 – Illustration of the different conformations adopted by an ideal (in green) and a self-avoiding (in yellow) chain with 54 monomers whether (a) free or (b) tethered to a wall. The wall is made of the blue particles and the red particles are the end monomers of the chains.

Figure 8.3 shows the end-to end probability distribution computed from MD simulations. For each chain's length, the results are the average over 500 runs with a straight chain as initial configuration and enough timesteps to reach an equilibrated configuration[1]. We clearly see how the repulsive excluded volume interactions between monomers tend to ”swell” the chain whether free or fixed. Also, we can observe a ”swelling” effect due to the anchoring of the chain whether ideal or self-avoiding.

---

[1] We checked the mean end-to-end distance to scale as theoretically expected $\sim N^{\nu}$

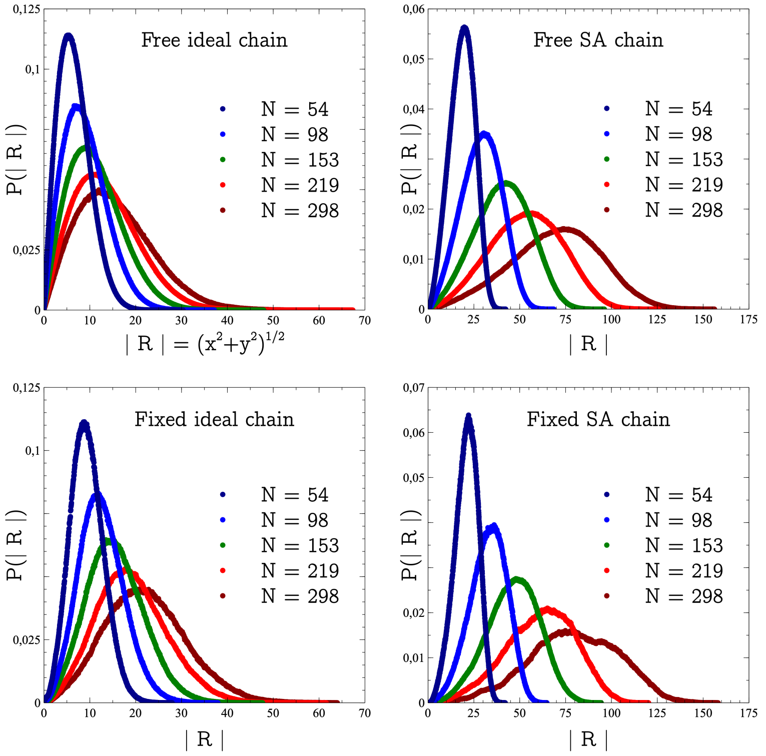

Figure 8.3 – Probability distributions of end-to-end distance for free (left column) and fixed (right column) ideal (top row) and self-avoiding (bottom row) chains.

Modelisation of distributions for end-to-end distance

One would assume such distributions to be understood and described since almost a century. While this statement is true for a free ideal chain, the self-avoindingness of a random walk yields inextricable mathematical difficulties. The results below may be found in [55]. For the sake of generality, we assume the existence of a function ϕ so that the end-to-end vector $\underline{R}$ distribution is given by:

$$P_N(\underline{R}) \sim \frac{1}{R_0^d}\phi\left(\frac{\underline{R}}{R_0}\right) \tag{8.1}$$

where R_0 is the characteristic size of the chain at equilibrium and d is the number of space dimension.

The prefactor $1/R_0^d$ appears as a result of the normalization condition. For sake of simplicity and since we only investigate 2D chains, we set $d = 2$ in the following. The distribution of end-to-end distance $P_N(|\underline{R}|)$ is directly obtained after integrating over all orientation θ in polar coordinates $(|\underline{R}|, \theta)$:

$$P_N(|\underline{R}|) \simeq \int_\theta d\theta |\underline{R}| P_N(\underline{R}) \sim \frac{|\underline{R}|}{R_0^2}\phi\left(\frac{|\underline{R}|}{R_0}\right) \tag{8.2}$$

For an ideal chain, the function ϕ is the well known Gaussian, thus:

$$P_N^{ideal}(|\underline{R}|) \simeq \frac{1}{R_0}\frac{|\underline{R}|}{R_0}\exp\left[-\left(|\underline{R}|/R_0\right)^2\right] \tag{8.3}$$

We can easily verify this result through our MD simulations, see Fig. 8.4. The end-to-end distance distribution is well fitted by the theoretical predictions and the $R_0 \sim N^{1/2}$ scaling law for the characteristic size of an ideal chain at equilibrium is obtained.

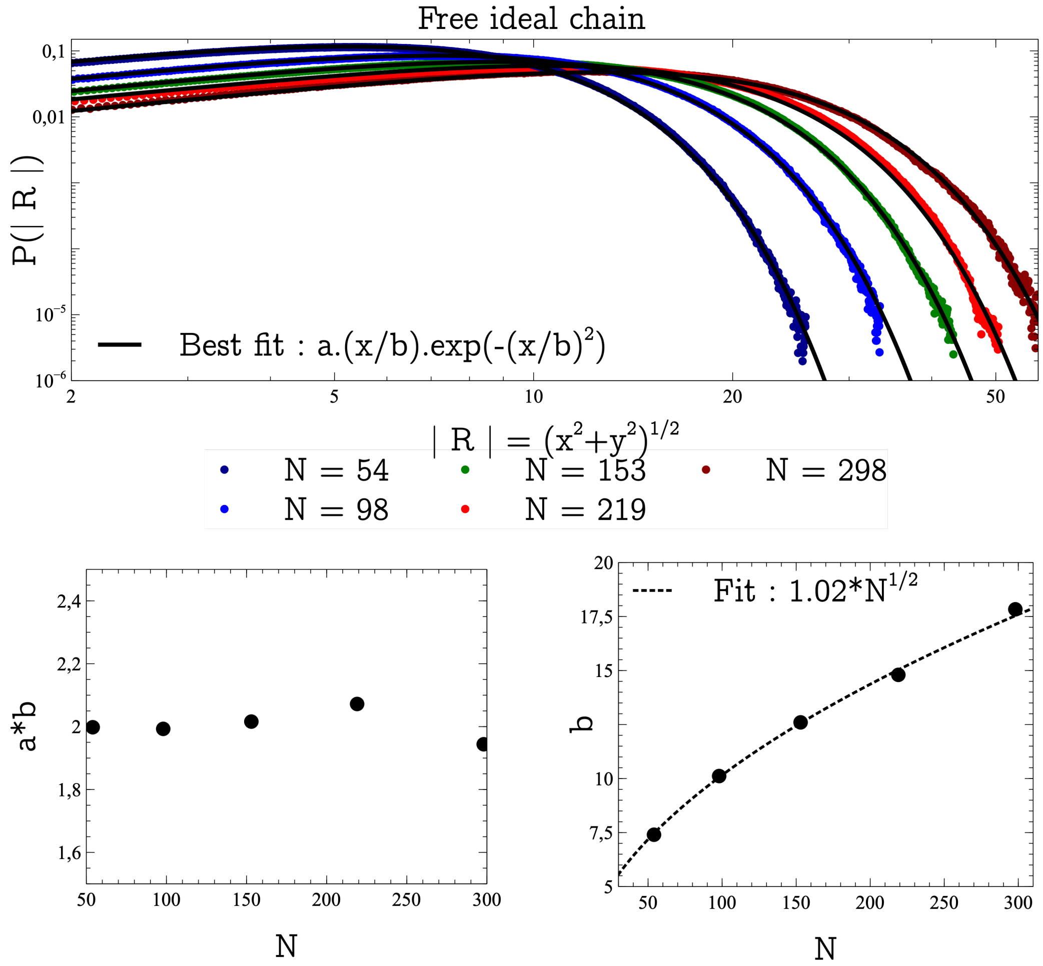

Figure 8.4 – Probability distribution of the end-to-end distance for an ideal chain, freely evolving in 2D. In the upper pannel the black solid curves are a best fit with the function $a(x/b)\exp(-(x/b)^2)$, where a and b are the fitting parameters. The bottom left pannel represents the evolution of the product ab and the bottom right pannel the evolution of b with the chain length N.

For a self-avoiding chain, there is a significant difference with an ideal chain at short end-to-end distances. Indeed, the excluded volume interactions tend to swell the self-avoiding chain. In order to circumvent this problem, one may consider, as in [55], the asymptotic limits of short and long end-to-end distance and bridge the two behaviours in the following fashion:

$$\begin{cases} \phi(x) \sim x^g \text{ when } |x| \ll 1, \\ \phi(x) \sim e^{-x^\delta} \text{ when } |x| \gg 1. \end{cases} \tag{8.4}$$

with $g = (\gamma - 1)/\nu \approx 4/9 \quad (\gamma \approx 4/3$ and $\nu = 3/4$ for 2D chains) while $\delta = 1/(1 - \nu) = 4$.
Combining both asymptotic regimes, the function ϕ may be written as:

$$\phi\Big(\frac{|\underline{R}|}{R_0}\Big) = \Big(\frac{|\underline{R}|}{R_0}\Big)^{4/9} \exp\left[-\Big(\frac{|\underline{R}|}{R_0}\Big)^4\right] \tag{8.5}$$

Finally, the end-to-end distance distribution for self-avoiding chains is given by:

$$P_N(|\underline{R}|) \simeq \frac{1}{R_0}\Big(\frac{|\underline{R}|}{R_0}\Big)^{13/9} \exp\left[-\Big(\frac{|\underline{R}|}{R_0}\Big)^4\right] \tag{8.6}$$

Again, we are able to check it with our MD simulations, see Fig. 8.5. The agreement between the simulations and the theory is satisfactory and we recover the $R_0 \sim N^{3/4}$ scaling law for the characteristic size of self-avoiding chains in 2D.

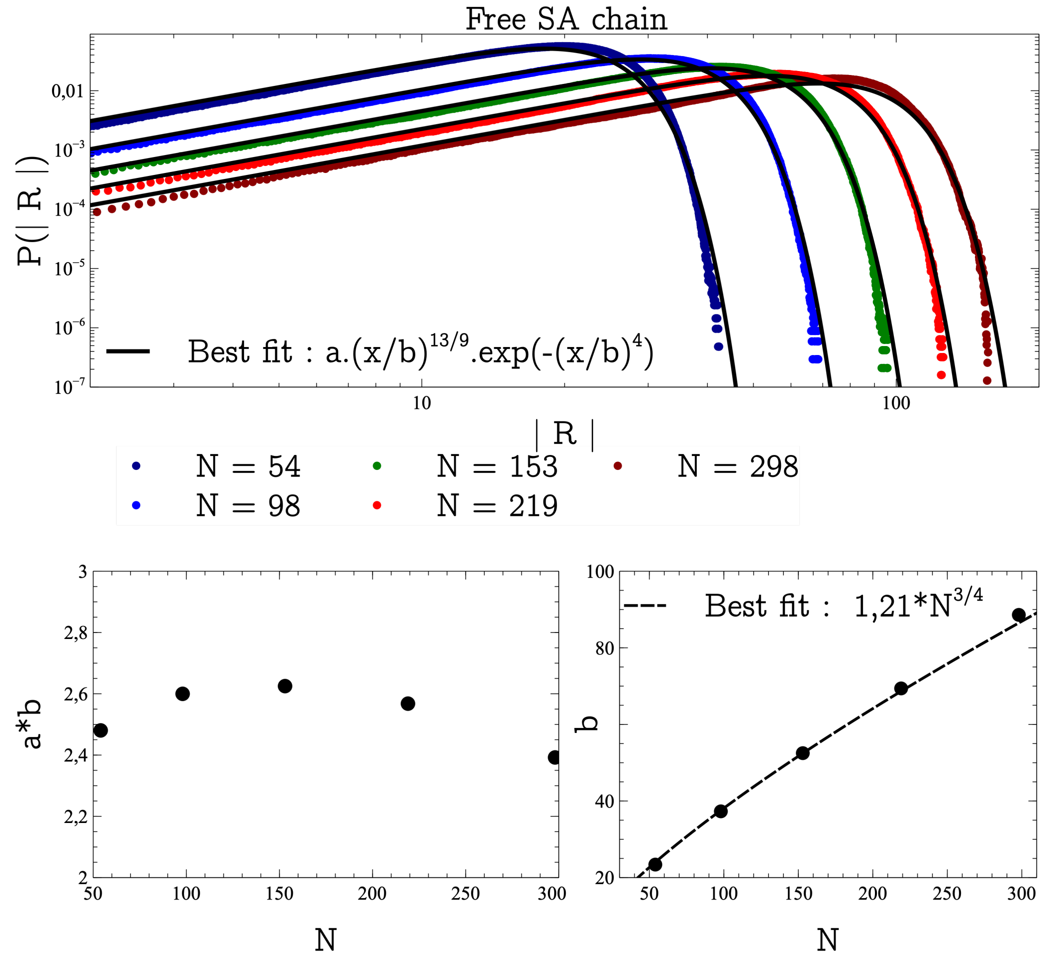

Figure 8.5 – Probability distribution of the end-to-end distance for a self-avoiding chain, freely evolving in 2D. In the upper pannel the black solid curves are a best fit with the function $a(x/b)\exp(-(x/b)^2)$, where a and b are the fitting parameters. The bottom left pannel represents the evolution of the product ab and the bottom right pannel the evolution of b with the chain length N.

To obtain an estimation of the probability distribution of end-to-end vector $G_N(\underline{R})$ for a chain tethered to a repulsive wall, whether ideal or self-avoiding, we use the method of images as suggested in [119] and as done in the previous chapter. That is $G_N(\underline{R}) = P_N(\underline{R} - \underline{\epsilon}) - P_N(\underline{R} + \underline{\epsilon})$, where $|\underline{\epsilon}|$ is arbitrarily small compared to $|\underline{R}|$ ($|\underline{\epsilon}|$ is typically of monomer size). Using the function ϕ, we can rewrite this equation as:

$$G_N(\underline{R}) = \frac{1}{R_0^2}\left[\phi\left(\frac{R-\epsilon}{R_0}\right) - \phi\left(\frac{R+\epsilon}{R_0}\right)\right] \tag{8.7}$$

A Taylor expansion around $\underline{\epsilon} = 0$ leads to:

$$G_N(\underline{R}) = \frac{-2\epsilon}{R_0^3}(\phi)' \tag{8.8}$$

For an ideal chain this directly reads:

$$G_N(\underline{R}) = \frac{4\epsilon}{R_0^3}\,\frac{R}{R_0}\,\exp\left[-\left(\frac{R}{R_0}\right)^2\right] \tag{8.9}$$

Which finally yields:

$$G_N(|\underline{R}|) \sim \frac{4\epsilon}{R_0^2}\left(\frac{R}{R_0}\right)^2 \exp\left[-\left(\frac{R}{R_0}\right)^2\right] \tag{8.10}$$

The results of the MD simulations for ideal chains with one end fixed on a rigid wall allows us to verify the proposed distribution (Fig. 8.6). The typical size of the chains follows a similar scaling law as for free chains, $R_0 \sim N^{1/2}$.

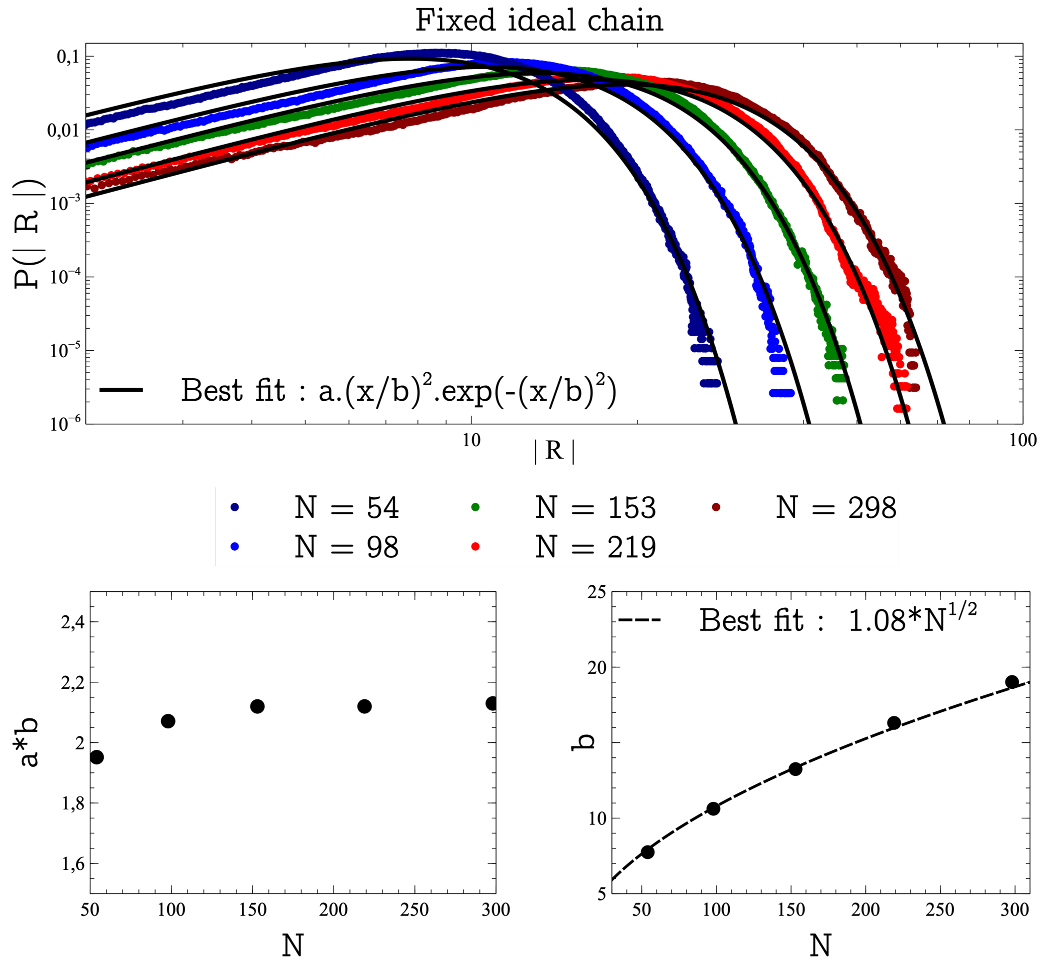

Figure 8.6 – Probability distribution of the end-to-end distance for an ideal chain in 2D, tethered to a wall. In the upper pannel the black solid curves are a best fit with the function $a(x/b)\exp(-(x/b)^2)$, where a and b are the fitting parameters. The bottom left pannel represents the evolution of the product ab and the bottom right pannel the evolution of b with the chain length N.

For a self-avoiding chain, one has to be more careful since we determined the free behaviour by bridging asymptotic behaviours. Incidentally, if we were to perform a Taylor expansion of ϕ on both asymptotic limits, we would have:

$$\begin{cases} \phi'(x) \sim g x^{g-1} \text{ when } |x| \ll 1, \\ \phi'(x) \sim -\delta x^{\delta-1} e^{(-x^{\delta})} \text{ when } |x| \gg 1. \end{cases} \tag{8.11}$$

Thus inserting Eq.8.11 in Eq.8.8:

$$G_N(\underline{R}) \sim \frac{2g\delta\epsilon}{R_0^2}\left(\frac{|\underline{R}|}{R_0}\right)^{g+\delta-2} e^{-\left(\frac{|\underline{R}|}{R_0}\right)^4} \tag{8.12}$$

Once integrated over all orientations, we would finally have the end-to-end distance distribution:

$$G_N(|\underline{R}|) \sim \frac{2g\delta\epsilon}{R_0}\left(\frac{|\underline{R}|}{R_0}\right)^{g+\delta-1} e^{-\left(\frac{|\underline{R}|}{R_0}\right)^4} \tag{8.13}$$

using the values of $g = 4/9$ and $\delta = 4$, this reads:

$$G_N(|\underline{R}|) \sim \frac{1}{R_0}\left(\frac{|\underline{R}|}{R_0}\right)^{31/9} e^{-\left(\frac{|\underline{R}|}{R_0}\right)^4} \tag{8.14}$$

As shown in Fig. 8.7, the end-to-end distance distributions obtained from MD simulations do not agree with this expression.

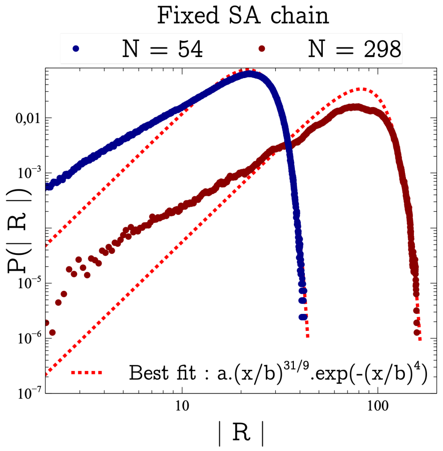

Figure 8.7 – Probability distribution of the end-to-end distance for a self-avoiding chain in 2D, tethered to a wall. The red dashed lines correspond to a best fit with the function $a(x/b)^{31/9}\exp(-(x/b)^4)$.

Keeping a similar shape for the distribution, $x^{\alpha}e^{-x^{\beta}}$, we found that the following relation agrees with the distribution computed from MD simulations:

$$G_N(R) \sim \left(\frac{R}{R_0}\right)^{22/9} \exp[-(R/R_0)^4] \tag{8.15}$$

We note however that this estimation of the distribution of tethered chains with excluded volume interactions remains questionable.

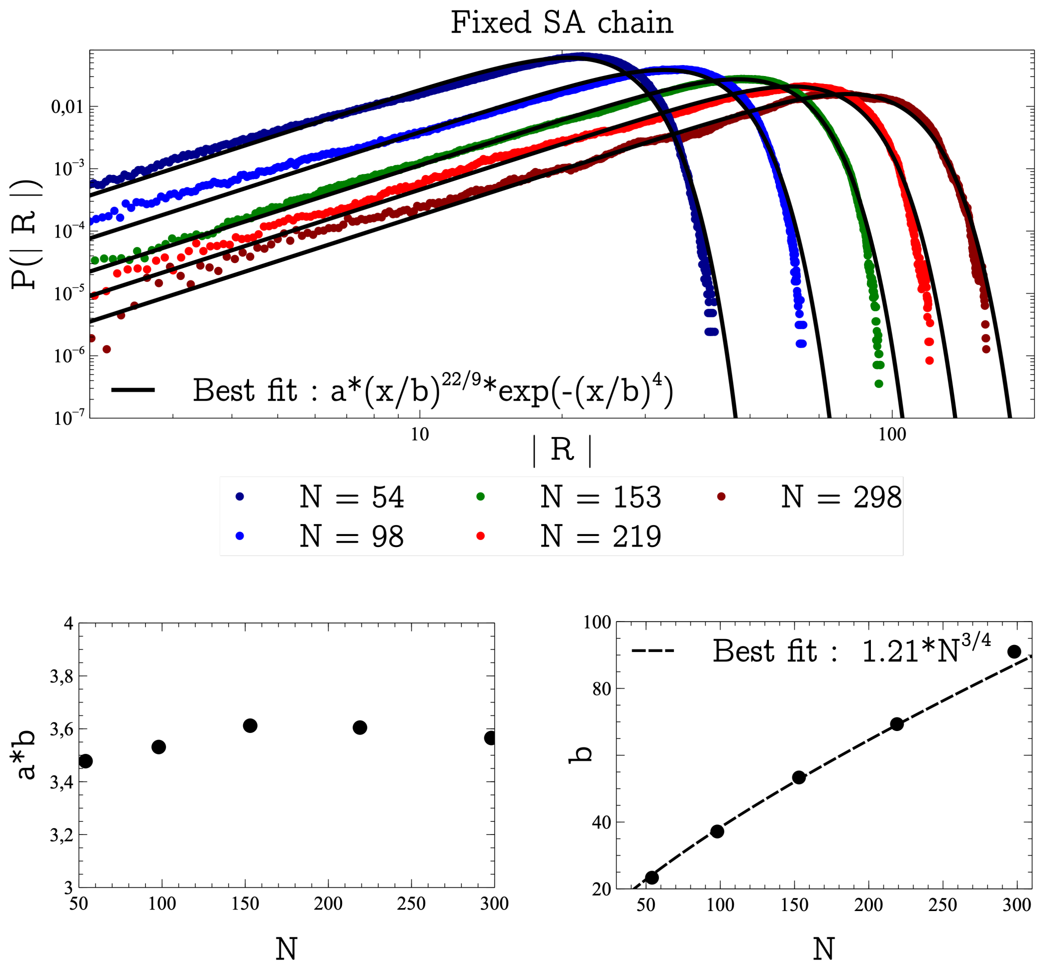

Figure 8.8 – Probability distribution of the end-to-end distance for a self-avoiding chain in 2D, tethered to a wall. In the upper pannel the black solid curves are a best fit with the function $a(x/b)\exp(-(x/b)^2)$, where a and b are the fitting parameters. The bottom left pannel represents the evolution of the product ab and the bottom right pannel the evolution of b with the chain length N.

8.1.2 Free energy

Along with [119], to obtain the free energy of a translocating chain, the chain is divided in two subchains, of lengths s and $N - s$. The free energy of each of these subchains is estimated by considering them as tethered to the repulsive wall. Under the assumption that each subchain is equilibrated at any time, its partition function can be derived from the end-to-end distribution and thus its free energy reads $F = k_B T \ln Z$, with T the temperature and Z the partition function. In order to perform calculations without discriminating ideal and self-avoiding chains, we use the generic equation $G_N = -2\epsilon\phi'/R_0^3$ (Eq. 8.8) for the end-to-end vector distribution.

The partition function of a fixed chain is easily derived from its end-to-end distribution without having to fully describe the distribution:

$$Z_i = \int_\Sigma G d\Sigma \tag{8.16}$$

where Σ is the volume of accessible states. In polar coordinate, the partition function becomes:

$$Z_i \sim -\int_0^\infty \int_{-\pi/2}^{\pi/2} 2\frac{\epsilon}{R_0^3}\phi'\Big(\frac{R}{R_0}\Big) R\; dR d\theta \tag{8.17}$$

Assuming there is no prefered orientation for the chain, the integral over the orientation yields a constant and thus one gets:

$$Z_i \sim -2\frac{\epsilon}{R_0}\int_0^\infty \phi'(R/R_0)\ (R/R_0)\ d(R/R_0) \tag{8.18}$$

$$\sim -2\frac{\epsilon}{R_0}\int_0^\infty \phi'(u)\ u\ du \tag{8.19}$$

$$Z_i = e^{-\beta F} = \text{Const.}\ \frac{\epsilon}{R_0} \tag{8.20}$$

Finally, the free energy of a tethered chain reads:

$$\beta F = \ln\left(\frac{R_0}{\epsilon}\right) + \text{Const.} = \nu \ln N + \text{Const.} \tag{8.21}$$

where $\epsilon \simeq a$ and $R_0 = aN^\nu$.

This expression is valid for both ideal and self-avoiding chains provided that the proper ν exponent is used.

Free energy of the whole chain during the translocation

The partition function of the whole chain simply corresponds to the product of the partition functions of each subchain under the assumption that they are independent. We thus have:

$$Z_{\text{chain}} = Z_s Z_{N-s} = \text{Const.}\ \frac{1}{R_s}\frac{1}{R_{N-s}} \tag{8.22}$$

where $R_i \sim i^\nu$ is the characteristic size of the subchain of length i.
The corresponding free energy is:

$$\beta F = -\ln(Z_{\text{chain}}) \sim \nu \ln\Big[s(N-s)\Big] \tag{8.23}$$

with $\beta = (k_B T)^{-1}$. The evolution of the free energy with the translocation coordinate s is plotted in Fig. 8.9. The difference between ideal and self-avoiding chains is minor, appearing only in the prefactor given by ν. As previously shown by Sung and Park, the free energy is maximum when $s = N/2$. The chain thus feels an entropic barrier to enter in the pore, due to the wall repulsion. In Fig. 8.9, we may also see that this barrier is relatively flat as long as the subchains have similar lengths.

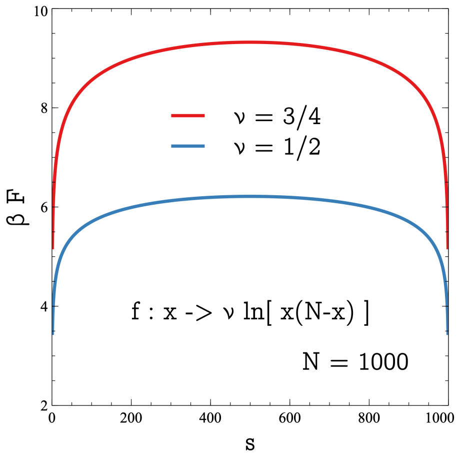

Figure 8.9 – Effect of the wall as a free energy barrier for an ideal chain ($\nu = 1/2$, blue curve) and a self-avoiding chain ($\nu = 3/4$, red curve) of 1000 monomers. This barrier, given by $f(x) = \nu \ln(x(N-x))$, is relatively flat and reached its maximum for the mid monomer.

8.1.3 Fokker-Planck equation

As stated at the beginning of this section, the translocation problem is reduced to a diffusive random process of the number s of the monomer in the pore. In the work of Sung and Park, they solved the Fokker-Planck equation to get the probability distribution $P(s,t)$:

$$\partial_t P(s,t) = L_{\mathrm{FP}}(s) P(s,t) \tag{8.24}$$

where $L_{\mathrm{FP}}(s)$ is the Fokker-Planck operator that we may express with the free energy previously determined:

$$L_{\mathrm{FP}}(s) = \frac{1}{b^2} \partial_s D(s) e^{-\beta F(s)} \partial_s e^{\beta F(s)} \tag{8.25}$$

with b is the monomer size, $D(s)$ the diffusion coefficient of the chain during translocation and $F(s)$ the free energy calculated beforehand, Eq.9.3. From Eq.8.25, we may obtain the time the chain needs to diffuse, *i.e.* the mean first passage time, *i.e.* the translocation time. However, one may reach the same conclusion as Sung and Park did but with a different and simpler approach. Indeed, starting from the Langevin equation:

$$\dot{x}(t) = -\frac{D}{k_{\mathrm{B}} T} \partial_x F + \sqrt{2D}\eta(t) \tag{8.26}$$

where F is the free energy landscape and η a normalized Gaussian white noise. Knowing from Eq.9.3, the function F, we have:

$$\partial_x F = -\frac{2x}{(N/2)^2 - x^2} \tag{8.27}$$

Therefore we may rescale x, introducing $y = 2x/N$, and Eq.8.27 is rewritten:

$$\dot{y} = 2D^* \frac{y}{1-y^2} + \sqrt{2D^*}\eta(t) \tag{8.28}$$

where we have introduced the effective diffusion coefficient:

$$D^* = \frac{4D}{N^2} \tag{8.29}$$

In Eq.8.28, the timescale is only set by D^*, thus we have this scaling behaviour for the translocation time:

$$\tau \sim 1/D^* \sim \frac{N^2}{D} \tag{8.30}$$

From this scaling law we may consider two limiting cases, friction may occur at the scale of the whole chain or at the scale the monomer located at the pore. Indeed, we may wonder if this diffusion coefficient is related to the motion of the chain on both sides of the wall or to the motion of the monomer located at the opening in the wall. This leads to two limits for the mean translocation time:

$$\begin{cases} \tau \sim N^2 \text{ if } D = D_0 \text{ the diffusion coefficient of a single monomer,} \\ \tau \sim N^3 \text{ if } D \sim \dfrac{D_0}{N} \text{ the coefficient of diffusion of the chain.} \end{cases} \tag{8.31}$$

8.1.4 Langevin equation

For such a 1D diffusive process, the translocation dynamics can be followed from a direct numerical resolution of a Langevin equation. In the overdamped regime and with a driving force, the Langevin differential equation becomes:

$$\gamma \dot{s} = F_{\mathrm{p}} + \eta(t) \tag{8.32}$$

where γ is the friction coefficient, F_{p} and η being the force deriving from the potential and the fluctuating force, respectively. The magnitude of the fluctuating force is given by $< \eta^2 >= 2k_{\mathrm{B}}T\gamma$.

From the free energy potential, $\beta F_{\mathrm{p}} \sim \nu \ln \left[s(N-s)\right]$, and considering two absorbing points ($s = 0$ and $s = N$), the 1D Brownian trajectory can be simulated. Figure 8.10 shows that average trajectories obtained from MD simulations and 1D Langevin (mean over 1000 runs) follow a similar behavior. As suggested by the Fokker-Planck analysis, the evolution of the mean translocation time with the chain size do not agree with the MD simulations results. For both ideal and self-avoiding chains, the Langevin simulations shows that $\tau \sim N^2$. No influence of the nature of the chain is observed.

The framework first proposed by Sung and Park in [119] appears convincing because the presence of the wall must impact the behaviour of the chain or at least lessen the number of allowed configurations for the chain. However, the resulting scaling laws for the mean translocation time are not in accordance with our results as well as the ones in

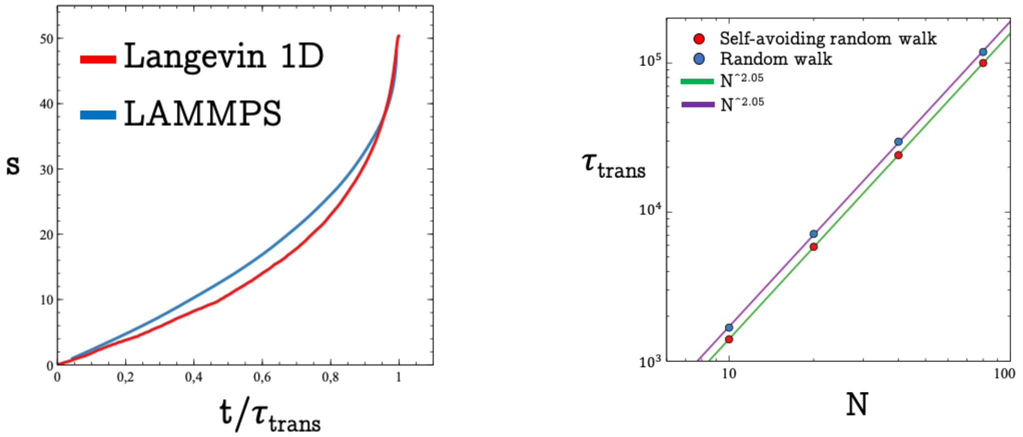

(a)

(b)

Figure 8.10 – (a) Comparison between MD simulations (LAMMPS) and numerical results from Eq.8.32 for the translocation trajectory s of an ideal chain of 100 monomers. (b) Evolution of the mean translocation time τ_{trans} with the chain size N. Dots are data points and solid lines are best fits with the function aN^b with a and b as fitting parameters.

the literature. More importantly, this theoretical framework does not provide any clue to discriminate between ideal and self-avoiding chains whether in 2D or in 3D, while we exhibited reproducible differences.

8.2 Panja's theoretical approach

Reducing the translocation of a chain composed of numerous units to the problem of a single particle escaping over a potential has proven to be too reductive. Indeed, the chain dynamics is impacted by several factors. We have already mentioned excluded volume interactions: a swollen chain should move differently from an ideal one. Another impact on the chain dynamics may be caused by hydrodynamic interactions, that is the complex interplay between the chain monomers and the solvent: a moving monomer unit locally creates a solvent flow which, in turn, affects other monomer units. These interactions go beyond the scope of our work. One final interaction, up to now overlooked, is chain connectivity, *i.e.* the fact that monomer units (or beads) adjacent along the chain constrain the motion of their nearest neighbors. These interactions decay very slowly with distance, and they can drastically influence the properties of the chain [31, 53].

As first suggested by Chuang et al., connectivity should impact translocation since monomer dynamics becomes anomalous [22]. The translocation process may be viewed as two sub-polymers on each side of the wall and exchanging monomers through the pore. When a monomer translocates, the polymer's chain tension close to the pore changes. Increasing/decreasing the number of monomers generates a transient compressive/stretching stress in the sub-chain that should relax.

Before describing this monomer exchange at the pore, we will exhibit the anomalous diffusion behaviour of a monomer inside a chain and how new timescales are then derived.

8.2.1 Anomalous diffusion of a monomer - Rouse dynamics

In the Rouse model of a chain, the chain connectivity is considered via i) an ideal polymer chain with elastic modulus given by, $\kappa \sim k_{\mathrm{B}}T/(Na^2)$, ii) a phantom chain, for which the segments may overlap, and iii) independent thermal forces acting on the monomer units. In essence, the Rouse model is a Brownian motion of coupled harmonic oscillators in the overdamped regime or a *phantom chain in immobile solvent* [55]. In this beads-and-springs picture of a chain, the monomers are connected via ideal harmonic springs, leading to the energy (in d dimensions):

$$U = \frac{dk_{\mathrm{B}}T}{a^2}\sum_{i=1}^{N}(\mathbf{r}_{i-1} - \mathbf{r}_i)^2 \tag{8.33}$$

where $dk_{\mathrm{B}}T/a^2 = \kappa$ is the spring stiffness.

Without additional interaction (excluded volume for instance), the chain adopts an ideal conformation, with Gaussian distribution and typical size:

$$R_{id} \sim \sqrt{N}a,$$

A Langevin equation can be written for the position r_n of each bead, indexed by n:

$$m\frac{d^2r_n}{dt^2} = -\gamma\frac{dr_n}{dt} - \frac{dU}{dr_n} + F_n(t) \tag{8.34}$$

where γ is the friction coefficient between the bead and solvent and F_n a random fluctuating thermal force. The term $-dU/dr$ describes the force exerted by the other beads on the moving bead.

In the overdamped regime, this set of Langevin equations become a system of $N+1$ linear differential equations:

$$\gamma d_t r_n = \kappa(r_{n+1} + r_{n-1} - 2r_n) + F_n(t) \tag{8.35}$$

This equation is the diffusion equation with noise, referenced as the Edwards-Wilkinson equation initially proposed to describe growing interfaces[40]. The random force acting on different beads are independent and verifies:

$$< F_n(t) >= 0 \quad < F_n(t)F_m(t') >= 2dk_{\mathrm{B}}T\gamma\delta(t-t')\delta_{n,m}$$

Within a continuous description of the chain, the position of a bead is not indexed by n

but given by $r(s)$, with s a curvilinear coordinate $[0, L]$, and we get:

$$\gamma \partial_t r(s,t) = \kappa \partial^2_{s^2} r(s,t) + F(s,t) \tag{8.36}$$

with the random force verifying:

$$< F(s,t)F(s',t') >= 2dk_\mathrm{B}T\gamma\delta(t-t')\delta(s-s')$$

and boundary conditions:

$$\left[\frac{\partial r(s,t)}{\partial s}\right]_{s=0,L} = 0$$

Both discrete and continuous systems of Rouse equations can be solved by Fourier transform, *i.e.*, by introducing the normal modes (u_p the amplitude of mode p). The imposed boundary conditions are only compatible with the cosinus function. In the continuous description, we have an infinite number of modes while in the discrete description there are N modes:

$$r_n(t) = r_n(0) + 2\sum_{p=1}^{\infty} u_p(t)\cos\frac{\pi p n}{N}$$
$$u_p = \frac{1}{N}\int_0^N dn\; r_n \cos(\frac{p\pi n}{N})$$

which yields the set of Langevin equations:

$$\gamma_p \frac{du_p}{dt} = -\kappa_p u_p + F_p(t) \quad (p \geq 1) \tag{8.37}$$

$$\text{with } \gamma_p \sim \frac{N}{p}\gamma \quad \text{and} \quad \kappa_p \sim \kappa\frac{p}{N} \tag{8.38}$$

where $\kappa \sim k_\mathrm{B}T/a^2$, see details in [31, 55].
The normal mode $p = 1$ describes the motion of the chain as a whole, *i.e.* of its center of mass. The corresponding Langevin equation reads:

$$\gamma_1 \frac{du_1}{dt} = F_0 \tag{8.39}$$

which is the stochastic equation of a Wiener process (pure diffusion), which yields:

$$< u_1(t)^2 >= 4Dt$$

in 2D with the diffusion coefficient $D = k_\mathrm{B}T/(N\gamma)$. This is expected from the fluctuation-dissipation theorem since we assumed the friction forces on beads to be uncorrelated, leading to an effective friction coefficient $\gamma_1 = N\gamma$.

For other modes ($p > 1$), the Langevin equations, Eq. 8.37, correspond to independent stochastic equations characteristics of a Ornstein-Uhlenbeck process. The dynamics become:

$$< u_p(t)^2 >= \frac{kT}{\kappa_p}\left(1 - e^{-2t/\tau_p}\right) \tag{8.40}$$

with the relaxation times:

$$\tau_p = \frac{\gamma_p}{\kappa_p} \sim \left(\frac{N}{p}\right)^2 \tau_N \tag{8.41}$$

where the shortest relaxation time, $\tau_N \sim \gamma/\kappa$ is the typical time needed for a single free bead to diffuse a distance of order its own size a. The longest relaxation time of the chain, called the Rouse time, is $\tau_1 = \tau_R \sim \gamma N^2 a^2/kT = \tau_0 N^2$. For longer times, the chain diffuses freely as a whole, i.e. with a bulk diffusion of the center of mass.

Therefore, for any given time $t \in [\tau_N, \tau_R]$ all Rouse modes can be separated into two classes: modes with relatively small p such that $t < \tau_p$ are not yet relaxed, while modes with larger p are already relaxed. These different timescales of relaxation have an impact on the motion of the monomers. Indeed, for short time intervals ($\Delta t < \tau_N$), a monomer of the chain does not feel its neighbors and behaves as a single particle while for long time intervals ($\Delta t > \tau_R$) the chain is fully relaxed and the monomers are not perturbed by their connectivity. In these two instances, a monomer inside a chain is alike a single particle and is simply freely diffusing. However, between intermediate time intervals ($\tau_N < \Delta t < \tau_R$), some of the Rouse modes are already relaxed while others are still relaxing, with the number of thermalized modes growing with time. Indeed, if we consider a portion of the chain containing N/p monomers, the mean square displacement of one monomer during the mode relaxation τ_p would be on the order of the mean square size of the chain portion $a^2(N/p)$; hence using Eq.8.41, we get the mean square displacement (MSD):

$$MSD(\Delta t = \tau_p) \sim a^2(N/p) \sim a^2\left(\frac{\Delta t}{\tau_N}\right)^{1/2} \tag{8.42}$$

We thus expect a subdiffusive behaviour for the MSD of a monomer inside the chain scaling as $MSD \sim t^{1/2}$ for an ideal chain. The analysis of MD Langevin simulations reproduces this behaviour. Fig.8.11 shows the MSD of a tagged monomer. After a transient ballistic regime, MSD$\sim t^2$, the subdiffusion regime is clearly observed for times smaller than the Rouse time of the chain. For longer times a classical diffusion with $MSD \sim t$ is recovered. Interestingly, the subdiffusion regime completely disappears in the MSD of the center of mass.

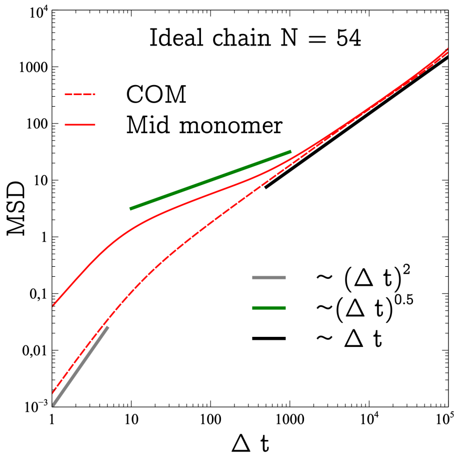

Figure 8.11 – Comparison between the MSD of a monomer located in the middle (solid line) and the one of the chain's center of mass (dashed line) of an ideal chain of length 54.

8.2.2 Anomalous diffusion of a monomer - self-avoiding chain

In the previous derivation of the Rouse model, the chains are considered ideal. For self-avoiding chains, Eq.8.34 would be modified to take into account the excluded volume interactions. However, Panja [100] has developped a scaling approach by considering that the arguments developped for an ideal chain pertaining the different timescales to relax the strain, induced by the chain connectivity, must hold for chains with excluded volume interactions. For a self-avoiding chain, the spring constants in Eq.8.38 have to be modified accordingly, following the scaling approach given in [16]:

$$\kappa_p \sim \kappa \left(\frac{p}{N} \right)^{2\nu} \tag{8.43}$$

And the relaxation time reads:

$$\tau_p = \frac{\gamma_p}{\kappa_p} \sim \left(\frac{N}{p} \right)^{1+2\nu} \tau_N \tag{8.44}$$

Therefore, adapting Eq.8.42 with Eqs.8.43 and 8.44, one obtains:

$$MSD(\Delta t = \tau_p) \sim a^2 (N/p)^{2\nu} \sim a^2 \left(\frac{\Delta t}{\tau_N} \right)^{2\nu/(1+2\nu)} \tag{8.45}$$

With this equation, we retrieve the previous result for an ideal chain.
Finally, at intermediate time scales, the MSD of a monomer inside a self-avoiding chain is expected to be $MSD \sim t^{3/5}$.
Thanks to our simulations, we again display the transient sub-diffusive behaviour of a monomer inside a self-avoiding chain, see Fig.8.12. For short times $t \leq \tau_0$, a ballistic motion of the monomer is observed MSD$\sim t^2$. Then for intermediate stages $\tau_0 < t < \tau_R$, we observe the anomalous diffusion of the monomer with MSD$\sim t^{0.5}$ for an ideal chain

and MSD$\sim t^{0.6}$ for a self-avoiding one. Finally, for long times $t \geq \tau_R$, the diffusion of the monomer follows the diffusion of the whole chain MSD$\sim t$.

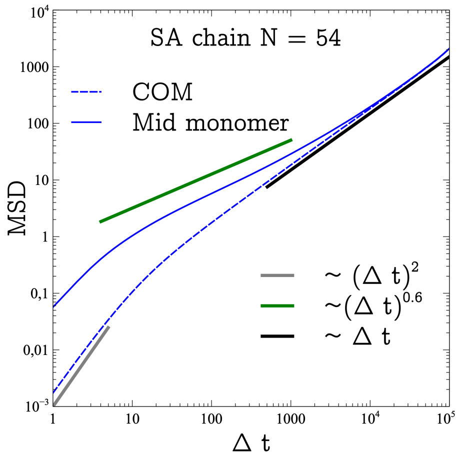

Figure 8.12 – Comparison between the MSD of a monomer located in the middle (solid line) and the one of the chain's center of mass (dashed line) of a self-avoiding chain of length 54.

Anomalous diffusion for shaken granular chains

With our experimental apparatus described in the previous Part, we also tried to see if anomalous diffusion could be observed during the shaken chain experiments. Figure 8.13 shows snapshots of an experiment with a granular chain of 50 monomers. For tracking purpose, some beads have been painted in black. At first sight, granular chains can be considered as 2D self-avoiding chains. During the experiment, we recorded and tracked the position of the tagged mid bead. The evolution of the MSD of the tagged bead with time is given in Fig. 8.14. Surprisingly, the MSD of a bead inside a granular chain is very close to what is obtained from the MD simulations: a ballistic regime at short times with MSD$\sim t^2$ and a classical diffusion regime at long times with MSD$\sim t$. In between these timescales, we observed without ambiguity a subdiffusive regime with MSD$\sim t^{0.7}$.

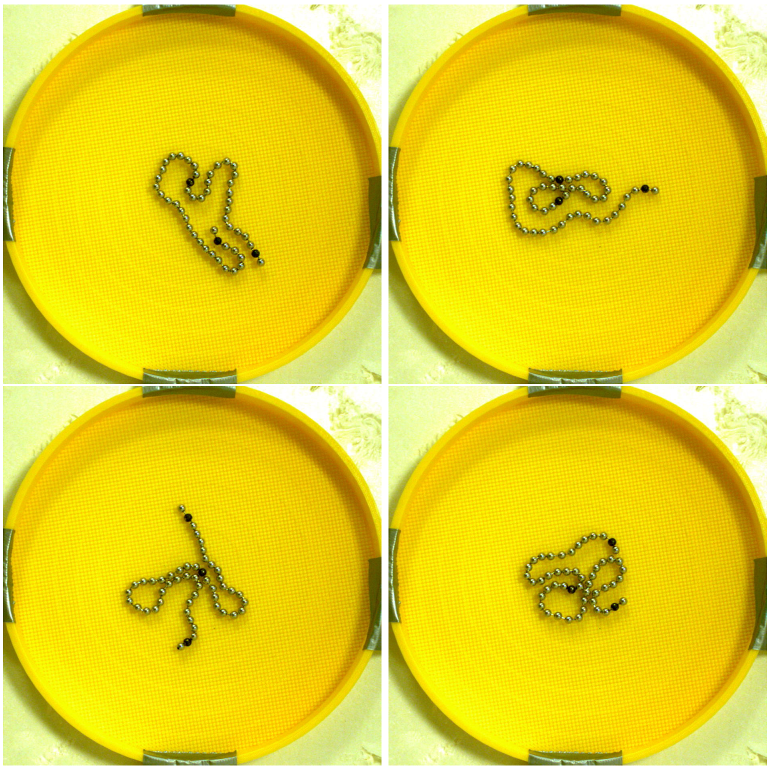

Figure 8.13 – Snapshots of a vibrated 50 monomers long granular chain taken at different times. The black beads are the ones tracked during the experiment.

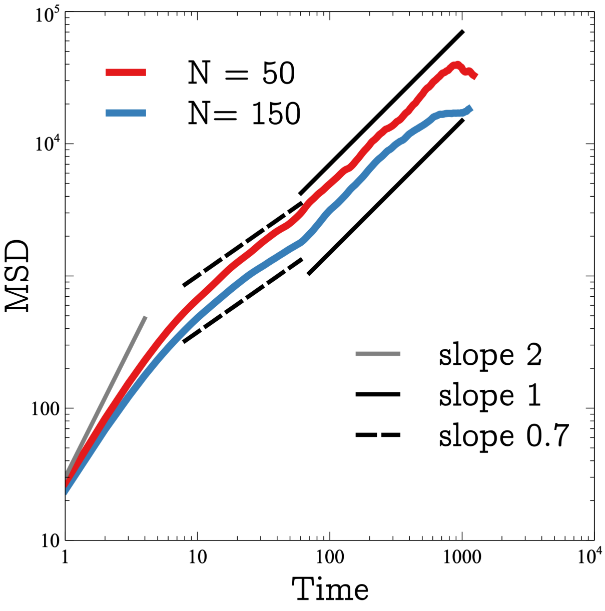

Figure 8.14 – Time evolution of the MSD of a tagged bead located at the center of a granular chain from our vibrated experiment.

8.2.3 Memory kernel and anomalous diffusion

In the Rouse model, the dynamics of a single chain is given by a system of N coupled Langevin equations. This model bears some analogies with the classical Caldeira-Leggett model of a free Brownian particle in interaction with a thermal bath of N harmonic oscillators [131, 106]. We had derived the generalized Langevin equation Eq.5.9 for such a system.
This yields in the overdamped regime:

$$m\dot{v} = -m \int_0^t dt' \mu(t-t')v(t') + X(t) \tag{8.46}$$

where the function $\mu(t)$ is the memory kernel and $X(t)$ a random force. At this point, the question mark concerns the memory function for the studied system.
Classically, there are two families of memory kernels:

1. $\mu(t) \sim t^{-\alpha}$

2. $\mu(t) \sim \sum_i e^{-t\tau_i}$

Interestingly, it has been shown, see *e.g.* [90, 72, 69, 86], that a memory kernel of the first family leads to anomalous diffusion at long times (sub or hyper diffusive depending on the value of α). An example of such anomalous diffusion can be drawn from the in vivo subdiffusive behaviour of macroparticles in cell cytoplasm.
However, as we have previously shown with the diffusion of a monomer inside a chain, diffusion may well be normal at long times and still exhibit anomalous diffusion at intermediate timescales. Another instance of such transient anomalous diffusion happens for a Brownian particle in a labyrinth, where the particle encountering a wall has to make a step in the opposite direction, leading to a memory effect.
According to [87], this transient anomalous behaviour is attributed to the second family of memory kernels.

8.2.4 Impact of anomalous diffusion on chain free translocation through a pore

As shown by the study of free chain diffusion, anomalous diffusion and memory kernel are intricate. Knowing that anomalous diffusion is also observed in chain translocation, Panja derived the relevant memory function of a translocating polymer. Panja reduced the translocation problem to the problem of injecting n extra monomers into an anchored chain [99] and the subsequent relaxation dynamics of the tension. First, in [98], Panja derived the memory function of a polymer to a localized step strain and obtained the following results:

$$\begin{cases} \mu(t) \sim t^{-1} & \text{for an ideal free chain,} \\ \mu(t) \sim t^{-1} & \text{for an ideal tethered chain,} \\ \mu(t) \sim t^{-2/(1+2\nu)} & \text{for a self-avoiding free chain,} \\ \mu(t) \sim t^{-(1+\nu)/(1+2\nu)} & \text{for a self-avoiding tethered chain.} \end{cases} \tag{8.47}$$

We note that while the derivation of the memory kernel for the ideal chain is exact, the one for the self-avoiding chain is based on a scaling approach following a similar scheme. A major issue in this approach is that when using the exponent $\nu = 1/2$ of an ideal chain in the relation given for the self-avoiding tethered chain, one does not recover the expression derived for the ideal chain.

The scaling arguments deployed by Panja for self-avoiding tethered chains are as follows. At short times the chain relaxes the tension produced by n compressed monomers. Considering that at time t, there are n_t monomers that have relaxed, with $n_t \sim t^{1/1+2\nu}$, and where the compressed monomers are given by $n + n_t$. To estimate the compression force felt by the monomers, we need to estimate the impacted size δr related to the compression and partial relaxation. The size of the relaxed chain segment being $R \sim n_t^{\nu}$, the compression thus becomes:

$$\delta r = R(n_t) - R(n + n_t) = n \left(\frac{\partial R}{\partial N} \right)_{n_t} \sim n\, n_t^{\nu - 1}$$

where, it is assumed that $n \ll n_t$.

With the spring constant as in Eq.8.43, the time evolution at short time intervals of the tension/compressive force is given by:

$$\begin{aligned} \mu(t) &\sim n_t^{-2\nu} n\, n_t^{\nu-1} \sim n\, n_t^{-(1+\nu)} \\ &\sim n\, t^{-(1+\nu)/(1+2\nu)} \end{aligned}$$

Therefore, the memory function for a polymer translocating through an opening in a wall is made of two parts:

1. a power law decay at short time intervals, corresponding to the relaxation of the compressed monomers;

2. an exponential decay at long times, corresponding to the relaxation of the whole chain.

Finally, the memory kernel reads:

$$\begin{cases} \mu(t) \sim t^{-1} exp(-t/\tau_R) & \text{for an ideal chain,} \\ \mu(t) \sim t^{-(1+\nu)(1+2\nu)} exp(-t/\tau_R) & \text{for a self-avoiding chain.} \end{cases} \tag{8.48}$$

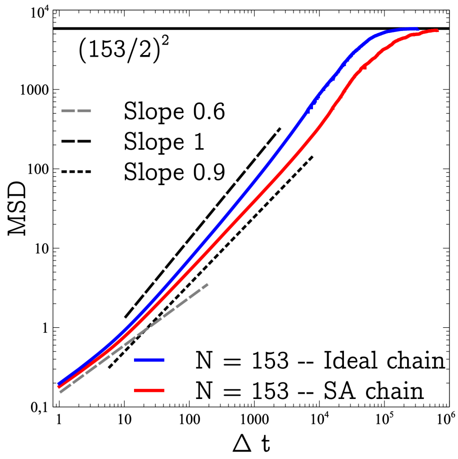

Figure 8.15 – MSD of the monomer number in the pore for an ideal (in blue) and a SA (in red) chain of length $N = 153$.

where τ_R is the Rouse relaxation time of the whole chain.

Assuming that the proposition $\mu(t) \sim t^{-\alpha} \Rightarrow MSD \sim t^{\alpha}$ is true, we thus have normal diffusion for the ideal chain and subdiffusion for the self-avoiding case with $MSD \sim t^{0.7}$ in 2D.
From our simulations, we indeed exhibit a difference in the MSD of an ideal and a self-avoiding chains, where the anomalous diffusion is clearer for the latter.

To estimate the translocation time τ^{ideal} of the ideal chain, since the diffusion is normal we simply have to express the fact that $MSD(\tau^{\text{ideal}}) \sim \tau^{\text{ideal}}$ and $MSD(\tau^{\text{ideal}}) \sim N^2$, hence:

$$\tau^{\text{ideal}} \sim N^2 \tag{8.49}$$

However, to estimate the translocation time τ^{SA} of the self-avoiding chain, we cannot directly use the previously determined time-dependance of the MSD. Indeed, for $\tau > \tau_R$, we have to consider anomalous diffusion up to τ_R and afterwards normal diffusion.
At the Rouse time, we have $MSD(\tau_R) \sim N^{1+\nu}$. Beyond the Rouse time, we thus have:

$$MSD(t > \tau_R) \sim \frac{MSD(\tau_R)}{\tau_R} t \sim N^{-\nu} t \tag{8.50}$$

At the translocation time, we have $MSD(\tau^{\text{SA}}) \sim N^2$. Hence, the translocation time finally corresponds to the time at which $N^{-\nu} t \sim N^2$, yielding:

$$\tau^{\text{SA}} \sim N^{2+\nu}. \tag{8.51}$$

Within this model, the translocation time for the whole chain, becomes proportionnal to N^2 for an ideal chain and to $N^{2.75}$ for a self-avoiding one in 2D. Observed values for the translocation time power law exponents are around 2 and 2.5 for an ideal and a SA chain, respectively.

8.2.5 Concluding remarks

In accordance with the literature, we have obtained the power law dependency of the mean translocation time of a linear chain in the form of $\tau \sim N^{\alpha}$ with N the length of the chain and α depending on the space dimension and the type of interactions between the monomers. We have confronted to our data and pushed to their limits the models developped to rationalize the translocation process. We have found that the first approach, based on the escape over an entropic barrier, does not allow to discriminate between different types of chains. While the second approach, based on memory effects, does allow to discriminate ideal and self-avoiding chains, we still have found discrepancies with experimental evidences. On one hand the disagreement between exact results and the predicted scaling for ideal chains casts doubt on the validity of the scaling approach proposed by Panja. On the other hand, the anomalous diffusion is clearly observed in our simulations as well as in our vibrated experiments. The first and the second approaches are both enticing but not entirely fulfilling. While the first one lacks the volume excluded interactions between monomers, the second one over-simplifies them. One may try to combine both approaches, yielding a generalized Langevin equation coupled to an entropic potential. Unbiased translocation problems suffer from the same drawback than the other problems where the scaling approach is ineffective to finely take into account excluded volume interactions.

Chapter 9

Chain initially confined

Contrary to free translocation, driven processes have a privileged direction for the translocation. There are several ways to introduce bias in translocation, in vitro and in vivo. One may cite for instance osmotic pressure, chemical and electrical gradient or fluid flow.

In this chapter, we focus mainly on translocation driven by a geometrical confinement of the polymer chain (Fig. 9.1). When the chain is initially confined, it faces two opposing traits. On one hand, confinement means that the accessible volume to the polymer is smaller than the one at equilibrium, hence an unfavorable state. On the other hand, to escape this unfavorable state the chain needs to ″find″ the opening which is statistically sparsely probable, even though the excluded volume effects tend to make it more statistically probable [71]. We thus separate these different phases: i) the time needed to find the opening and ii) the translocation of the chain itself. As we will show, the translocation process itself may be split into several subparts.

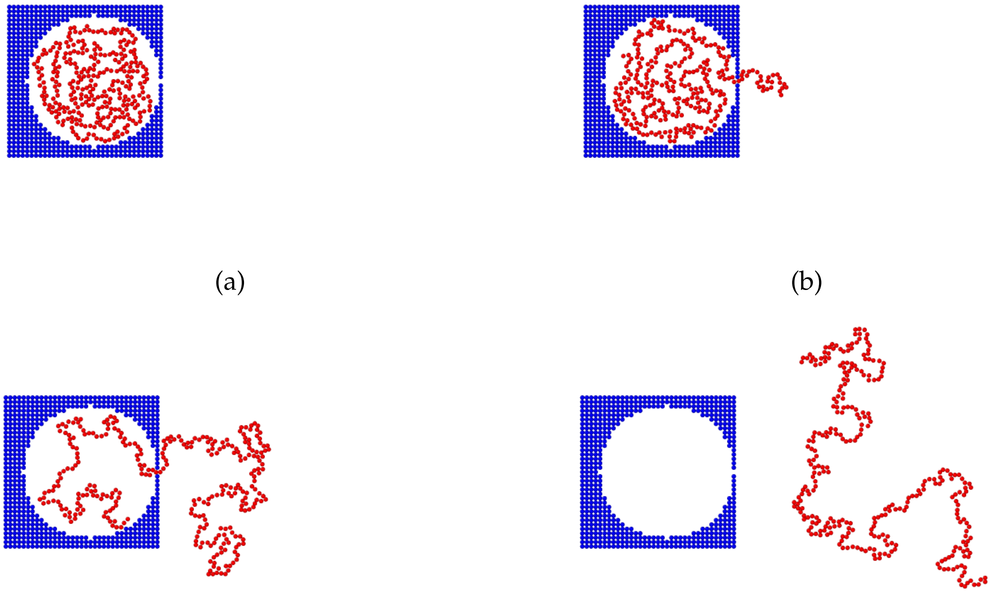

(a) (b)

(c) (d)

Figure 9.1 – Snapshots of a self-avoiding chain with $N = 298$ monomers escaping a cavity, from LAMMPS simulations at times (a) $t = 0$ (b) t_1 (c) $t_2 = 3 \cdot t_1$ and (d) $t_4 = 12 \cdot t_1$.

9.1 Pressure driven translocation

A first step in understanding the translocation driven by confinement is to study the effect of confinement on a chain. To do so, we first derive the free energy of a chain confined in a cavity and then the resulting internal pressure.

According to Sakaue and Raphaël [111], a chain inside a closed cavity can be described as a succession of blobs. Equipartition ensures that the free energy depends linearly on the number of blobs, N_{blob}:

$$\Delta F = k_{\text{B}} T N_{\text{blob}} \tag{9.1}$$

In 2D, the number of blobs is obtained via the ratio of the size of the cavity and the size of a blob $N_{\text{blob}} \sim R^2/\xi^2$, where R and ξ stand for the radius of the enclosing cavity and the size of a blob, respectively. The chain inside a blob contains g monomers and is unperturbed, leading to $\xi \sim a g^{\nu}$, $\nu = 3/4$ being the Flory exponent. The volume fraction of monomers inside the blob should be equal to the total volume fraction of monomers inside the cavity, $\phi \sim g a^2/\xi^2 \sim N a^2/R^2$. From this relation, we derive the scaling law of the blob size:

$$\xi \sim R \left(\frac{R}{N^{\nu} a} \right)^{1/(2\nu-1)} \sim R \left(\frac{R}{R_{\text{F}}} \right)^{1/(2\nu-1)} . \tag{9.2}$$

Combining these relations, we obtain the free energy expressed through the degree of

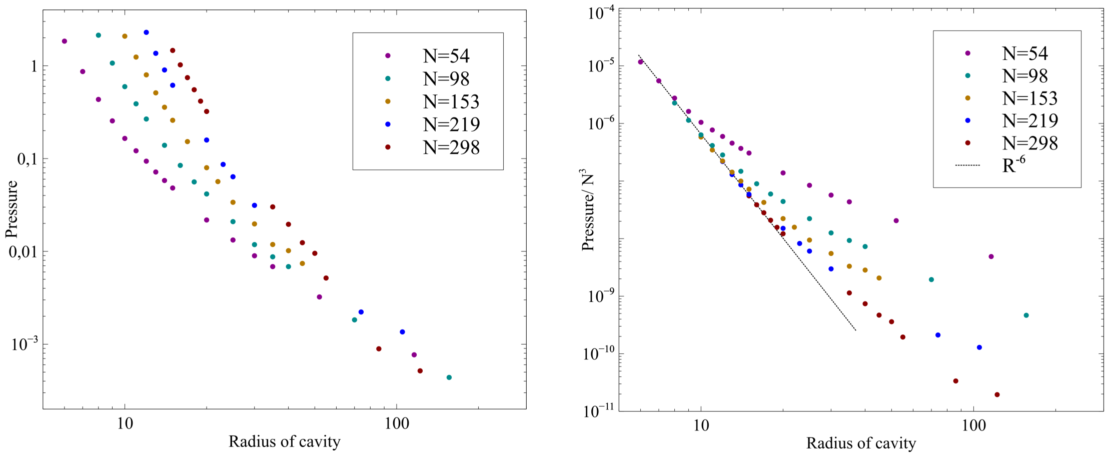

(a) (b)

Figure 9.2 – (a) Raw and (b) Normalized by N^3 pressures P for a self-avoiding chain in a closed circular 2D cavity.

confinement R_F/R:

$$\Delta F \sim k_B T \left(\frac{R_\mathrm{F}}{R}\right)^{2/(2\nu-1)} \tag{9.3}$$

with $R_\mathrm{F} \sim aN^\nu$. For 2D chains with excluded volume interactions, $2/(2\nu-1) = 4$.

The pressure can be derived from the free energy through $P = -\partial_V \Delta F$, the volume being given by $V \sim aR^2$. The differentiation of Eq. 9.3 yields:

$$P \sim -\frac{1}{aR}\;(\partial_R \Delta F) \sim k_\mathrm{B} T \left(\frac{R_\mathrm{F}^4}{aR^6}\right) \propto \frac{N^3}{R^6} \tag{9.4}$$

To test the validity of this approach, we performed a series of MD simulations for chains confined in a closed cavity. Different chain lengths and cavity sizes are considered. We used the same parameters as in chapter 2 but only considered chains with excluded volume interactions. In Fig. 9.2, the pressure, calculated via the knowledge of the Cauchy stress tensor for every monomer, is plotted against the radius of the cavity.

In rescaling the pressure by the number of monomers to the power three, the data collapse on a single curve following the scaling law R^{-6} up to a certain point. Indeed, we notice a deviation from this scaling law when the cavity becomes too large. We attribute this effect to a lack of confinement, for large cavities for which the pressure should be constant. The blob picture used to derive the pressure remains indeed valid as long as $\xi < R_\mathrm{F}$ which implies that $R < R_\mathrm{F}$. The chain is obviously confined as long as the size of the cavity is smaller than the chain's radius of gyration. We could define a critical radius of cavity $R_\mathrm{c} \propto R_\mathrm{F} \sim aN^{3/4}$ that should follow a power law with the chain length. In spite of the difficulty to determine their exact values, the cavity radii corresponding to the onset of deviation are plotted in Fig 9.3a. The R_c's increase with the chain length but they do not follow the expected $N^{3/4}$ dependance with the number of monomers.

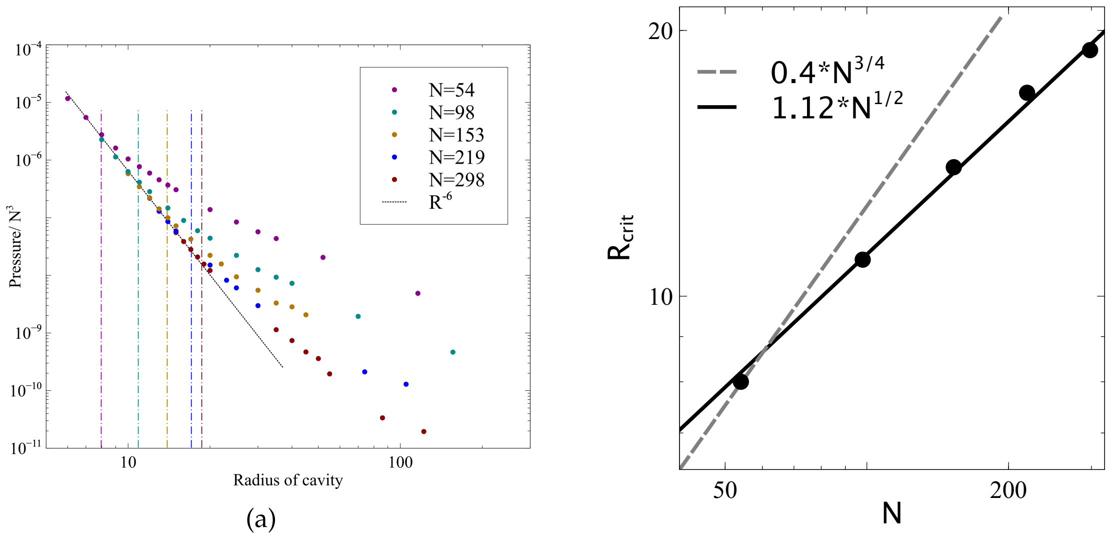

(a)

(b)

Figure 9.3 – (a) Determination of the cavity's radius at which deviation from theoretical law starts (dashed lines). The solid black line correponds to the function R^{-6}. (b) Evolution of R_{crit} with the chain's length.

9.1.1 Mean escape time from the cavity

In the first chapter of this part, we already highlighted in Fig.7.17 that a small increase in the radius of the cavity, whatever the length of the chain, leads to a very large increase in the translocation time. To produce a master curve of all escape times, a scaling law for the mean time $\tau \sim N^4 f(R/R_F)$ has been proposed with the unknown function f in the first chapter of this part.

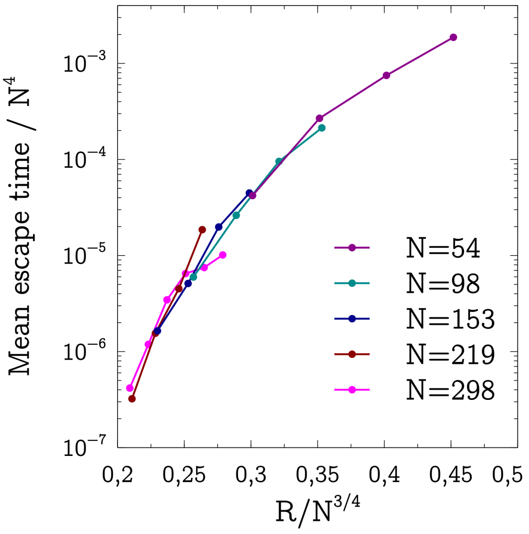

Figure 9.4 – Figure already displayed in the first chapter of this part Fig.7.17 but redisplayed here for sake of simplicity.

The release of the chain from the cavity should exhibit different regimes since the confinement varies continuously during the escape process, from severe confinement in the beginning to unconfined chain at the end of the release. The role of the first monomers expelled at high pressure and stretching the chain is not less complex to achieve a global theoretical modelization of the escape. To have an insight about the mean escape time, we can nevertheless propose an oversimplified model of the escape by considering a constant pressure. The confinement pressure generates a force at the pore given by, $P \cdot a^2$, a^2 being the pore area that is balanced by a friction force to yield:

$$\gamma \dot{s} = \frac{k_B T a^5}{R^6} (N-s)^3 \simeq \frac{k_B T a^5}{R^6} N^3$$

solving this equation for complete escape, $s = N$ gives an estimation of the mean escape time:

$$\tau \sim \frac{R^6}{k_B T a^5 N^2}$$

that can be written as,

$$\frac{\tau}{N^{5/2}} \sim \left(\frac{R}{R_F}\right)^6$$

Fig. 9.5 shows an attempt to use this relation to generate a master curve of the data. Considering the very crude approximations used here, the agreement between theory and experiments is not so bad. The agreement is even good for the evolution of mean escape time for not too severe confinements (*i.e.*, larger values of R/R_F).

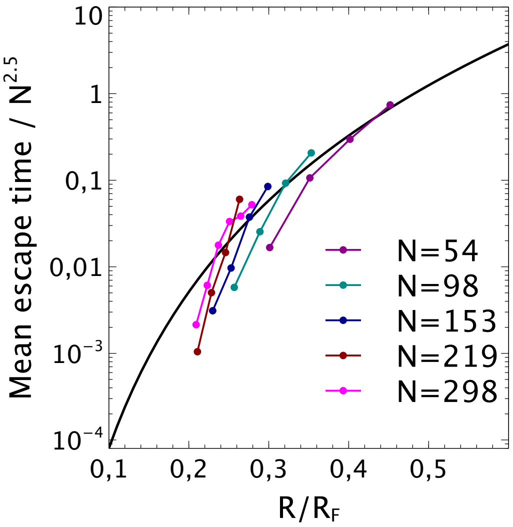

Figure 9.5 – Evolution of the rescaled, by $N^{5/2}$, mean escape time with the degree of initial confinement R/R_F.

Sakaue proposed another model of the escape process based on the free energy of a confined chain and a viscous dissipation. Due to the confinement, we can use Eq.9.3 for the free energy. During translocation, a variation of energy must occur and under the assumption that this variation is mostly due to heat loss caused by viscous friction at the pore, we may write:

$$\dot{\triangle F} = -T\dot{S} \tag{9.5}$$

where F is the free energy and S the entropy.
Because of the interactions between the pore and the translocating monomers, we may expect a velocity gradient amongst the monomers. This gradient propagating on the size of a blob, can be approximated by:

$$\nabla V \simeq \frac{a\dot{N}}{\xi} \tag{9.6}$$

with V being the velocity of a monomer and N the number of monomers. Hence, the dissipation at the pore can be written as:

$$T\dot{S} = \eta(\nabla V)^2\Omega \tag{9.7}$$

where Ω is the impacted volume. For 2D systems, $\Omega = a\xi^2$

Combining these relations, we obtain the following ordinary differential equation:

$$\frac{d}{dt}\left[k_{\mathrm{B}}T\left(\frac{a}{R}\right)^{\frac{2}{2\nu-1}}N^{\frac{2\nu}{2\nu-1}}\right] = -\eta\left(\frac{a\dot{N}}{\xi}\right)^2 a\xi^2$$

The solution of this equation reads:

$$n(t) = N\left(1 + \frac{4\nu(1-\nu)}{2\nu-1}\frac{k_{\mathrm{B}}T}{\eta}a^{-3}\left(\frac{a}{R}\right)^{\frac{2}{2\nu-1}}N^{\frac{-2(\nu-1)}{2\nu-1}}t\right)^{\frac{2\nu-1}{2(\nu-1)}}$$

Finally, we can reduce the time evolution of the number of monomers inside the cavity as:

$$n(t) = N\left(1 + \frac{t}{\tau}\right)^{\beta} \tag{9.8}$$

where N is the total number of monomers of the chain, $\beta = (2\nu-1)/2(\nu-1)$ and the characteristic escape time is:

$$\tau = \frac{2\nu-1}{4\nu(1-\nu)}\frac{\eta}{k_{\mathrm{B}}T}a^3\left(\frac{R}{a}\right)^{2/(2\nu-1)}N^{2(\nu-1)/(2\nu-1)}$$

Using the value of the Flory exponent, we get:

$$\tau = \frac{2}{3}\frac{\eta}{k_B T a}\frac{R^4}{N} \quad \text{or} \quad \frac{\tau}{N^2} \sim \left(\frac{R}{R_F}\right)^4$$

The relation derived from Sakaue's approach unfortunately produces a worse agreement with the experimental data than the crude model proposed here above. This model has obviously the same drawbacks, *i.e.* considering a strong confinement regime during all the escape process.

The model of Sakaue predicts the time evolution of the number of escaped monomers, $N - n(t)$, see Eq. 9.8. In Fig.9.6, we have plotted the number of monomers outside the cavity against time normalized by $\tau \sim R^4/N$. We have only represented the results for two different chain lengths, $N = 54$ and 298. The curves do not collapse on a single one and the function given by Eq. 9.8 does not agree with our results. It even seems that the translocation happens faster than predicted by the Sakaue's model based on constant pressure and friction dissipation.

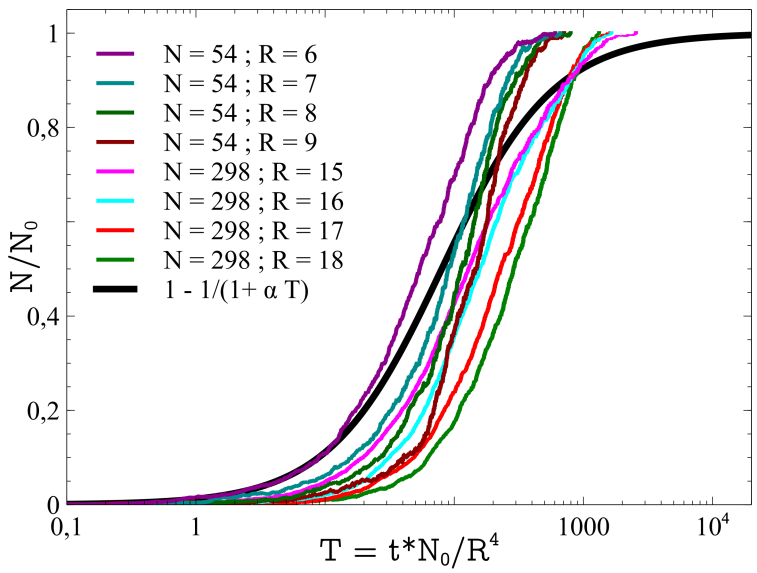

Figure 9.6 – Number of monomers oustide the cavity with respect to a normalized time $T = tN_0/R^4$.

The two proposed models of the chain escape from a cavity capture the essence of the escape dynamics and their basic features: sigmoidal evolution of the number of monomers escaped and a mean escape time given by $\tau/N^\alpha \sim (R/R_F)^\beta$. Within the crude approximations used up to now – a constant pressure and without considering chain stretching and subsequent relaxation – building a more adapted model is probably impossible.

9.1.2 Mean first passage time

Another interesting quantity is the mean time for the chain to "find" the opening of the cavity. In our simulations, the chain is initially created in a spiral fashion, one end at the center and one end nearer to the cavity walls. However, before creating an opening in the cavity, the chain is allowed to equilibrate for a time longer than the Rouse time. Therefore, the knowledge of the chain's ends position is obviously lost. As shown in

Fig. 9.7, the exit time for the first monomer increases very rapidly with the radius of the cavity. As proposed for the mean escape time, it is possible to build a master curve of these exit times by using the scaling $\tau/N^{\alpha} \sim (R/R_F)^{\beta}$, with $\alpha = 5/2, \beta = 8$.
However, building a theoretical framework to study this quantity seems for now an open question.

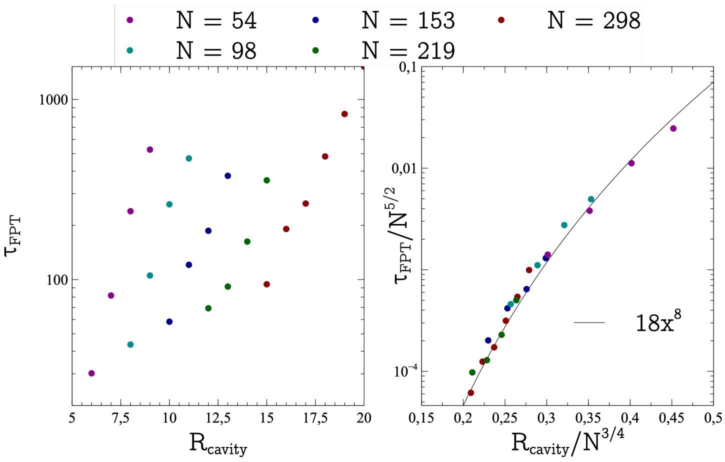

Figure 9.7 – Mean first passage time for the first monomer of the chain to escape the cavity.

9.2 Example of another biased translocation

There are many ways to introduce a bias in the translocation process so that a preferential direction emerges. We have already mentioned an electrical field, a fluid flow or a gradient across the wall to enhance the translocation and we have already studied the case of geometrical confinement. However, another way, inspired by in vivo speculation, is chaperone assisted translocation. That is, for some reason[1], a type of monomer once across the wall in the privileged direction cannot cross it back. Like the Brownian ratchet, this translocation is called ratchet translocation.
The full study of this type of translocation is beyond the scope of our study but we may display some preliminary results.

9.2.1 Ratchet translocation

In these simulations, the chain is self-avoiding and its initial configuration is such that a monomer is on one side of the wall and the rest on the other side. Some monomers are different from the others in the sens that they cannot go in the cis side once in the trans side. On Fig.9.8, they are represented in red. Three different cases to gradually increase the number of ratchets in the chain. First, only the head monomer cannot cross back, Fig.9.8a . Then, the mid-monomer also becomes a ratchet point, Fig.9.8b. Finally, a density of one ratchet every ten monomers is used, Fig.9.8c.

---

[1] *e.g.* conformational changes or chemical reactions.

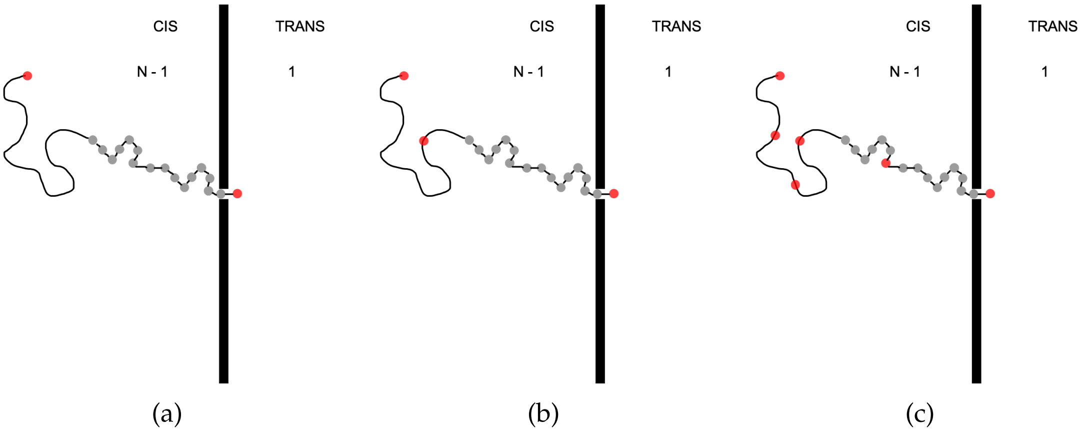

Figure 9.8 – Initial configurations when the chain has: (a) One head ratchet , (b) One head ratchet & ratchet in the middle and (c) A ratchet every 10 monomers.

In Fig.9.9, we can see that as one might expect, the more there are ratchets in the chain, the faster the translocation happens. Describing this increase would require longer chains with a finer screening in the ratchet densities.

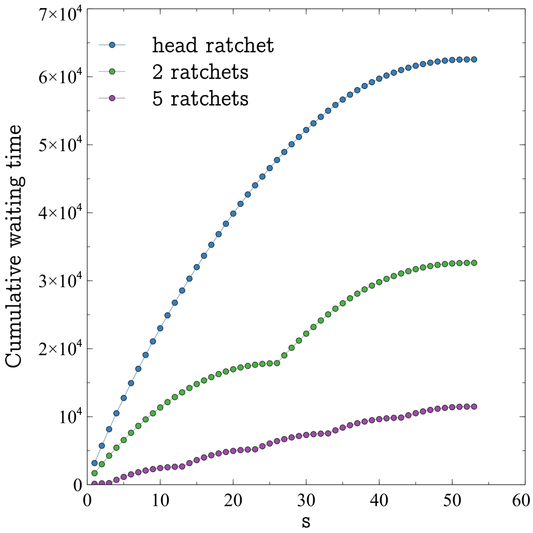

Figure 9.9 – Cumulative waiting time for a self-avoiding chain of length 54 with different number of ratchets amongst its monomers.

9.3 Concluding remarks

The translocation bias induced by the confinement is very effective and the dynamics of the translocation drastically impacted since the mean translocation time depends on the size of the confining cavity to a power α. In the model proposed by Sakaue $\alpha = 4$ while on the model we derived $\alpha = 6$. However, both models fail to capture the complete translocation dynamics because the confinement of the chain is only a transient feature. Indeed, translocation implies monomers leaving the confining cavity and thus decreasing the internal pressure. At some point, one cannot solely invoke confinement to explain translocation. Other mechanisms have to be envisioned, such as an entropic force due to the likely stretching of the subchain outside of the cavity, to fully describe the translocation process. One may even try to apply the models developped for the unbiased case to the transocation out of a cavity once the confinement has lost its strength. Another way of introducing a bias in the translocation is to consider ratchets in the chain so that the translocation becomes irreversible. In vivo, this can be chemical reactions leading to the addition of a molecule or to conformational changes.

General conclusion and outlooks

Reaching the end of this thesis, our use of the granular chain as a polymer equivalent has proved to be adequate both in a static assembly and under mechanical excitation. Remarkably, just like for the microscopic realm, the bulk properties are well modeled but when single particle or quasi 2D geometries are considered, existing theoretical frameworks suffer from the same drawbacks than those already known at the microscopic scale.

In the first part, the assembly of granular chains was investigated via an indirect method: indentation. The experimental data suggest that, like any aggregate of macroscopic particles in contact, friction drives the cohesion of the assembly but, unlike other assembly, its internal structure is a basic key to understand the amplification of the friction. We have used the polymer analogy to describe the intertwined granular chains as a polymer melt and thus been able to quantify the contacts between them through a statistical approach. We pushed this polymer melt analogy further to the semi-dilute case that we experimentally investigated by mixing granular chains and simple beads. The proposed model is in a good quantitative agreement with the experimental data, as long as we consider their mean behaviour. However, if we study separately each mechanical response of the chain's assembly under indentation, avalanche-like events happen. The distribution of these events surely provides information on the internal structure. It, thus, would be interesting to further analyze this behaviour.

In the second part, we built an experimental setup whose purpose was to inject mechanical energy to the granular chain. The core of this setup is an electrodynamic shaker providing monoaxial vibrations, with controllable frequency spectrum and acceleration. Typically, the vibrations are along the gravity axis and the motion of the vibrated particle in the perpendicular plane. We bypassed the key question of the definition of temperature by restricting ourselves in considering the temperature to be linearly proportional to the mean acceleration of the mechanical vibrations. We have also shown that for the motion of the vibrated particle to be equivalent to the Brownian motion, one has to properly design the environment of the particle under test. Surprisingly, the most efficient environment is to render rough the surface on which the particle moves. We then 3D-printed different experimental arenas: a flat one and one with two connected wells. With the first arena we verified the Brownian motion characteristics of the particle and with the second one we challenged macroscopic and archetypal microscopic results with a good agreement.

In the last part, we used our experimental setup to study the motion of a granular chain. Granular chains exhibited the anomalous diffusion of a monomer inside the chain for intermediate times. This transient regime is absent for the motion of the chain's center of mass. We used molecular dynamics simulations to study the motion of a linear chain in two confined geometries: biased and unbiased translocation. As to the free translocation, even though we were able to obtain, from our simulations, the dependency of the translocation time with the chain length, we were only able to stress out the downsides of both the coarse-grained and the microscopic models proposed in the literature. Since the results from the simulations are insufficient to finely describe the translocation process, one could then use the granular chain in a suitably designed arena to add experimental results to the debate. Regarding the translocation driven by initial confinement, we provided an adequate model for the early stage of translocation. However, no model could take into account the decrease in confinement caused by the translocation.

Bibliography

[1] Héctor Alarcón et al. “Self-amplification of solid friction in interleaved assemblies”. In: *Physical review letters* 116.1 (2016), p. 015502.

[2] I Ali, D Marenduzzo, and JM Yeomans. “Polymer packaging and ejection in viral capsids: shape matters”. In: *Physical review letters* 96.20 (2006), p. 208102.

[3] Tomaso Aste, Tiziana Di Matteo, and E Galleani d’Agliano. “Stress transmission in granular matter”. In: *Journal of Physics: Condensed Matter* 14.9 (2002), p. 2391.

[4] Gaston Bachelard. *The psychoanalysis of fire*. Vol. 277. Beacon Press, 1964.

[5] William Barlow. *Probable Nature of the Internal Symmetry of Crystals 1*. 1883.

[6] GW Baxter and JS Olafsen. “Gaussian statistics in granular gases”. In: *Nature* 425.6959 (2003), pp. 680–680.

[7] Behringer. *Webpage of Bob Behringer*. `https://webhome.phy.duke.edu/~bob/`.

[8] Robert P Behringer and Bulbul Chakraborty. “The physics of jamming for granular materials: a review”. In: *Reports on Progress in Physics* 82.1 (2018), p. 012601.

[9] O Bénichou et al. “Optimizing intermittent reaction paths”. In: *Physical Chemistry Chemical Physics* 10.47 (2008), pp. 7059–7072.

[10] JD Bernal and J_ Mason. “Packing of spheres: co-ordination of randomly packed spheres”. In: *Nature* 188.4754 (1960), pp. 910–911.

[11] John D Bernal. “A geometrical approach to the structure of liquids”. In: *Nature* 183.4655 (1959), pp. 141–147.

[12] John D Bernal. “The Bakerian lecture, 1962. The structure of liquids”. In: *Proceedings of the Royal Society of London. Series A, Mathematical and Physical Sciences* 280.1382 (1964), pp. 299–322.

[13] Jöns Jacob Berzelius. *Théorie des proportions chimiques et table synoptique des poids atomiques des corps simples, et de leurs combinaisons les plus importantes*. Firmin Didot frères, 1835.

[14] Sergey M Bezrukov, Igor Vodyanoy, and V Adrian Parsegian. “Counting polymers moving through a single ion channel”. In: *Nature* 370.6487 (1994), pp. 279–281.

[15] Max Born and HS Green. “A general kinetic theory of liquids I. The molecular distribution functions”. In: *Proceedings of the Royal Society of London. Series A. Mathematical and Physical Sciences* 188.1012 (1946), pp. 10–18.

[16] Françoise Brochard-Wyart, Pierre Nassoy, and Pierre-Henri Puech. *Physique de la matière molle*. Dunod, 2018.

[17] Eric Brown et al. “Strain stiffening in random packings of entangled granular chains”. In: *Physical review letters* 108.10 (2012), p. 108302.

[18] Stephen G Brush. *The Kind of Motion We Call Heat. A History of the Kinetic Theory of Gases in the 19th Century. Book 1: Physics and the Atomists. Book 2: Statistical Physics and Irreversibel Processes*. Amsterdam, 1976.

[19] AO Caldeira and Anthony J Leggett. “Quantum tunnelling in a dissipative system”. In: *Annals of physics* 149.2 (1983), pp. 374–456.

[20] H Campbell and WC Bauer. “Cause and cure of demixing in solid-solid mixers”. In: *Chem. Eng* 73.19 (1966), p. 129.

[21] Clément Chatelain, Yacov Kantor, and Mehran Kardar. “Probability distributions for polymer translocation”. In: *Physical Review E* 78.2 (2008), p. 021129.

[22] Jeffrey Chuang, Yacov Kantor, and Mehran Kardar. “Anomalous dynamics of translocation”. In: *Physical Review E* 65.1 (2001).

[23] Rudolf Clausius. “XI. On the nature of the motion which we call heat”. In: *The London, Edinburgh, and Dublin Philosophical Magazine and Journal of Science* 14.91 (1857), pp. 108–127.

[24] Wallace H Coulter. *Means for counting particles suspended in a fluid*. US Patent 2,656,508. 1953.

[25] Gwennou Coupier et al. “Local symmetries and order-disorder transitions in small macroscopic Wigner islands”. In: *Physical Review E* 71.4 (2005), p. 046105.

[26] Jean Cuvier. *Eloge historique de M. Hauy*. 1823.

[27] John Dalton. *A new system of chemical philosophy, Vol. 1, Part 2*. Bickerstaff, 1810.

[28] Gianfranco D’Anna et al. “Observing brownian motion in vibration-fluidized granular matter”. In: *Nature* 424.6951 (2003), pp. 909–912.

[29] Willey David. *Tearing two interlaced phone books apart using two 18 wheeler trucks*. `https://www.youtube.com/watch?v=qjKpQxlIlUw`.

[30] RW DeBlois and CP Bean. “Counting and sizing of submicron particles by the resistive pulse technique”. In: *Review of Scientific Instruments* 41.7 (1970), pp. 909–916.

[31] Masao Doi and Samuel Frederick Edwards. *The theory of polymer dynamics*. Vol. 73. oxford university press, 1988.

[32] MB Donald and B Roseman. "Mixing and demixing of solid particles. Parts I, II and III". In: *Br. Chem. Eng.* 1 (1962), p. 749.

[33] Aleksandar Donev, Salvatore Torquato, and Frank H Stillinger. "Pair correlation function characteristics of nearly jammed disordered and ordered hard-sphere packings". In: *Physical Review E* 71.1 (2005), p. 011105.

[34] Aleksandar Donev et al. "Improving the density of jammed disordered packings using ellipsoids". In: *Science* 303.5660 (2004), pp. 990–993.

[35] Joseph L Doob. "The Brownian movement and stochastic equations". In: *Annals of Mathematics* (1942), pp. 351–369.

[36] JLA Dubbeldam et al. "Polymer translocation through a nanopore: A showcase of anomalous diffusion". In: *Physical Review E* 76.1 (2007), p. 010801.

[37] Denis Dumont et al. "Emergent strain stiffening in interlocked granular chains". In: *Physical review letters* 120.8 (2018), p. 088001.

[38] Christopher M Edmonds et al. "Polymer translocation in solid-state nanopores: Dependence of scaling behavior on pore dimensions and applied voltage". In: *The Journal of chemical physics* 136.6 (2012), 02B610.

[39] Sam F Edwards and RBS Oakeshott. "Theory of powders". In: *Physica A: Statistical Mechanics and its Applications* 157.3 (1989), pp. 1080–1090.

[40] Samuel Frederick Edwards and DR Wilkinson. "The surface statistics of a granular aggregate". In: *Proceedings of the Royal Society of London. A. Mathematical and Physical Sciences* 381.1780 (1982), pp. 17–31.

[41] Albert Einstein. "Ether and the Theory of Relativity". In: *Ltd, London* (1922).

[42] Albert Einstein. "On the theory of the Brownian movement". In: *Ann. Phys* 19.4 (1906), pp. 371–381.

[43] Albert Einstein. *The world as I see it*. Open Road Media, 2011.

[44] Nicolas Estrada et al. "Identification of rolling resistance as a shape parameter in sheared granular media". In: *Physical Review E* 84.1 (2011), p. 011306.

[45] Michael L Falk and James S Langer. "Dynamics of viscoplastic deformation in amorphous solids". In: *Physical Review E* 57.6 (1998), p. 7192.

[46] John L Finney. "Bernal's road to random packing and the structure of liquids". In: *Philosophical Magazine* 93.31-33 (2013), pp. 3940–3969.

[47] John L Finney and Leslie V Woodcock. "Renaissance of Bernal's random close packing and hypercritical line in the theory of liquids". In: *Journal of Physics: Condensed Matter* 26.46 (2014), p. 463102.

[48] Paul J Flory. *Principles of polymer chemistry*. Cornell University Press, 1953.

[49] Scott V Franklin. "Geometric cohesion in granular materials". In: *Physics Today* 65.9 (2012), p. 70.

[50] Walter Friedrich, Paul Knipping, and Max Laue. "Interferenzerscheinungen bei roentgenstrahlen". In: *Annalen der Physik* 346.10 (1913), pp. 971–988.

[51] Galileo Galilei. *Dialogues concerning two new sciences*. Dover, 1914.

[52] Junfei Geng et al. "Footprints in sand: the response of a granular material to local perturbations". In: *Physical Review Letters* 87.3 (2001), p. 035506.

[53] Pierre-Gilles de. Gennes. *Scaling concepts in polymer physics*. Cornell Univ. Press, 2005.

[54] Alexander Y Grosberg and Yitzhak Rabin. "DNA capture into a nanopore: interplay of diffusion and electrohydrodynamics". In: *The Journal of chemical physics* 133.16 (2010), 10B617.

[55] Alexander Yu. Grosberg and Alexei R. Khokhlov. *Statistical physics of macromolecules*. American Institute of Physics, 1994.

[56] B Gutenberg and CF Richter. "Magnitude and energy of earthquakes". In: *Nature* 176.4486 (1955), pp. 795–795.

[57] Beno Gutenberg and Carl F Richter. "Earthquake magnitude, intensity, energy, and acceleration: (Second paper)". In: *Bulletin of the seismological society of America* 46.2 (1956), pp. 105–145.

[58] Beno Gutenberg and Charles Francis Richter. "Earthquake magnitude, intensity, energy, and acceleration". In: *Bulletin of the Seismological society of America* 32.3 (1942), pp. 163–191.

[59] Hendrick W de Haan and Gary W Slater. "Mapping the variation of the translocation α scaling exponent with nanopore width". In: *Physical Review E* 81.5 (2010), p. 051802.

[60] Hendrick W de Haan and Gary W Slater. "Memory effects during the unbiased translocation of a polymer through a nanopore". In: *The Journal of chemical physics* 136.15 (2012), p. 154903.

[61] Thomas C Hales. "A proof of the Kepler conjecture". In: *Annals of mathematics* 162.3 (2005), pp. 1065–1185.

[62] Daniel M Harris and John WM Bush. "Generating uniaxial vibration with an electrodynamic shaker and external air bearing". In: *Journal of Sound and Vibration* 334 (2015), pp. 255–269.

[63] René Just Haüy. *Essai d'une theorie sur la structure des crystaux, appliquee a plusieurs genres de substances crystallisees; par M. l'abbe Hauy*. chez Gogue & Nee de La Rochelle, libraires quai des Augustins, 1784.

[64] SB Hladky and DA Haydon. “Discreteness of conductance change in bimolecular lipid membranes in the presence of certain antibiotics”. In: *Nature* 225.5231 (1970), pp. 451–453.

[65] Ilkka Huopaniemi et al. “Langevin dynamics simulations of polymer translocation through nanopores”. In: *The Journal of Chemical Physics* 125.12 (2006), p. 124901.

[66] John J Kasianowicz et al. “Characterization of individual polynucleotide molecules using a membrane channel”. In: *Proceedings of the National Academy of Sciences* 93.24 (1996), pp. 13770–13773.

[67] Johannes Kepler. “De nive sexangula, 1611”. In: *An English translation (by Colin Hardie) was published in* (1966).

[68] John G Kirkwood. “Statistical mechanics of fluid mixtures”. In: *The Journal of Chemical Physics* 3.5 (1935), pp. 300–313.

[69] Gerald Kneller. “Generalized Kubo relations and conditions for anomalous diffusion: Physical insights from a mathematical theorem”. In: *The Journal of chemical physics* 134 (June 2011), p. 224106.

[70] James B Knight et al. “Density relaxation in a vibrated granular material”. In: *Physical review E* 51.5 (1995), p. 3957.

[71] CY Kong and M Muthukumar. “Polymer translocation through a nanopore. II. Excluded volume effect”. In: *The Journal of chemical physics* 120.7 (2004), pp. 3460–3466.

[72] Samuel C Kou et al. “Stochastic modeling in nanoscale biophysics: subdiffusion within proteins”. In: *The Annals of Applied Statistics* 2.2 (2008), pp. 501–535.

[73] Hendrik Anthony Kramers. “Brownian motion in a field of force and the diffusion model of chemical reactions”. In: *Physica* 7.4 (1940), pp. 284–304.

[74] R Kubo, M Toda, and N Hashitsume. “Statistical Physics II (Spriger-Verlag, Berlin, 1985)”. In: *J. Schwinger, J. Math. Phys.* 13 (), p. 2.

[75] Jaeger lab. *Image reconstructed from the X-ray tomography of a chain packing*. `https://jfi.uchicago.edu/~jaeger/group/Granular_Matter_by_Design/Projects/Entries/2011/9/14_Strain-stiffening_in_granular_polymers.html`.

[76] Paul Langevin. “Sur la théorie du mouvement brownien”. In: *C. R. Acad. Sci. (Paris)* 146 (1908), 530–533.

[77] Andrea J Liu and Sidney R Nagel. “Jamming is not just cool any more”. In: *Nature* 396.6706 (1998), pp. 21–22.

[78] W Losert et al. “Velocity statistics in excited granular media”. In: *Chaos: An Interdisciplinary Journal of Nonlinear Science* 9.3 (1999), pp. 682–690.

[79] Kaifu Luo, Tapio Ala-Nissila, and See-Chen Ying. “Polymer translocation through a nanopore: A two-dimensional Monte Carlo study”. In: *The Journal of chemical physics* 124.3 (2006), p. 034714.

[80] Kaifu Luo et al. “Dynamical scaling exponents for polymer translocation through a nanopore”. In: *Physical Review E* 78.5 (2008), p. 050901.

[81] Paul Lévy. “Processus stochastiques et mouvement Brownien, Suivi d’une note de M. Loeve”. In: *Gauthier-Villars, Paris* (1948).

[82] AJ Matheson. “Computation of a random packing of hard spheres”. In: *Journal of Physics C: Solid State Physics* 7.15 (1974), p. 2569.

[83] Christopher K Mathews. *Reproduction of large virulent bacteriophages*. Springer, 1977, pp. 179–294.

[84] James Clerk Maxwell. “Iv. on the dynamical theory of gases”. In: *Philosophical transactions of the Royal Society of London* 157 (1867), pp. 49–88.

[85] James Clerk Maxwell. “V. Illustrations of the dynamical theory of gases.—Part I. On the motions and collisions of perfectly elastic spheres”. In: *The London, Edinburgh, and Dublin Philosophical Magazine and Journal of Science* 19.124 (1860), pp. 19–32.

[86] Scott A McKinley and Hung D Nguyen. “Anomalous diffusion and the generalized Langevin equation”. In: *SIAM Journal on Mathematical Analysis* 50.5 (2018), pp. 5119–5160.

[87] Scott A McKinley, Lingxing Yao, and M Gregory Forest. “Transient anomalous diffusion of tracer particles in soft matter”. In: *Journal of Rheology* 53.6 (2009), pp. 1487–1506.

[88] Amit Meller, Lucas Nivon, and Daniel Branton. “Voltage-driven DNA translocations through a nanopore”. In: *Physical Review Letters* 86.15 (2001), p. 3435.

[89] L Menéndez-Arias and F Gago. *Structure and Physics of Viruses: An Integrated Textbook, edited by GM Mateu*. 2013.

[90] Rafael Morgado et al. “Relation between anomalous and normal diffusion in systems with memory”. In: *Physical review letters* 89.10 (2002), p. 100601.

[91] Cristian F Moukarzel. “Isostatic phase transition and instability in stiff granular materials”. In: *Physical review letters* 81.8 (1998), p. 1634.

[92] Yuval Mulla, Anders Aufderhorst-Roberts, and Gijsje H Koenderink. “Shaping up synthetic cells”. In: *Physical biology* 15.4 (2018), p. 041001.

[93] M Muthukumar. “Theory of capture rate in polymer translocation”. In: *The Journal of chemical physics* 132.19 (2010), 05B605.

[94] Erwin Neher and Bert Sakmann. “Single-channel currents recorded from membrane of denervated frog muscle fibres”. In: *Nature* 260.5554 (1976), pp. 799–802.

[95] Jessica Nicastro et al. *Bacteriophage Applications-Historical Perspective and Future Potential*. Springer, 2016.

[96] JS Olafsen and Jeffery S Urbach. "Velocity distributions and density fluctuations in a granular gas". In: *Physical Review E* 60.3 (1999), R2468.

[97] Srdjan Ostojic, Ellák Somfai, and Bernard Nienhuis. "Scale invariance and universality of force networks in static granular matter". In: *Nature* 439.7078 (2006), pp. 828–830.

[98] Debabrata Panja. "Response of single polymers to localized step strains". In: *Physical Review E* 79.1 (2009), p. 011803.

[99] Debabrata Panja and Gerard T Barkema. "Simulations of two-dimensional unbiased polymer translocation using the bond fluctuation model". In: *The Journal of chemical physics* 132.1 (2010), p. 014902.

[100] Debabrata Panja, Gerard T Barkema, and Robin C Ball. "Anomalous dynamics of unbiased polymer translocation through a narrow pore". In: *Journal of Physics: Condensed Matter* 19.43 (2007), p. 432202.

[101] Debabrata Panja, Gerard T Barkema, and Robin C Ball. "Polymer translocation out of planar confinements". In: *Journal of Physics: Condensed Matter* 20.7 (2008), p. 075101.

[102] Debabrata Panja, Gerard T Barkema, and Anatoly B Kolomeisky. "Through the eye of the needle: recent advances in understanding biopolymer translocation". In: *Journal of Physics: Condensed Matter* 25.41 (2013), p. 413101.

[103] Albert P Philipse. "The random contact equation and its implications for (colloidal) rods in packings, suspensions, and anisotropic powders". In: *Langmuir* 12.5 (1996), pp. 1127–1133.

[104] Albert P Philipse and Alain Verberkmoes. "Statistical geometry of caging effects in random thin-rod structures". In: *Physica A: Statistical Mechanics and its Applications* 235.1-2 (1997), pp. 186–193.

[105] Christine M Pooley and David Tabor. "Friction and molecular structure: the behaviour of some thermoplastics". In: *Proceedings of the Royal Society of London. A. Mathematical and Physical Sciences* 329.1578 (1972), pp. 251–274.

[106] Noëlle Pottier. *Nonequilibrium statistical physics: linear irreversible processes*. Oxford University Press, 2009.

[107] JA Prins and H Petersen. "Theoretical diffraction patterns corresponding to some simple types of molecular arrangement in liquids". In: *Physica* 3.1-4 (1936), pp. 147–153.

[108] Pedro M Reis, Rohit A Ingale, and Mark D Shattuck. "Forcing independent velocity distributions in an experimental granular fluid". In: *Physical Review E* 75.5 (2007), p. 051311.

[109] Florence Rouyer and Narayanan Menon. "Velocity fluctuations in a homogeneous 2D granular gas in steady state". In: *Physical review letters* 85.17 (2000), p. 3676.

[110] Payam Rowghanian and Alexander Y Grosberg. "Electrophoretic capture of a DNA chain into a nanopore". In: *Physical Review E* 87.4 (2013), p. 042722.

[111] Takahiro Sakaue and Elie Raphaël. "Polymer Chains in Confined Spaces and Flow-Injection Problems: Some Remarks". In: *Macromolecules* 39.7 (2006), 2621–2628.

[112] Erwin Schrodinger. *What is life*. 1944.

[113] G David Scott. "Packing of spheres: packing of equal spheres". In: *Nature* 188.4754 (1960), pp. 908–909.

[114] GD Scott and DM Kilgour. "The density of random close packing of spheres". In: *Journal of Physics D: Applied Physics* 2.6 (1969), p. 863.

[115] Steven D Stellman. "A spherical chicken". In: (1973).

[116] GW Stewart. "Theory of X-Ray Diffraction in Liquids". In: *Physical Review* 32.4 (1928), p. 558.

[117] GW Stewart. "X-ray diffraction in liquids". In: *Reviews of Modern Physics* 2.1 (1930), p. 116.

[118] IM Stuart. "Capstan equation for strings with rigidity". In: *British Journal of Applied Physics* 12.10 (1961), p. 559.

[119] W. Sung and P. J. Park. "Polymer Translocation through a Pore in a Membrane". In: *Physical Review Letters* 77.4 (1996), 783–786.

[120] Alexei V Tkachenko and Thomas A Witten. "Stress propagation through frictionless granular material". In: *Physical review E* 60.1 (1999), p. 687.

[121] Salvatore Torquato and Frank H Stillinger. "Jammed hard-particle packings: From Kepler to Bernal and beyond". In: *Reviews of modern physics* 82.3 (2010), p. 2633.

[122] Melissa Trepanier and Scott V Franklin. "Column collapse of granular rods". In: *Physical Review E* 82.1 (2010), p. 011308.

[123] Mark Tuckerman. *Statistical mechanics: theory and molecular simulation*. Oxford university press, 2010.

[124] Dongshan Wei et al. "Unforced translocation of a polymer chain through a nanopore: The solvent effect". In: *The Journal of chemical physics* 126.20 (2007), 05B610.

[125] Norbert Wiener. "Differential-Space". In: *Journal of Mathematics and Physics* 2.1-4 (1923), pp. 131–174.

[126] RD Wildman, JM Huntley, and DJ Parker. "Granular temperature profiles in three-dimensional vibrofluidized granular beds". In: *Physical Review E* 63.6 (2001), p. 061311.

[127] RD Wildman and DJ Parker. “Coexistence of two granular temperatures in binary vibrofluidized beds”. In: *Physical review letters* 88.6 (2002), p. 064301.

[128] Matthieu Wyart. “On the rigidity of amorphous solids”. In: *arXiv preprint cond-mat/0512155* (2005).

[129] Xiaoyu Yang et al. “Measurements of grain motion in a dense, three-dimensional granular fluid”. In: *Physical review letters* 88.4 (2002), p. 044301.

[130] Ling-Nan Zou et al. “The packing of granular polymer chains”. In: *Science* 326.5951 (2009), pp. 408–410.

[131] Robert Zwanzig. *Nonequilibrium statistical mechanics*. Oxford University Press, 2001.

Abstract / Résumé

Chains dynamics, specially when repulsive interactions come at play, remains an unsolved problem of polymer physics, although understanding this dynamics could improve our knowledge about crucial phenomena at the cellular level. For instance, the transport of RNA across the nuclear pore or the injection of viral DNA plasmid by bacteriophages into a bacteria. Alas, studying repulsive polymers in confined geometries is as experimentally difficult as it is biologically relevant. In spite of recent advances in « nanorheology », from the Brownian motion of local probes, or in computer simulation, designing experiments matching the biological parameters is near impossible. All this leads to unchallenged theoretical tools. Even the straightforward problem of polymer translocation remains lively debated. As a way out of this impasse, we propose to use granular chain as a macroscopic equivalent of a polymer. First we were interested in the internal structure of a stack of granular chains at rest and we rationalized it with polymer analogy. Then we added energy in our experimental system via mechanical excitations which appears to be analogous to the equilibration with a thermal bath. Finally we studied the dynamics of chains in specific confined geometries and compared it to both molecular dynamics simulation and theoretical tools.

La dynamique des chaînes est encore de nos jours une question ouverte en physique des polymères, tout particulièrement lorsque les interactions répulsives sont prises en compte. Néanmoins, répondre à cette question améliorerait nos connaissances sur la machinerie cellulaire. On peut penser, par exemple, au transport de l'ARN du noyau au cytoplasme ou encore à l'injection du matériel génétique de bactériophages dans les bactéries. Malheureusement, étudier ces polymères en situation confinée est aussi expérimentalement difficile que biologiquement pertinent. En dépit des récentes avancées en nanorhéologie et en simulation de dynamique moléculaire, concevoir des expériences reprenant les mêmes paramètres que rencontrés in vivo est proche de l'impossible. Les théories en place ne peuvent donc être contestées par l'expérience. Même le problème, simple en apparence, de la translocation est encore aujourd'hui âprement discuté. Nous proposons, pour sortir de l'impasse actuelle, d'utiliser un équivalent d'un polymère à l'échelle macroscopique : la chaîne granulaire. Nous nous sommes tout d'abord intéressé à la structure interne d'un empilement de chaînes granulaires, au repos, et nous proposons pour la comprendre d'adopter une analogie avec les polymères. Après quoi, nous introduisons, par le biais d'une excitation mécanique, de l'énergie dans notre système expérimental et nous montrons que c'est statistiquement analogue à l'équilibre thermique à l'échelle microscopique. Enfin, nous étudions la dynamique de chaînes granulaires dans des géométries confinées et nous comparons nos résultats à ceux obtenus par simulation de dynamique moléculaire et ceux théoriquement attendus.